Crystallisation of Gypsum and Prevention of Foaming in Wet Flue Gas Desulphurisation (FGD) Plants

Hansen, Brian Brun

Publication date:
2008

Document Version
Publisher's PDF, also known as Version of record

Crystallisation of Gypsum and Prevention of Foaming in Wet Flue Gas Desulphurisation (FGD) Plants

Ph.D. Thesis

Brian Brun Hansen

Supervisors:
Søren Kiil
Jan E. Johnsson

CHEC Research Centre
Department of Chemical and Biochemical Engineering
Technical University of Denmark

ISBN-10 87-91435-91-9
ISBN-13 978-87-91435-91-1
Printed by J&R Frydenberg A/S, Copenhagen, Denmark

Preface

This thesis is written in partial fulfilment of the requirements to obtain the Doctor of Philosophy degree (PhD) at the Technical University of Denmark (DTU). The work has been carried out from March 2005 to June 2008 at the Combustion and Harmful Emission Control (CHEC) Research Centre, Department of Chemical Engineering, DTU. The project has been supervised by Ass. Prof. Søren Kiil and Prof. Jan E. Johnsson. The work was financed by DTU, Elsam A/S, Energi E2 A/S and the Danish Agency for Science, Technology and Innovation through the Graduate School in Chemical Engineering (MP_2T).

I would like to express my sincere thanks to a number of people who have contributed to this project. First of all my supervisors for their guidance, inspiration and swift feedback. Students Maria H. Pedersen, Jonas Kok, Klaus B. Sønder and Yang Cui for their hard work. Engineers Folmer Fogh, Henrik Rostgaard, Niels-Ole Knudsen, Mikkel Bruun and Jørgen Peter Jensen for their cooperation and valuable comments regarding power plants and full-scale conditions. Ass. Prof. Flemming Frandsen for his interest in my work and the proofreading of this thesis. Finally thanks to my family, friends, fellow PhD students and other colleagues at CHEC for their help and support during the last three years.

Brian Brun Hansen
Kgs. Lyngby, Denmark
May 30th, 2008

Abstract

The aim of this project is to investigate two operational problems, which have been experienced during wet flue gas desulphurisation (FGD) operation, i.e. poor gypsum dewatering properties and foaming. The results of this work can be used for the optimization of wet FGD-plants in terms of reliability of operation and consistency of the gypsum quality obtained. This work may furthermore be of interest to other industrial systems in which foaming or gypsum crystallisation may take place.

FGD is an industrial process, which removes sulphur dioxide (SO_2) from flue gasses generated by fossil fuel combustion at power plants and other heavy industries, thereby abating the detrimental effects known as "acid rain". The majority of the 680 FGD-plants installed at power plants worldwide in 1999 ($2.41 \cdot 10^5$ MW_e) were using the wet FGD-technology. This process absorbs ~ 99 % of the SO_2 by an alkaline slurry, where it is oxidised to sulphate (SO_4^{2-}) and crystallised as gypsum ($CaSO_4 \cdot 2H_2O$) - a commercial product.

The crystallisation process and the operating conditions under which it takes place, will determine the particle size distribution (PSD), the crystal morphology and thereby the dewatering properties. Experiments in a falling film wet FGD pilot plant have shown a strong non-linear behaviour (in a $\ln(n(l))$ vs. l plot) at the lower end of the particle size range, compared to the well-known linear "mixed suspension mixed product removal (MSMPR)" model. A transient population balance model, fitted to experimental breakage data, was able to model an increase in the fraction of small particles, but not to the extent observed for the experimental steady state PSD. A three-parameter, size-dependent growth model, previously used in the literature to describe sodium sulphate decahydrate ($Na_2SO_4 \cdot 10H_2O$) and potassium aluminium sulphate ($KAl(SO_4)_2 \cdot 12H_2O$) crystallisation, was able to describe the experimental data, indicating a surface integration controlled growth mechanism. The PSD at three full-scale wet FGD-plants were comparable to the gypsum produced in the pilot plant. However, the crystals had fewer distinct crystals faces and more amorphous shapes. An episode with deteriorating gypsum dewatering properties at unit 3 of Amager Power Plant was linked to a change in crystal morphology, possibly due to adsorption of growth retarding aluminium fluoride compounds at specific crystal faces.

Excessive foaming within wet FGD-plants has been associated with a range of operational problems as well as an increased degree of SO_2 absorption. Foaming agents include surfactants, macromolecules (such as polymers or proteins), and finely dispersed solids. The foaming ability of particles, electrolytes and buffers, present in a wet FGD-plant, has been investigated by laboratory scale Bikerman experiments. Adipic acid, as well as a combination of small particles and an electrolyte, have been demonstrated to generate weak transient foams. Pilot plant experiments showed an increased absorption efficiency of SO_2 using a foaming solution of calcium chloride ($CaCl_2$) with small quartz particles, compared to pure non-foaming tap water.

Resume

Formålet med dette projekt er at undersøge 2 driftsproblemer, som kan opstå i et vådt røggasafsvovlingsanlæg, nærmere bestemt forringede afvandingsegenskaber af den producerede gips og skumdannelse. Resultaterne af dette arbejde kan benyttes til at optimere våde røggasafsvovlingsanlæg med hensyn til driftssikkerhed og opnåelse af en konsistent gips kvalitet. Resultaterne kan desuden have interesse for andre industrielle systemer, hvor skumdannelse eller gipskrystallisation kan forekomme.

Røggasafsvovling er en industriel proces, som benyttes til at rense svovldioxidholdige (SO_2) røggasser dannet ved afbrænding af fossile brændsler på kraftværker og indenfor anden tung industri. De skadelige konsekvenser af SO_2-emission til atmosfæren, kendt som "syreregn", afhjælpes derved. Våde røggasafsvovlingsanlæg udgjorde størstedelen af den installerede afsvovlingskapacitet på verdens kraftværker i 1999 (680 stk., $2.41 \cdot 10^5$ MW_e). Denne proces absorberer ~ 99 % af SO_2'en ved kontakt med en alkalisk opslemning af kalksten, hvor en oxidation til sulfat (SO_4^{2-}) og en udkrystallisation som kommercielt gips ($CaSO_4 \cdot 2H_2O$) finder sted.

Krystallisationsprocessen afgør hvilken partikelstørrelsesfordeling, morfologi og derved hvilke afvandingsegenskaber, som opnås. Gipskrystaller produceret i et pilotskala røggasafsvovlingsanlæg (faldfilmskolonne) udviste en stærk ulineær opførsel, i en $\ln(n(l))$ mod l afbildning, sammenlignet med den velkendte lineære MSMPR model. En transient populationsbalance model for partikelnedbrydning, som er udviklet på basis af eksperimentelle målinger, kan modellere en forøget fraktion af små partikler, men ikke i det eksperimentelt målte omfang. En 3-parameters model for størrelsesafhængig vækst, som tidligere er blevet benyttet i litteraturen til at beskrive krystallisation af natriumsulfat dekahydrat ($Na_2SO_4 \cdot 10H_2O$) og kalium-aluminium-sulfat ($KAl(SO_4)_2 \cdot 12H_2O$), er i stand til at modellere de eksperimentelle målinger. Dette indikerer at krystalvæksten er kontrolleret af ionoptagelsen i krystalgitteret. Partikelstørrelsesfordelingen af den producerede gips fra 3 fuldskala røggasafsvovlingsanlæg var sammenlignelig med gips produceret i pilotskala anlægget. Krystallerne udviste dog færre markante krystaloverflader og havde amorfe morfologier. En episode med en forringelse af gipsens afvandingsegenskaber på

Amagerværkets blok 3 blev relateret til en ændring i krystal morfologi, muligvis forårsaget af adsorption af væksthæmmende aluminium fluorid forbindelser på specifikke krystaloverflader.

Markant skumning i våde røggasafsvovlingsanlæg kan medføre en række driftsproblemer men også en forøget SO_2 absorptionsgrad. Skumningstendensen kan påvirkes af overfladeaktive stoffer, makromolekyler (polymerer og proteiner) samt små partikler. Potentialet for skumdannelse af en række partikler, elektrolytter og buffere, som kan være tilstede i et vådt røggasafsvovlingsanlæg, er blevet undersøgt i laboratorieskala ved Bikerman eksperimenter. Adipinsyre samt en kombination af små partikler og en elektrolyt dannede et svagt transient skumlag. En forøget SO_2 absorptionsgrad blev målt i pilotanlægget når en svagt skummende opløsning af calcium klorid ($CaCl_2$) og små kvarts partikler blev anvendt, sammenlignet med rent ikke skummende vandhanevand.

Contents

List of Figures

List of Tables

Chapter 1

Background

This chapter provides an overview of the various commercial flue gas desulphurisation (FGD)-technologies used at power plants and their worldwide application. A special emphasis is placed on wet scrubbers using limestone as reactant, because this process is the focus of the work presented in the subsequent chapters. Finally the aims of this thesis are outlined.

1.1 Introduction

The combustion of fossil fuels containing sulphur, such as coal and oil, supply a substantial part of the worlds present energy demand and is expected to continue to do so in the coming years, despite an increasing interest in alternative fuel sources.[1] The sulphur may be present in both inorganic form (i.e. sulphides (S^{2-}) and sulphates (SO_4^{2-})) and in organic form (i.e. thiols and thiophenes).[2] The sulphur content of some fossil fuels may exceed 7 wt.%, while much lower fractions are present in fuels such as natural gas, wood, straw etc. During combustion the sulphur is oxidised rapidly through a sequence of steps initiated by reactions with sulphur containing radicals. The primary compound formed by the combustion process is gaseous sulphur dioxide (SO_2), however, small amounts of gaseous sulphur trioxide (SO_3) and various sulphates are also formed.

Oxidation of SO_2 and reaction with water vapour can take place in the atmosphere forming sulphuric acid aerosols. The resulting acid rain has been associated with detrimental effects such as a reduction in atmospheric visibility, damage to buildings, flora and fauna and an increase in the occurrence of respiratory diseases.[3] National legislation and international protocols concerning SO_2 emissions have been introduced since the 1970s to abate these

adverse effects, through thresholds values, emission caps and taxes.[4] Initially a switch towards fuels containing less sulphur was sufficient to comply with the environmental regulations. Stricter regulations concerning the power plants, as well as a desire to utilise a wide range of fuels, necessitated additional measures. A range of FGD-technologies have subsequently been developed and installed at power plants all over the world.

1.2 FGD-Technologies

1.2.1 The wet scrubber FGD-process

The wet scrubber technologies bring the SO_2 containing flue gas into contact with an alkaline slurry/solution in an absorber. The SO_2 is transferred to the liquid phase by diffusion through the gas film and the liquid film. Depending on the SO_2-concentration in the flue gas and the reactant used, the diffusion process can be influenced by the gas film resistance and the liquid film resistance. The different wet FGD-technologies may be subdivided according to the absorber design as well as the reactant used. In the Jet Bubbling Reactor (JBR) the flue gas is bubbled through the liquid phase, while the counter-current spray-tower and the co-current packed tower distribute the liquid phase as droplets by atomising nozzles or as a film across grid elements.[5] Most installations use limestone ($CaCO_3$) as reactant, because of its wide availability, low price and the production of a commercial product (i.e. gypsum, $CaSO_4 \cdot 2H_2O$). To obtain an acceptable reactivity/dissolution rate a grinding of the limestone particles is, however, often necessary. Reactants such as slaked lime ($Ca(OH)_2$) or magnesium-containing slaked lime ($Ca(OH)_2$ and $Mg(OH)_2$) provide an increased reactivity, thereby facilitating the use of a more compact absorber, at the expense of higher operating costs.[5] Installations located by the sea and onboard ocean-going vessels may utilise the natural alkalinity of seawater (bicarbonate, HCO_3^-) for desulphurisation, producing a discharge containing a SO_4^{2-}-concentration within natural variations.[6] Finally scrubbers using ammonia as reactant may produce ammonium sulphate ($(NH_4)_2SO_4$, a commercial fertilizer).[4] The following process description focuses on the limestone-based wet scrubber process.

The outline of a wet FGD spray-tower scrubber is shown in Figure 1.1. The liquid to gas ratio in the absorber is an important operating parameter with a strong influence on the desulphurisation degree. The limestone slurry leaving the absorber is collected in a holding/reaction tank, which often is an integrated part of the absorber. New limestone slurry is added to the holding tank based on the SO_2 load (flue gas flow and SO_2-concentration) and a control of the slurry pH. A slurry recycle stream is furthermore withdrawn from the holding tank and returned to the absorber. Based on an online measurement of the slurry density in the holding tank the crystal product is withdrawn, washed and dewatered by e.g. hydrocyclones, centrifuges or belt filters, yielding liquid bleed and recycle streams. The flue gas leaving the holding tank passes though demisters, which captures entrained droplets, and is reheated to avoid condensation, before it is emitted.

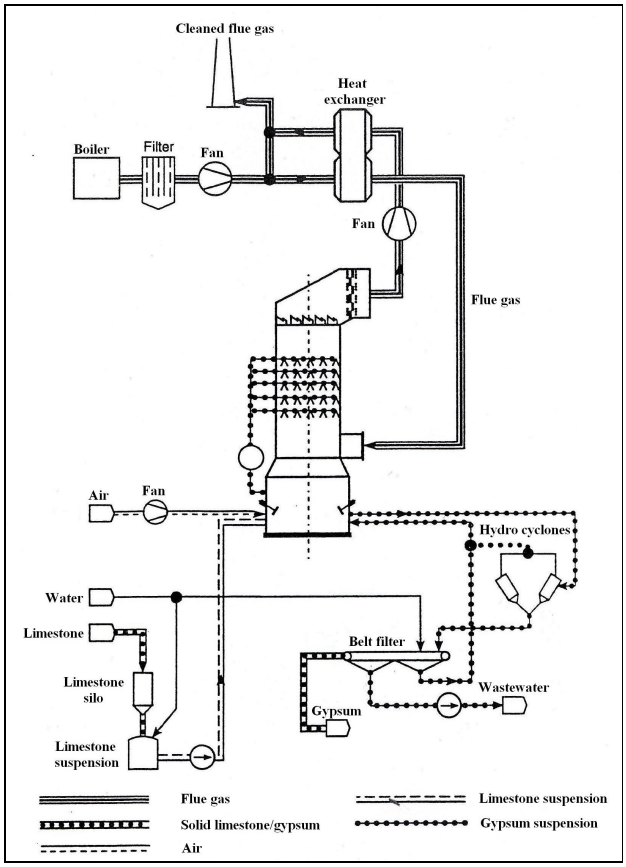

Figure 1.1: Outline of full-scale wet FGD-plant consisting of flue gas scrubber (centre), the reactant preparation line (lower left) and the gypsum dewatering line (lower right).[7] Reproduced with the permission of Dong Energy A/S.

The overall desulphurisation operation of the limestone-based wet scrubber, is comprised of a number of sub-operations/sub-reactions, equation 1.01 to 1.05.[8]

$$SO_2(g) + H_2O \Leftrightarrow H_2SO_3(aq) \Leftrightarrow H^+(aq) + HSO_3^-(aq) \quad (1.01)$$

$$HSO_3^-(aq) \Leftrightarrow H^+(aq) + SO_3^{2-}(aq)$$

$$CaCO_3(s) \Leftrightarrow Ca^{2+}(aq) + CO_3^{2-}(aq) \quad (1.02)$$

$$Ca^{2+}(aq) + CO_3^{2-}(aq) + H_2O \Leftrightarrow Ca^{2+}(aq) + HCO_3^-(aq) + OH^-(aq)$$

$$CaCO_3(s) + 2H^+(aq) \Leftrightarrow Ca^{2+}(aq) + H_2O + CO_2(g) \quad (1.03)$$

$$HSO_3^-(aq) + \tfrac{1}{2}O_2(g) \Rightarrow H^+(aq) + SO_4^{2-}(aq) \quad (1.04)$$

$$Ca^{2+}(aq) + SO_4^{2-}(aq) + 2H_2O \Leftrightarrow CaSO_4 \cdot 2H_2O(s) \quad (1.05)$$

The mass transfer of SO_2 to the liquid phase is described by equilibrium reaction 1.01 and the dissolution of limestone by equation 1.02 and 1.03, with only a minor contribution from equation 1.02. Depending on the availability of oxygen the hydrogen sulphite (HSO_3^-) can be oxidised to SO_4^{2-}, equation 1.04, with the increasing HSO_3^--concentration at low pH values favouring the oxidation rate.[9] Additional oxidation air is supplied in most modern plants, to ensure a complete conversion to SO_4^{2-} and the subsequent crystallisation as gypsum, equation 1.05. Depending on the commercial use of the gypsum (wallboard or cement production) different quality specifications may exist. In the case of wallboard production specifications regarding purity ($\geq$ 92 %), moisture content ($<$ 10 %) and chloride content ($Cl^- < 100$ ppm) have been reported.[8]

Episodes concerning poor gypsum dewatering properties and unexpected/non-wanted foaming have been encountered in several Danish wet FGD-plants. A deterioration of gypsum dewatering properties can lead to an increased processing time/cost and a higher moisture content of the final product. Such a change of gypsum dewatering properties can be caused by increased fractions of small particles and a change of morphology. Foaming has caused scaling at the demister, interference with slurry density measurements and FGD-unit shutdown, due to foam overflow from the reactor.

1.2.2 Other FGD-technologies

The spray-dry scrubber

The spray-dry scrubber brings the flue gas into contact with alkaline slurry droplets in a carbon steel vessel. The SO_2 is absorbed by the droplets in the upper part of the spray-dryer, while only dry particles, consisting of an un-reacted core and an outer product layer, remains in the lower part. The operating temperature and the presence of deliquescent salts influence the droplet lifetime and thereby the desulphurisation degree and reactant utillisation.[5,6] Operation at an excess of reactant, i.e. molar calcium to sulphur ratios of 1.1 to 1.6, ensures a high degree of desulphurisation.[5] The obtained solid mixture of unused reactant, calcium sulphite ($CaSO_3$) and calcium sulphate ($CaSO_4$) are collected at the bottom of the spray-dryer and in a particulate control device. The collected solids are usually either disposed off or used as reactant for nearby wet FGD-plants.

The sorbent injection processes

By injecting reactants into the flue gas stream the duct/furnace can be used as reaction vessels. A special case is the circulating fluidized bed (CFB), in which the flue gas passes through a separate reaction vessel. An upgraded particulate control device collects the obtained solid mixture of unused reactant, $CaSO_3$ and $CaSO_4$. The obtainable desulphurisation degree depends on the choice of reactant, the humidification and the excess of reactant. The operation is usually performed at a considerable excess of reactant, i.e. molar calcium to sulphur ratios of two to three.[5]

The regenerable reactant processes

This type of FGD-processes usually consists of a pre-scrubber that removes any deactivating impurities from the flue gas, a scrubber for SO_2 capture and a vessel for either chemical or thermal regeneration of the reactant. Reactants include sodium sulphite (Na_2SO_3), magnesium sulphite ($MgSO_3$), sodium carbonate (Na_2CO_3), amines (R_3N) and activated carbon.[5,6] Commercial products such as sulphuric acid, elemental sulphur or liquid SO_2 are obtained.

Combined SO_2/NO_x removal

The concept of this type of FGD-process is to reduce the overall cost of flue gas cleaning, and to limit the space requirements, by combining the removal of SO_2 and nitrogen oxides (NO_x). Several novel technologies have been suggested, but few have reached commercial operation. Commercial examples include the Topsøe SNOX^{TM} process, producing sulphuric acid, and the regenerable NOXSO process.[5]

1.3 Comparison of technologies and overview of installations

1.3.1 Overview of installations

The most recent data found on the worldwide installed FGD capacity at coal-fired power plants are from 1999.[4] 680 power plant units with a total capacity of 241000 MW_e were equipped with FGD-technologies and the construction of an additional 140 FGD-units were planned. Figure 1.2 illustrates the technological distribution of the installed FGD capacity. Wet scrubbers accounted for the majority (87.5 %) of the installed capacity well ahead of spray-dry scrubbers (7.6 %). The other FGD-processes only had obtained limited application.

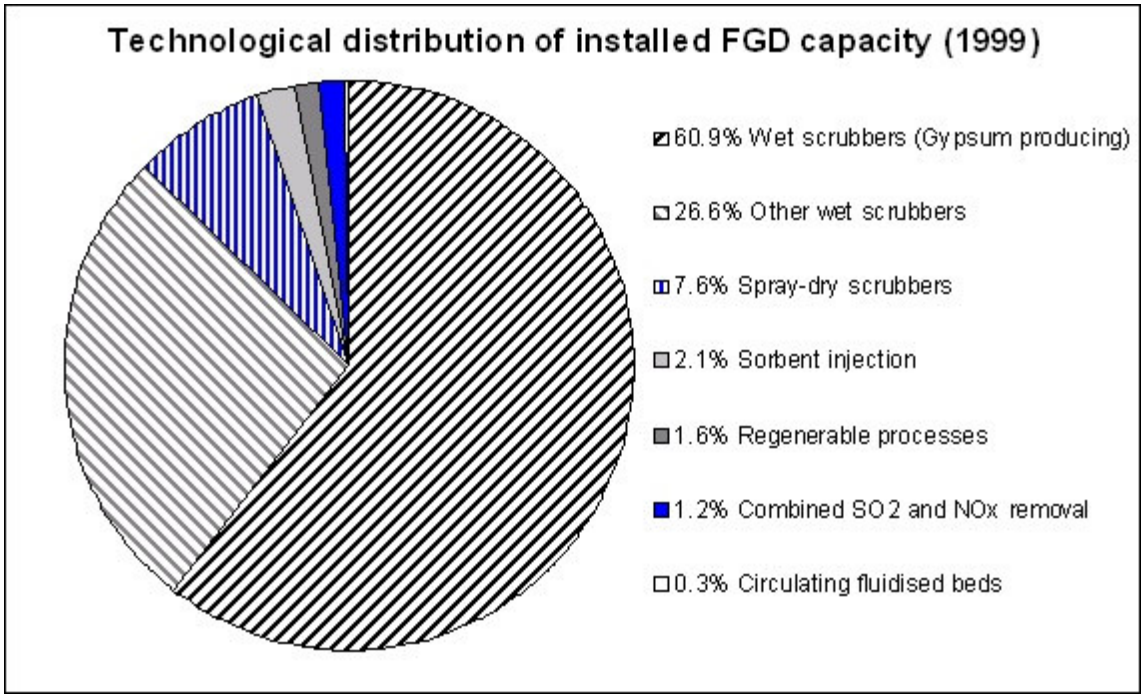

Figure 1.2: Technological distribution of installed FGD capacity on coal-fired power plants in 1999, based on data from ref 4.

North America comprised most of the installed FGD capacity in 1999 (43 %), with 39 % being located in Europe (mainly Germany) and 18 % in East Asia (Japan, Taiwan, South Korea and Thailand).[4] An ambitious Chinese air quality program featuring the installation of 300 FGD-units is about to change this picture in the coming years. China is predicted to have overtaken the installed FGD capacity of the USA by 2012, despite the increasing retrofitting activity in the US facilitated by the "Clean Air Interstate Rule.[10] India is furthermore reported to be in the initial stages of what could become a major air quality programme. The majority of these new installations will be limestone-based wet scrubbers, but approximately 15 % of the commissions are CFB's or spray-dry scrubbers.[10]

Table 1.1 lists the 12 FGD-plants currently installed at Danish power plants. Some power plant units may not be equipped with a FGD-plant, due to the fuel used, and unit numbers may furthermore cover a historical facility that has been closed down. Some small FGD-units are furthermore installed at other locations, such as waste incinerators, and unit 1 of Amager Power Plant (APP) is being equipped with a wet FGD-unit. As in the rest of the world, the limestone-based wet scrubber process is the predominant FGD-technology used in Denmark

Table 1.1: FGD-units installed at Danish power plants

Plant	Unit no.	Capacity	FGD-technology
Amagerværket (APP)	3	250 MW_e	Wet scrubber
Asnæsværket (ASPP)	5	640 MW_e	Wet scrubber
Avedøreværket (AVPP)	1	250 MW_e	Wet scrubber
Avedøreværket (AVPP)	2	570 MW_e	Wet scrubber
Enstedværket (ENPP)	3	600 MW_e	Wet scrubber
Esbjergværket (ESPP)	3	378 MW_e	Wet scrubber
Fynsværket (FPP)	7	401 MW_e	Spray dryer
Nordjyllandsværket (NJPP)	2	285 MW_e	Combined SO_2 and NO_x (WSA-SNOX)
Nordjyllandsværket (NJPP)	3	380 MW_e	Wet scrubber
Stigsnæsværket (STPP))	2	266 MW_e	Wet scrubber
Studstrupværket (SSPP)	3	350 MW_e	Spray dryer
Studstrupværket (SSPP)	4	350 MW_e	Spray dryer

1.3.2 Comparison of FGD-technologies

The following section will briefly highlight the main differences, in terms of performance and costs, of the different FGD-technologies applied at power plants.

Siegfriedt et. al (2007)[11] compared the performance and the levelised cost of three FGD-technologies (spray-dry scrubbers, CFB's and limestone-based wet scrubbers) for three coal types (0.6; 1.3 and 2.0 wt.% sulphur), two unit sizes (400 and 500 MW_e) and the cases of retro-fitting and the construction of a new unit. The present high levels of activity within the FGD supplier sector, as well as the high demand of construction materials, have most likely influenced the following estimates of the levelised cost for the construction of a new FGD-unit.

- Wet scrubber: 0.91-1.07 ¢ kWh^{-1}
- Circulating fluidised bed: 0.84-1.12 ¢ kWh^{-1}
- Spray-dry scrubber: 0.82-1.07 ¢ kWh^{-1}

Significant differences in the fixed (capital costs) and the operating costs of the different FGD-processes do, however, exist. The capital cost covers the design and construction of the unit and will depend on the process complexity (i.e. engineering calculations), the construction materials used and the number of units operations involved. The operating cost covers expenses for maintenance, reactant purchase, product disposal and utilities (steam, power and water).[12] The selection of the optimal FGD-technology will consequently depend on a number of factors including: local legislation, reactant availability, disposal opportunities, plant size, sulphur content of the fuel and expected plant lifetime.[12] Table 1.2 summarise some of the main features and differences between 4 different FGD-technologies, from which some general conclusions can be drawn.

Table 1.2: Comparison of FGD-technologies based on data from ref 4, 5, 6, 11 and 13.

	Wet scrubber	**Spray-dry scrubber**	**Circulating fluidised bed**	**WSA-SNOX**
Cleaning capabilities				
SO_2	~ 99 %	~ 98 %	~ 97 %	~ 95 %
NO_x				~ 95 %
Reactant	Limestone	Slaked lime	Slaked lime	NH_3 for NO_x removal
Reactant consumption (Ca/S molar ratio)	1.01 to 1.05	1.1 to 1.6	1.2 to 1.5	
Commercial product?	Yes	No	No	Yes
Product	$CaSO_4 \cdot 2H_2O$	$CaSO_3/CaSO_4$	$CaSO_3/CaSO_4$	H_2SO_4
Complexity	High	Moderate	Moderate	High
Material quality	Alloys Lined carbon steel	Carbon steel	Carbon steel	Glass condenser
Multiple units required	> 1000 MW_e	> 400 MW_e	> 700 MW_e	
Energy consumption	1-2 %[a]	0.5-1.0 %[a]		[b]

[a] Percentage of power plant output.

[b] Break even in the case of a fuel sulphur content of 2-3 wt. %.

The limestone-based wet scrubbers are associated with relative high capital costs, because of the corrosive/abrasive operation environment and the unit operations required for the processing of the obtained product and the generated wastewater. The efficient utilisation of a cheap reactant, and the commercial product obtained do, however, provide this process with favourable operating costs. The process is consequently well suited for the desulphurisation of large flue gas streams from power plants, with considerable remaining lifetimes, combusting coal/oil containing several percent of sulphur. The process is able to comply with strict emission limits (η_{SO2} ~ 99 %) and a single scrubber can handle power plant units up to 1000 MW_e.[4,5,14]

The spray-dry scrubbers, CFB's and sorbent injection units are associated with low to moderate capital costs, because of a lower degree of complexity and the use of cheaper construction materials. The more costly reactant is, however, not utilised as efficiently and expenses are associated wit the disposal of the obtained products. These processes are consequently well suited for the desulphurisation of flue gas streams from small to medium-sized power plants, with short remaining lifetimes, combusting fuels with a low to moderate sulphur content. The spray-dry scrubbers and CFB are able to comply with relative strict emission limits (η_{SO2} ~ 97 %), while the desulphurisation potential of the sorbent injection processes are limited (η_{SO2} ~ 80 %).[4,5,14]

The regenerable FGD-processes and the combined SO_2 and NO_x removal processes are associated with relative high capital costs and utility expenses, because of the process complexity, the reactant reactivation and the processing of the obtained product. The favourable energy consumption of the WSA-SNOX process is a notable exception. An income is, however, generated from the commercials product obtained. These features have limited the application of these processes within the power plant sector.

1.4 Project objective

It is the aim of the work presented in the subsequent chapters to increase the understanding of the gypsum crystallisation taking place in a limestone-based wet scrubber and to study its influence on the product quality in terms of purity and dewatering properties. A better understanding of the gypsum crystallisation process could facilitate a more consistent gypsum quality and an increased control of the limestone-based wet FGD-process. It is furthermore the aim of this project to investigate the origin of the sudden and unwanted occurrence of foaming in wet FGD-plants. If the foaming mechanism was to be identified, this could point towards methods to control the foaming and its associated operational problems.

1.5 Outline

The thesis consists of a literature survey as well as three chapters containing the articles, which were completed during this study. The articles are presented in the same form as they were submitted, with only minor layout changes and a slight editing to avoid repetitions.

In chapter two a literature survey concerning gypsum crystallisation and foaming is presented. The information obtained, alongside the introduction to the FGD-process in this chapter, provides the theoretical foundation for the subsequent investigation of crystallisation and foaming.

In chapter three the crystal formation (nucleation), growth and breakage in a pilot-scale wet FGD-plant is investigated. The influence of these processes, on the obtained particle size distribution (PSD), is evaluated based on experimental data and simulations.

The operating conditions and the gypsum quality obtained at full-scale wet FGD-plants are investigated in chapter four. Special attention is paid to the PSD and morphology of the crystals, due to these parameters influence on the gypsum dewatering properties.

Chapter five consists of an investigation of the occurrence of foaming within wet FGD-plants. The influence of particles, electrolytes and buffers on this operational problem will be investigated in laboratory scale.

Finally conclusions and suggestions for further work will be outlined in chapter six.

Chapter 2

Literature review

2.1 Introduction

In this chapter the literature concerning crystallisation and foaming is reviewed. The major part of this chapter concerns the crystallisation process in general, and the crystallisation of gypsum in particular, but a brief introduction to foaming is also given. The following chapters containing the experimental and published work from this project include more specific literature reviews, thereby expanding the theoretical framework provided by this chapter.

2.2 Crystallisation theory

Crystallisation can be encountered in nature and it can be used industrially as a separation and production technique. The process consists of the formation of new crystals from a supersaturated liquid phase (nucleation) and the subsequent growth of these crystals.

2.2.1 Driving force of crystallisation

The growth affinity (β_g), equation 2.01, is the dimensionless driving force of the crystallisation process. It is related to the molecular change in the chemical potential obtained by integration into the crystal lattice.[15] The degree of saturation, equation 2.02, is a property easier to evaluate based on the ionic concentrations in solution. An approximated degree of saturation, equation 2.03, is quite often being used in crystallisation studies.

$$\beta_g = \ln(S) = \frac{\Delta\mu}{R_u \cdot T} \qquad (2.01)$$

$$S_{CaSO_4 \cdot 2H_2O} = \frac{a_{Ca^{2+}} \cdot a_{SO_4^{2-}} \cdot a_{H_2O}^2}{\left(a_{Ca^{2+}} \cdot a_{SO_4^{2-}} \cdot a_{H_2O}^2\right)_{eq}} = \frac{\gamma_{Ca^{2+}} \cdot c_{Ca^{2+}} \cdot \gamma_{SO_4^{2-}} \cdot c_{SO_4^{2-}} \cdot \left(\gamma_{H_2O} \cdot c_{H_2O}\right)^2}{K_{so,CaSO_4 \cdot 2H_2O}} \quad (2.02)$$

$$S'_{CaSO_4 \cdot 2H_2O} = \frac{C_{CaSO_4 \cdot 2H_2O}}{(C_{CaSO_4 \cdot 2H_2O})_{eq}} \quad (2.03)$$

In order for crystallisation to proceed, the solution must be supersaturated (i.e. S > 1.0). At low degrees of supersaturation a meta-stable zone exist, where precipitation mainly takes place as crystal growth, while a burst of spontaneous nucleation causes the precipitation rate to increase at higher supersaturations.[15] The extent of the meta-stable zone will depend on the crystallising system as well as the operating conditions.

2.2.2 Nucleation and growth

Nucleation may take place as a direct consequence of supersaturation (homogenous nucleation), precipitation on foreign particles (heterogeneous nucleation) and mechanical attrition of crystals (secondary nucleation).[9,16] The nucleation rate in an industrial crystalliser will therefore depend on the saturation of the liquid phase, the properties of any particles present and the mechanical inputs (stirring, pumping etc.) to the system.

Homogenous nucleation can be described by an Arrhenius expression, such as equation 2.04.[17]

$$B^0 = k_{nu} \cdot \exp\left(\frac{-\Delta Gi}{R_U \cdot T}\right) \quad (2.04)$$

The size of the formed nuclei, will determine whether it is thermodynamically favourable to dissolve or grow, as illustrated qualitatively by Figure 2.1. The smallest nuclei size, at which a decrease in free energy is obtained by growth, is denoted the critical nuclei size. The free energy required to form a nuclei of critical size (ΔGi_{nu}) and thereby the nucleation rate is dependent on the supersaturation. Heterogeneous nucleation may also be described by

equations like equation 2.04, provided that a correction factor is included to account for the lower activation energy required to initiate nucleation.

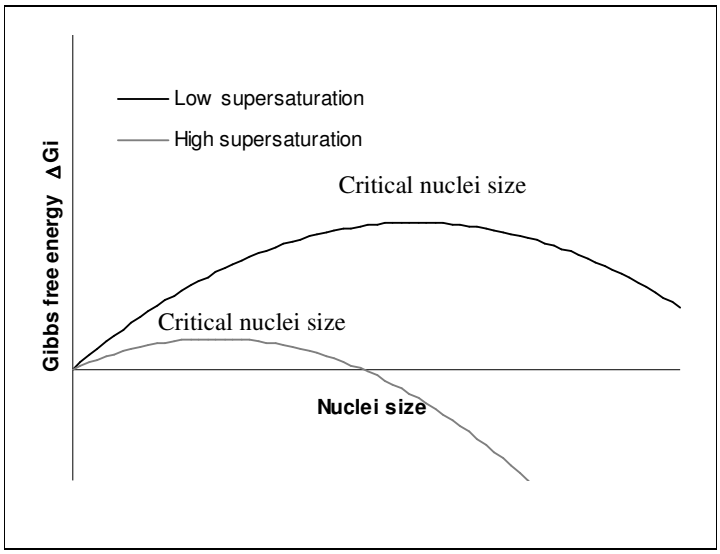

Figure 2.1: Gibbs free energy as a function of nuclei size and supersaturation.

The nucleation rate in industrial crystallisers is usually dominated by secondary nucleation, but some homogenous and heterogeneous nucleation may take place.[16] Empirical correlations, such as equation 2.05, are often used to describe the nucleation rate in such systems. In some cases the stirring rate (N_{st}) is incorporated into the rate constant.[9,16,17]

$$B^0 = k_{nu} \cdot N_{st}^{e_1} \cdot M_T^{e_2} \cdot G^{e_3} \qquad e_1 \in [2;4];\ e_2 \sim 1 \text{ and } e_3 \in [1;2.5]^{16} \qquad (2.05)$$

The stirring rate influences the frequency and force of the impeller – crystal collisions, while the crystal concentration (M_T) determines the likelihood of crystal – crystal collisions. The crystal growth rate (G) account for the extent of homogenous nucleation taking place and it is a function of the supersaturation of the solution (S-1) and thereby also the temperature.

The subsequent growth of the nuclei will influence the crystal morphology, the crystal size and the extent of impurity incorporation. Crystal growth consists of the transport of the solute to the crystal surface, desolvation, diffusion at the surface and the subsequent integration into the crystal lattice.[16,18] The overall crystal growth rate may consequently be influenced by the supersaturation, the agitation of the slurry and the growth mechanism. The relative

concentrations and characteristics of the lattice ions may furthermore influence the growth rate, due to differences in molecular size and degree of hydration.[19] The properties of the crystal surface, on the molecular level, will influence the mechanism by which the ions are integrated into the crystal lattice and thereby the surface growth rate. Depending on the roughness of the surface different kinds of binding sites may exist, as illustrated by Figure 2.2. The most favourable sites allow three neighbouring bonds to be formed (kink sites), the intermediate two bonds (step site) and the least favourable only a single bond (terrace or flat site).[15]

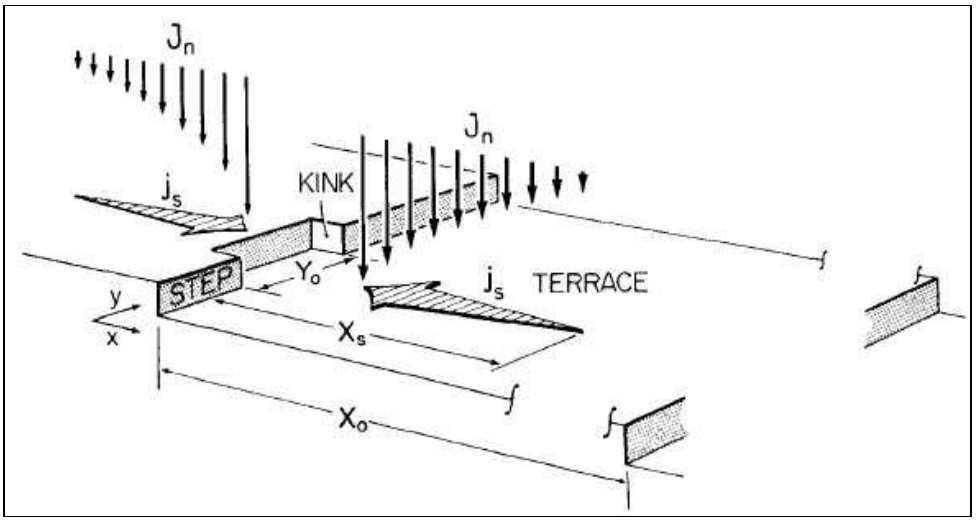

Figure 2.2: Crystal surface structure with diffusion towards kink and step growth sites.[20] Reprinted with permission of Elsevier Ltd.

The surface roughness, equation 2.06, affects the interaction between the crystal surface and the supersaturated solution and thereby the growth mechanism. The anisotropy factor, ξ, is connected to the bonding energies of the crystal surface layers.[15]

$$\alpha = \frac{\xi \cdot H}{k_b \cdot T} \qquad (2.06)$$

Molecular rough surfaces, offering multiple kink and step binding sites, are associated with α-factors below two to three.[15,16] The numerous binding sites allow an immediate integration of the solute molecules upon arrival at the crystal surface. The growth of such a surface is continuous, controlled by diffusion and proportional to the supersaturation. Crystals with α-

factors between three and five are associated with islands/plateaus spreading across flat surfaces. The growth is described as “birth and spread” or “polynuclear growth” and new islands form as a consequence of surface nucleation and spread due to the kink and step sites formed.[15] Crystals with α-factors above five are associated with smooth surfaces. The considerable energy barriers present discourage surface nucleation and the subsequent formation of favourable binding sites[15]. Crystal growth on such surfaces will mainly occur around lattice dislocations/defects, such as screw dislocations (i.e. spiral ramps on the crystal surface formed by the dislocation of atomic planes). The Burton-Cabrera-Frank (BCF) relationship, equation 2.07, derived for crystal growth from vapour, describes the crystal growth rate generated by screw dislocations.[15,21]

$$G = K_1 \cdot T \cdot (S-1) \cdot \ln(S) \cdot \tanh\left(\frac{K_2}{T \cdot \ln(S)}\right) \qquad (2.07)$$

K_1 and K_2 are system constants that depend on the spacing between dislocations. The crystal growth rate changes from a parabolic $(S-1)^2$ to a linear $(S-1)$ dependence as the supersaturation increases.

A simple power law growth rate expression, equation 2,08, can be used to describe experimental data for which no prior knowledge of the growth mechanism exists.[17] Diffusion-controlled growth will yield a linear supersaturation dependence, and so will the BCF relationship, equation 2.07, at high supersaturations.

$$G = k_g \cdot (S-1)^{e_4} \qquad (2.08)$$

2.2.3 Crystal morphology

The overall crystal growth rate is determined by the growth rates of the individual crystal faces. The area initially occupied by the fastest growing faces will diminish and disappear as the crystal grows and the slowest growing faces will therefore determine the final crystal habit. Factors that affect the growth rate include: the internal crystal structure, the supersaturation, the temperature and the incorporation of impurities. The faces of a crystal can be described by the Miller indices ($m_1m_2m_3$) based on their intercept of a crystallographic

axial system.[15] The Miller indices are inversely proportional with the axial intercepts, i.e. a plane parallel to the y-axis and z-axis may be denoted (100). When the topography of the crystal surface offers only few favourable binding sites, then an even small amount of a foreign species preferably adsorbed onto these "active" sites may have a significant effect on the rate of ion incorporation (crystal growth) and the resulting crystal morphology.[16] High supersaturations may furthermore enhance the differences in the growth rates of the crystal surfaces thereby facilitating a change in morphology. Apart from changes in morphology and crystal growth rate, the incorporation of foreign species into the crystal lattice may also influence the colour of the crystals.

2.2.4 Modelling crystallisers

The PSD in a crystalliser depends on operating conditions and crystallisation processes such as mixing, residence time, nucleation, breakage/attrition and crystal growth. Population balance techniques can be used to simulate the resulting PSD.[22] The general population balance for a well-mixed crystallisation vessel, in which particle growth, slurry flow and particle birth and death take place, is given by equation 2.09.

$$\frac{\partial(n(l))}{\partial t} + \frac{\partial(G \cdot n(l))}{\partial l} + \frac{n(l)}{\bar{t}} + n(l) \cdot \frac{d(\ln V)}{dt} = B(l) - D(l) \qquad (2.09)$$

Assuming that no breakage/agglomeration is taking place, the absence of crystals in the feed stream, a constant suspension volume and steady state, the continuous mixed-suspension mixed-product removal (MSMPR) model, equation 2.10, can be derived.

$$\frac{d(G \cdot n(l))}{dl} + \frac{n(l)}{\bar{t}} = 0 \qquad (2.10)$$

In the case of a size-independent growth rate, i.e. McCabe's Δl law,[22] integration yields equation 2.11.

$$n(l) = n(l_0) \cdot \exp\left(\frac{-l}{G \cdot \bar{t}}\right) = \left(\frac{B^0}{G}\right) \cdot \exp\left(\frac{-l}{G \cdot \bar{t}}\right) \qquad (2.11)$$

A semi logarithmic plot of the population density, ln($n(l)$), versus the characteristic particle size, l, will in this case yield a straight line, illustrated by Figure 2.3. This allows the easy extraction of the crystal growth rate (G) and the nucleation rate (B^0) for systems, which comply with the assumptions of the model.

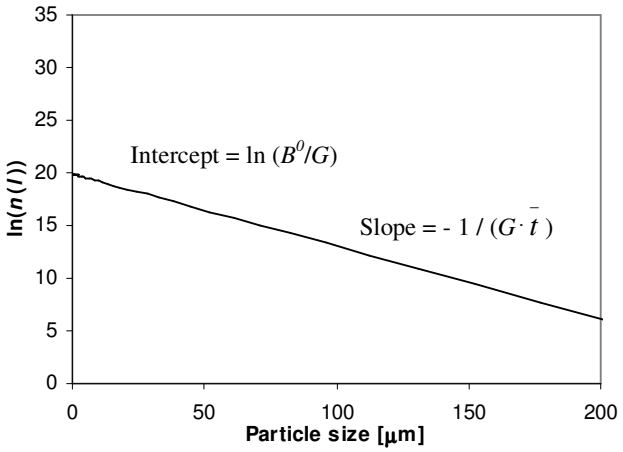

Figure 2.3: Semi-logarithmic plot of the MSMPR model as a function of the characteristic particle size (l).

Several crystallising systems have, however, been reported to display non-linearity through a considerable curvature, especially at the lower particle sizes.[23,24,25,26,27] Such non-linearity may arise due to any shortcomings of the assumptions of the MSMPR model. Examples include: growth rate dispersion, size-dependent growth, classification and crystal breakage. Such systems may be modelled by inserting size-dependent growth rate equations into equation 2.10, various semi-empirical equations have been suggested for this purpose.[25,28] Another approach, which can give a simple approximation of such systems, is the extraction of apparent values of B^0 and G from the linear part of the semi-logarithmic population density plot.[21]

2.3 Calcium sulphates

Calcium sulphate may exist as anhydrite ($CaSO_4$), hemihydrate/plaster of Paris ($CaSO_4 \cdot ½H_2O$) or dihydrate/gypsum ($CaSO_4 \cdot 2H_2O$). Gypsum is a commonly occurring mineral formed in nature by precipitation when lakes or oceans dry out. The different mineral forms of gypsum, i.e. selenite, alabaster and satin-spar, have traditionally been obtained from mining, but increasing amounts are being obtained as by-products of industrial processes, such as the wet FGD-process and phosphoric acid production.[8,29] The raw gypsum may dehydrate into hemihydrate or anhydrite by heating. Two different forms (α and β) of hemihydrate and three forms of anhydrite may be obtained depending on the heating profile and the partial pressure of water.[30,31] In pure water, as well as in seawater, gypsum is the thermodynamically stable form of calcium sulphate that precipitate below temperatures ~ 40 ^oC, whereas anhydrite is the thermodynamically stable form above this temperature.[32] Despite being meta-stable at all temperatures, hemihydrate is the form of calcium sulphate that usually precipitate above ~ 40 ^oC, due to the slow nucleation and growth of anhydrite. Precipitated gypsum can, however, persist for prolonged periods of time above 40 ^oC.[32]

When rehydrated hemihydrate changes into gypsum at ambient temperatures, a rigid and strong crystal lattice forms. This allows gypsum to be easily cast into various shapes through moulds. Historically gypsum and plaster of Paris have been used for mortar as well as sculptures in ancient Egypt and for decorations and stuccowork during the rococo and baroque style periods.[30] Today gypsum and plaster of Paris are still used for decorative purposes as well as for the production of wallboards and as a conditioning agent in cement.

2.3.1 Gypsum crystallisation

Due to its long history as a building material, the settling of gypsum plaster was the focus of research interest as early as 1768.[31] The dewatering properties of the gypsum crystals formed as a by-product of the wet FGD-process and during phosphoric acid production have been the focus of more recent research.

2.3.2 Gypsum crystal growth mechanism

Randolph & Etherton (1981)[9] studied the effect of supersaturation, pH, agitation, slurry density and additives on the gypsum crystallisation in simulated wet FGD-slurries. Seeded crystallisation experiments were performed in a 1 L bench-scale crystalliser and the MSMPR population balance model were used to extract the crystallisation kinetics. Equation 2.12 and 2.13 were fitted to correlate the experimentally obtained growth rate and nucleation rate.

$$G = \exp(13.11) \cdot \left(C_m - C_{m,eq}\right)^{2.226} \quad [\mu m\ min^{-1}] \tag{2.12}$$

$$B^0 = \exp(16.72) \cdot G^{1.48} \cdot M_T^{1.27} \quad [cm^{-3}\ min^{-1}] \tag{2.13}$$

Increased precipitation rates were observed at $S^{'} = 1.5$, which compared well with the data of Ottmars et. al. (1974).[33] Some of the increased precipitation in the study did, however, originate from an increased crystal growth rate and not from the shower of nucleation expected beyond the meta-stable zone. The influence of slurry pH-values ranging from three to eight was investigated by constant as well as transient pH-experiments. Decreasing pH values caused an increase in the nucleation rate, possibly due to an increased ionic activity of limiting chemical species. Agglomeration was furthermore observed during experiments with high nucleation rates. A 50 % increase in the stirring rate (to 450 RPM) yielded a 60 % increase in the nucleation rate. The effect of the stirring rate is included in the nucleation rate constant in this study, while it may appear as a separate term in other sources from the literature.[16]

Zhang and Nancollas (1991)[18] studied the effect of the calcium/sulphate molar ratio (Ca^{2+}/SO_4^{2-}) on the growth kinetics of gypsum. Seeded gypsum growth experiments were performed at constant solution composition, i.e. ionic strengths of 0.5 M potassium chloride (KCl) and 1 M sodium chloride (NaCl) at 25 ^oC. The crystal growth rate was found to depend on, not only the supersaturation, but also the relative concentrations and characteristics of the lattice ions. Decreasing Ca^{2+}/SO_4^{2-} molar ratios increased the crystal growth rate, indicating a surface-integration dependent growth mechanism, such as spiral growth. The presence of water in the crystal lattice might facilitate the integration of Ca^{2+}-ions, while rotational energy barriers make SO_4^{2-} the limiting species. The obtained crystal habit is described as elongated

due to a relative fast growth of the (111) crystal face compared to the (120) and (010) faces. A habit change towards tabular crystals was reported at the highest concentrations of sodium (Na^+) possibly due to a selective adsorption.

Christoffersen et. al. (1982)[34] performed seeded gypsum growth rate experiments at 25 ^oC at low degrees of saturation, S' = 1.03-1.15. Constant as well as transient electrical conductance experiments were performed. The measured crystal growth rates only constituted less than 5 % of the growth rate expected in the case of transport/diffusion limited growth, indicating a surface-integration controlled growth mechanism. A combination of surface-integration effects such as individual and cooperating spiral growth and outgrowth of concave crystals parts was suggested to explain the experimentally observed growth rates. An initial vigorous shaking of the crystals furthermore caused an increased growth rate.

Liu and Nancollas (1970)[35] performed seeded growth rate experiments with gypsum crystals in the temperature range 15-45 ^oC at transient solution compositions. A two-fold increase in the stirring rate, as well as the use of vibratory stirring, did not change the rate of crystal growth, indicating surface-integration controlled growth. The changes in surface area during growth did not influence the growth rate, which is consistent with the concept of growth at the active sites (screw dislocations) initially present on the surface of the seed crystals. Low crystal concentrations (36 mg/100 ml) and high ionic concentrations (0.053 M Ca^{2+}) caused surface nucleation facilitating surface roughening and an increased number of active sites. The obtained molar growth rates were described by equation 2.14 showing a linear dependence on the number of growth sites (N_{gr}) and a parabolic dependence on the concentration difference.

$$-\frac{d[C_{CaSO_4}]}{dt} = k_p \cdot N_{gr} \cdot (C_{Ca^{2+}} - C_{Ca^{2+},eq})^2 \qquad (2.14)$$

A decrease of the Ca^{2+}/SO_4^{2-} molar ratio, from 1.0 to 0.5, caused an increase in the growth rate constant, once again indicating that the crystal growth was limited by the integration of the SO_4^{2-}-ions into the crystal lattice.

Abdel-Aal et. al. (2004)[36] studied the influence of the supersaturation and the Ca^{2+}/SO_4^{2-} molar ratio on the size, shape and filtration rate of gypsum crystals formed during phosphoric acid production at 80 °C in a 1 L bench-scale crystalliser. Increasing SO_4^{2-}-concentrations, $C_{m,SO_4^{2-}} \in [1.5;\ 5.5\ \text{wt.}\%]$, facilitated the production of larger crystals, indicating that the diffusion and integration of SO_4^{2-}-ions were the growth-limiting step. The crystals formed at intermediate and high saturations ($S^{'}$ = 1.502 and 1.979) were needle-like, with a pronounced agglomeration taking place at the highest supersaturations.

The gypsum crystallisation taking place in wet FGD-plants may be influenced by several of the findings mentioned above. Crystallisation within the meta-stable zone is expected in the holding tank of a wet FGD-plant, because of the considerable crystal surface area available for precipitation. Bursts of nucleation facilitated by high supersaturations or low pH values may, however, be envisioned in the absorber and in the case of poor mixing in the holding tank. The mechanical inputs (stirring and pumping) in a wet FGD-plant are expected to provide a significant contribution to the overall nucleation rate. The surface-integration controlled gypsum growth rate makes the supersaturation an important parameter in terms of obtaining the maximal crystal growth rate.

2.3.3 Gypsum crystal morphology and the effect of impurities

Several studies concerning the influence of impurities on the calcium sulphates formed during phosphoric acid production have been reported in the literature.[37,38,39,40,41,42,43] The impurities originate from the phosphate ores, which are digested by sulphuric acid at elevated temperatures (70-80 °C).[37] Gypsum crystals have in the absence of impurities been reported to exhibit thick plate or rod-like shapes at low growth rates, while higher growth rates will yield longer and thinner shapes such as needle-like crystals.[19] In the case of the commercial cake filtration of gypsum from phosphoric acid production, acceptable filtration characteristics are obtained with a porous filter cake and not too small particles, which may block the filter cloth.[36] Equant crystals of a uniform size can produce such a filter cake, while plate-like crystals will yield a highly impervious filter cake.[40]

Kruger at. al. (2001)[37] studied the effect of ionic contaminants (Na^+, K^+, Mg^{2+}, Al^{3+}, F^- and Fe^{3+}) on the gypsum crystallisation during phosphoric acid production. The gypsum crystals produced by this process is reported to be either flat or needle-like. A cationic concentration of 0.1 wt.% was reported to yield an increased rate of precipitation and the maximal filtration rate through a filter cloth. The ferric ions (Fe^{3+}) were retained in the acid after filtration and did not alter the needle-like crystal morphology, but a non-uniform bimodal particle size developed with increasing concentration. The fluoride (F^-)-ions were removed from the acid during precipitation and the aluminium ions were portioned between the acid and the gypsum. An increasing aluminium (Al^{3+})-concentration was reported to yield decreasing filtration rates while increasing Al^{3+}/F^- ratios caused increasing particle sizes and decreasing aspect ratios.

Gilbert (1966)[38] studied gypsum crystallisation during laboratory-scale phosphoric acid production at 70 ^oC. Needle-like crystals forming stars from a central nucleolus were observed at high SO_4^{2-}-concentrations, rhomb-shaped crystals with length to width ratios of two to three were observed at intermediate SO_4^{2-}-concentrations and small thin plates were formed at low SO_4^{2-}-concentrations. Experiments with the acid from a full-scale phosphoric acid plant yielded rhomb-shaped crystals. Removal or inactivation of the organic material in the phosphoric acid, by active carbon treatment or calcinations at 1500 ^oC, yielded elongated needle-like crystals, indicating the presence of organic crystal habit modifiers. The addition of aluminium oxide (Al_2O_3), $C_{m,Al_2O_3} \in [1.4;\ 1.7\ \text{wt.}\%]$, yielded smaller and less elongated crystals, possibly due to aluminium adsorption at previously fast growing surfaces.

Martynowicz at. al. (1996a and 1996b)[39,40] studied the effect of aluminium fluoride (AlF_3) on the crystallisation of calcium sulphates during bench-scale wet phosphoric acid production at 75 and 90 ^oC. The presence of 95 mmol AlF_3 (kg solution)$^{-1}$ caused precipitation of gypsum at operating conditions where hemihydrate usually precipitated. This effect may be the consequence of growth retardation of the hemihydrate and gypsum, caused by aluminium fluoride complexes (AlF^{2+} to AlF_6^{3}), thereby creating a decreased precipitation rate and a corresponding increased supersaturation. The pronounced extent of crystal agglomeration observed furthermore supports this explanation. If the supersaturation exceeds the solubility product of gypsum, this hydrate may now be the one formed due to favourable kinetics as predicted by Ostwald's rule of stages.[40] The gypsum morphology observed in the presence of

aluminium fluoride were plate-like, due to substitution of SO_4^{2-}-ions by AlF_5^{2-} at the $(\bar{1}11)$ and (011) crystal faces causing growth retardation, as illustrated by Figure 2.4.

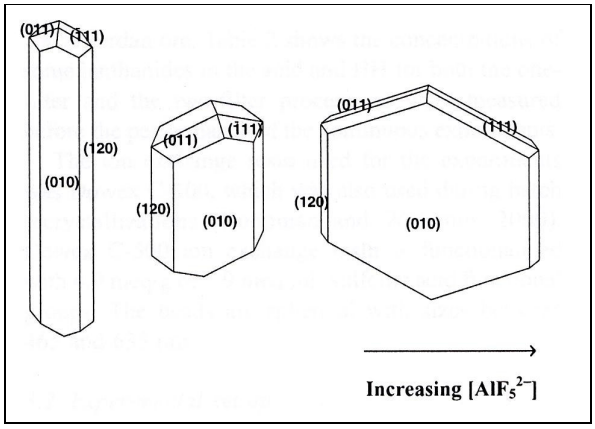

Figure 2.4: Changes in morphology as a function of AlF_5^{2-}-concentration.[41, 42]
Reproduced with the permission of Delft University of Technology and Elsevier.

Rashad et. Al. (2004)[43] studied the effect of ionic contaminants (Al^{3+} and Mg^{2+}) on the gypsum crystallisation during laboratory-scale phosphoric acid production at S' = [1.088;1.979] and 80 ^oC. The gypsum morphology changed from needle-like to thick rhombic in the presence of Al^{3+}-ions. The nucleation rate decreased 19 % compared to the baseline in the presence of 1 wt. % Al_2O_3 and increased 4 % in the presence of 1 wt. % magnesium oxide (MgO). The fraction of particles below 20 μm decreased at aluminium concentrations ≤ 2 wt. %, suggesting a decreased nucleation rate and possibly an increased crystal growth rate.

The ionic impurities present in phosphate rock are also expected to enter wet FGD-plants through the impurities in the used mineral limestone, the capture of fly ash from coal combustion and plant corrosion. A similar influence on the crystal nucleation rate, growth rate and morphology are expected, despite differences in the operating conditions of the two processes (i.e. temperature and pH).

2.4 Foaming theory

Foaming and flotation are used at industrial scale to clean vegetables and to harvest minerals from ground ore.[44] The unexpected occurrence of foaming in other industrial processes may, however, cause considerable problems, such as overflow from the reactor to the surroundings/subsequent piping. In essence foaming is the accumulation of bubbles at the liquid surface, due to either an increased arrival rate of bubbles or an increased bubble persistence (lifetime). The rate of bubble generation in a system is influenced by the extent of air injection, stirring and pumping that is being performed. The persistence of the bubble layer will be determined by the drainage rate of the liquid film, separating the individual bubbles, and the frequency of bubble rupture. The structure of the liquid film separating the individual bubbles in the foam layer is illustrated by Figure 2.5.

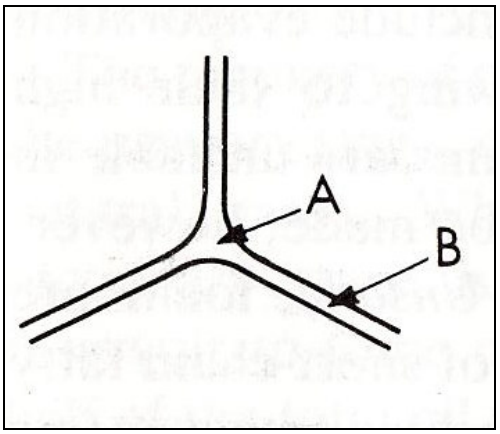

Figure 2.5: Plateau border at the intersection of three bubbles; the curvature at point "A" causes a lower pressure of the liquid than that at point "B", thereby inducing capillary flow toward the Plateau border.[45] Reprinted with the permission of Elsevier.

Foaming agents that provide increased bubble persistence include surfactants, macromolecules (such as polymers or proteins), or finely dispersed solids.[46]

Surfactants and macromolecules preferably arrange themselves at the liquid/gas interface, thereby providing several foam generating/stabilising mechanisms. The decreased surface tension created by the arrival of surfactants/macromolecules at the surface, reduces the additional energy required to generate the increased surface area present in foams. Secondly an increased lamella elasticity/resistance towards local film thinning will be provided by the

Marangoni effect, i.e. the restoring liquid flow induced by a decreased surfactant concentration at any thinned region (increased surface area). A decreased drainage rate, due to an increased viscosity, and a repulsive force generated by sterical/electrostatic double-layer interaction as two surfaces approach, will furthermore improve bubble persistence.[44,47]

Particles may also adhere at the gas/liquid interface if they possess a certain extent of hydrophobicity, such foaming systems are called froths. The adhesion process can be aided by electrolytes present in solution, through interactions with the particle surface and a reduction of the electrostatic repulsion between the particles and the air bubbles (a thinner electrostatic double layer).[47,48] The thickness of the electrostatic double layer (κ^{-1}), as expressed by equation 2.15, depends on the type, charge, and concentration of the electrolyte.

$$\kappa^{-1} = \sqrt{\frac{\varepsilon_0 \cdot \varepsilon_r \cdot k_b \cdot T}{N_a \cdot q^2 \cdot \sum_j C_{j,b} \cdot z_j^2}} \qquad (2.15)$$

The particles adhered at the gas/liquid interface may stabilise the bubbles by a decreased drainage rate of the lamella and an increased strength of the froth. The stabilising effect will depend on the size, shape, and hydrophobicity/wettability of the particles.[47,48]

Physical as well as chemical approaches can be used to break unwanted foam and prevent further foaming from taking place.[49,50] The foam may be broken mechanically by stirring, ultrasonics etc. Chemical defoaming additives include hydrophobic particles, oils and particle/oil mixtures. Oils can spread across the bubble surfaces, causing a reduction in film thickness and an increased likelihood of film rupture. Oil droplets may furthermore act as hydrophobic bridges through the lamella causing bubble collapse. Hydrophobic particles with a contact angle larger than 90° , such as coal dust, sulphur, quartz or Teflon, may act as air bridges through the lamella thereby destabilizing the froth. The particles may furthermore facilitate an increased spreading and penetration depth of oil-based defoamers.

The wet FGD-process may contain all three kinds of foaming agents (i.e. surfactants, macromolecules and fine solids). Buffers added to the slurry to enhance the absorption efficiency may also act as surfactants, biological activity may yield macromolecules (i.e. proteins) and limestone, gypsum and fly ash particles will be present in the slurry. Potential defoamers include oils and hydrophobic particles, but these compounds may also have unwanted side effects, such as an enhanced biological activity in the case of oils and a discolouring of the gypsum in the case of hydrophobic particles.

2.5 Conclusions

In this chapter part of the existing literature on crystallisation and foaming has been reviewed. The PSD obtained in a crystalliser, such as a wet FGD scrubber, will depend on the crystallisation process (i.e. nucleation and crystal growth) as well as breakage, mixing and classification. The literature indicates that gypsum crystal growth is located around defects on the crystal surfaces, with the integration of SO_4^{2-} into the crystal lattice being the limiting step. A molecular flat crystal surface with few favourable growth sites is associated with this growth mechanism. The breakage/attrition rate will depend on the frequency and the power of the impeller-crystal and crystal-crystal collisions taking place. The crystal purity and morphology obtained in a crystalliser depend on the growth rate of the different crystal as well as the incorporation of impurities into the crystal lattice. Studies concerning gypsum crystallisation during phosphoric acid production, have shown that the mineral impurities present in the phosphate rock can have a significant effect on the obtained gypsum morphology. These mineral impurities may also be encountered in a wet FGD-plant, due to the use of mineral limestone and the capture of fly ash from coal combustion.

Foaming may arise when the bubbles in a liquid phase, created by air injection or stirring, possess an increased persistence and thereby a prolonged lifetime. Agents, which may facilitate foaming, include surfactants, macromolecules (such as polymers or proteins), or finely dispersed solids. Defoamers such as oils or hydrophobic particles can be used to counter unwanted foaming.

Chapter 3

Quantification of Gypsum Crystallisation in a Wet FGD Pilot Plant

This chapter contains an investigation of the nucleation rate, the crystal growth rate and particle breakage in a wet FGD pilot plant, and the influence of these processes on the gypsum PSD. The results have been collected in the article "Quantification of gypsum crystal nucleation, growth and breakage rates in a wet flue gas desulphurisation pilot plant", which has been accepted for publication in the AICHE journal. This article was written by Brian Brun Hansen, Søren Kiil and Jan Erik Johnsson (The Department of Chemical and Biochemical Engineering, Technical University of Denmark). The article is presented in the same form as it was submitted, with only minor layout changes and a slight editing to avoid repetitions.

Abstract

The aim of this work is to study the influence of nucleation, growth and breakage on the PSD of gypsum crystals produced by the wet FGD process. The steady state PSD, obtained in a falling film wet FGD pilot plant during desulphurisation of a 1000 ppm(v) SO_2 gas stream, displayed a strong non-linear behaviour (in a ln(n(l)) vs. l plot) at the lower end of the particle size range, compared to the well-known linear MSMPR model. A transient population balance breakage model, fitted to experimental data, was able to model an increase in the fraction of small particles, but not to the extent observed experimentally. A three-parameter, size-dependent growth model, previously used for sodium sulphate decahydrate and potash alum, was able to describe the experimental data, indicating either size-dependent integration kinetics or growth rate dispersion.

3.1 Introduction

The majority of the installed FGD capacity consists of the wet scrubber FGD technology,[4] in which the flue gas is brought into contact with a $Ca(OH)_2$ solution or a limestone slurry. Additional air is often supplied to the slurry, called forced oxidation mode, ensuring an almost complete conversion of the reactant and the absorbed SO_2 to $CaSO_4 \cdot 2H_2O$. Equation 3.01 provides the overall reaction of the forced oxidation process.

$$CaCO_3(s) + SO_2(g) + 2H_2O(l) + ½O_2(g) \Leftrightarrow CaSO_4 \cdot 2H_2O(s) + CO_2(g) \qquad (3.01)$$

Most European power plants use this gypsum producing process because of the gypsum sales potential for either wallboard or cement production. The sales potential will be influenced by material properties such as the PSD, the impurity content, and the moisture content. These properties will in turn be determined by the crystallisation process,[21] which may include: Nucleation, crystal growth (diffusion to and integration of ions into the crystal lattice), crystal agglomeration, crystal breakage and size-dependent dissolution (Ostwald ripening).

The gypsum produced is withdrawn, washed and dewatered by e.g. hydrocyclones, centrifuges or belt filters, until a commercial product is obtained. Poor dewatering properties may be the result of an increased fraction of small particles (nucleation/breakage) or a change of morphology. Breakage of crystals may take place due to collisions with the reactor walls, the impellor or other particles and fragments ranging in size from nuclei to the size of the parent particle may be formed. Within industrial crystallisers breakage are considered the primary source of nucleation.[23] Previous bench-scale investigations of gypsum crystallisation kinetics, at wet FGD conditions, have used McCabe analysis to extract apparent growth and nucleation rates, which have subsequently been fitted to empirical kinetic expressions.[9] This article will expand the present knowledge concerning gypsum crystallisation in wet FGD plants, by quantifying the rates of nucleation, crystal growth and crystal breakage taking place in a wet FGD pilot plant and by studying the influence of these processes on the obtained PSD.

3.2. Strategy of investigation

This investigation of the nucleation, crystal growth and breakage in the wet FGD process was performed in a pilot-scale plant. The pilot-scale plant enables a high degree of control of the experimental conditions such as crystal residence time and crystal concentration. The crystal concentrations encountered in industrial plants are usually in the range 10 to 25 wt %, balancing concerns about bursts of nucleation/scaling and sedimentation/breakage. Depending on the choice of crystal concentration, plant design, and the sulphur content of the fuel the crystal residence time may vary from 20 hrs to more than 100 hrs. The 144.2 g L_{slurry}^{-1} (13.3 wt %) gypsum slurry obtained by desulphurisation of a 1000 ppm(v) SO_2 gas stream was used to evaluate the crystallisation process at a mean slurry residence time ($\bar{t}$) of 28.13 hrs. This slurry was furthermore used as starting material in two breakage experiments performed at conditions of industrial relevance (Table 3.1) and in the absence of flue gas desulphurisation, eliminating the effect of crystal growth. Due to sedimentation no experiments above 144 g/L were completed. A three-parameter population balance breakage model was used to describe the experimentally observed changes in PSD as a function of time. The steady state PSD in the pilot plant during desulphurisation operation was evaluated based on the breakage model obtained, and estimated values of nucleation rate (B^0) and growth rate (G). Finally, considerations regarding the importance of the different crystallisation mechanisms (breakage, size-dependent growth and growth rate dispersion) in the pilot plant as well as conditions at industrial scale were made.

Table 3.1: Experimental conditions

Experiment	Crystal concentration	Last sampling
Experiment 1	144.2 g L_{slurry}^{-1} (13.3 wt %)	336 hrs
Experiment 2	75.0 g L_{slurry}^{-1} (7.2 wt %)	600 hrs

3.3 Model formulation and solution

The PSD within a crystalliser depends on operating conditions and crystallisation processes such as mixing, residence time, nucleation rate, breakage and crystal growth rate. Population balance techniques can be used to simulate the PSD resulting from these conditions.[22] The general population balance for a well-mixed crystallization vessel, in which particle growth, slurry flow and particle birth and death takes place, is given by equation 3.02.

$$\frac{\partial(n(l))}{\partial t}+\frac{\partial(G\cdot n(l))}{\partial l}+\frac{n(l)}{\bar{t}}+n(l)\cdot\frac{d(l\ln V)}{dt}=B(l)-D(l) \qquad (3.02)$$

The gypsum crystallisation taking place in a wet FGD plant has been evaluated by the following approaches:

- McCabe analysis (G and B^0) of steady-sate pilot plant PSD and solid concentration.
- Least squares fitting of breakage kernel parameters based on breakage experiment PSD.
- Simulation of steady state PSD
  (Previously estimated G, B^o and breakage kernel parameters).
- Least squares fitting of size-dependent growth rate parameters based on steady state PSD and solid concentration.

3.3.1 McCabe analysis

The well-known MSMPR model, equation 3.03, allows the easy extraction of the growth rate and the nucleation rate from the linear semi-logarithmic plot of the population density, $n(l)$, versus the characteristic particle size, l.

$$n(l)=n(l_0)\cdot\exp\left(\frac{-l}{G\cdot\bar{t}}\right)=\left(\frac{B^0}{G}\right)\cdot\exp\left(\frac{-l}{G\cdot\bar{t}}\right) \qquad (3.03)$$

$$\Rightarrow \ln(n(l))=\ln\left(\frac{B^0}{G}\right)+\left(\frac{-l}{G\cdot\bar{t}}\right)$$

Several crystallising systems have, however, been reported to display non-linearity through a considerable curvature, especially at the lower particle sizes.[23,24,25,26,27] Such non-linearity may arise because of shortcomings of any of the assumptions of the MSMPR model: steady state, a constant well-mixed suspension volume, the absence of crystals in the feed stream, no breakage/agglomeration and a size-independent growth rate, i.e. McCabe's Δl law.[22]

3.3.2 Breakage modelling

The population balance on a particle volume basis, $n_v(v)$, is used when processes that change the number of particles is of interest (i.e. particle agglomeration or breakage).[22] Equation 3.04 describes a well-mixed crystallization vessel in which only particle birth and death is taking place.

$$\frac{\partial n_v(v)}{\partial t} = B(v) - D(v) = \left(\int_v^{v_{\max}} \beta(v,w) \cdot N_b(w) \cdot D(w) \cdot dw \right) - D(v) \qquad (3.04)$$

The birth term consists of the breakage kernel (β), describing the probability of formation of a fragment of volume "v" from the parent particle volume "w", the number of new particles formed per parent particle ($N_b(w)$) and the death term of the parent particle ($D(w)$). The breakage kernel may take the form of various mathematical functions[51,52] as well as the very simple two pieces of equal size function used in the literature[21,22] to model breakage processes. In the present study the cumulative Weibull distribution function, equation 3.05, has been used as breakage kernel.

$$F_v(l) = 1 - e^{-(l/\lambda)^{k_{we}}} \quad \rightarrow \quad \beta(l_v, l_w) = \frac{\left. \partial F_v(l) \middle/ \partial l \right|_{l_v}}{F_v(l_w)} = \frac{\left. \partial F_v(l) \middle/ \partial l \right|_{l_v}}{0.999} \qquad (3.05)$$

Where the parameter k_{we} and λ describes the shape and width of the distribution, respectively. The pieces formed are distributed between the size of the parent particle (l_w), chosen as the 99.9 % quantile, and down towards the size of nuclei. A major advantage of the Weibull distribution function is its ability to approximate other distribution functions, such as the exponential distribution function when k_{we} is equal to 1. The integral form of the Weibull

distribution is the well-known Rosin-Rammler distribution used to describe the cumulative particle size distribution resulting from crushing and milling of materials.[53]

Power law functions are often used in the literature to describe the death term.[21,22] The power law function used in this study, equation 3.06, includes an additional empirical exponent (e_5) to account for the strong particle number and volume dependence observed in the experimental data.

$$D(v) = k_d \cdot v^{e_5} \cdot n_v(v)^{e_5} \tag{3.06}$$

To facilitate the solution of equation 3.04, the population balance model is discretized into a range of intervals each of which is represented by a characteristic grid point "*x*". The discretization used in this study is based on the 64 particle size intervals used in the PSD analysis. The lower boundary of the first interval is, however, changed to 0 μm to preserve the mass of the system. The population model is solved by the "SIRUKE" FORTRAN integration routine,[54] based on the initial population density and a given set of kinetic parameters (k_d, e_5, k_{we} and λ). The width of the Weibull distribution (λ) will not influence the simulation, because the pieces formed will always be distributed between the size of the parent particle (l_w) and down towards the size of nuclei. The remaining kinetic parameters (k_d, e_5, k_{we}) are determined based on a stepwise iteration aiming at a minimization of the sum of least squares of the PSD after 336 hrs of breakage. A 64-interval discretization was sufficient to obtain convergence.

3.3.3 Pilot plant PSD – Nucleation, growth and breakage

The maximal accumulation of fragments at small particle sizes, and thereby the most pronounced impact of breakage, will take place when the fragments only have a limited growth rate. In this work the growth rate of the breakage fragments will therefore be considered negligible compared to the growth rate of crystals formed by nucleation. The formation of slow growing breakage fragments has been proposed previously in the literature[24,25] and has been demonstrated in the case of pentaerythritol[23] and ammonium sulphate[55] crystallisation. The assumption of a negligible fragment growth rate furthermore enables a separation of the particle growth and breakage calculations.

The simulation procedure treats one interval at the time and consists of a calculation of the number of crystals entering the interval through growth, equation 3.07, and the particle number being redistributed through breakage, equations 3.04, 3.06 and 3.08. The previously estimated kinetic parameters (G, B^0, k_d, e_5 and k_{we}) alongside a 64-interval discretization have been used for this simulation. The extent of breakage depends on the time the crystals spend in a given interval (t_j). The birth terms require the knowledge of all death terms, and will consequently be calculated as the last part of the simulation. The 64-interval discretization is sufficient to obtain convergence of the solution, as it also was seen for the breakage-only simulation.

$$\rightarrow \ln\left(n(l_j)_{MSMPR}\right) = \ln\left(n(l_{j-1})\right) - \frac{\left(l_j - l_{j-1}\right)}{G \cdot \bar{t}} \qquad with\ \mathrm{n}\left(l_0\right) = \frac{B^0}{G} \tag{3.07}$$

$$n_v\left(v_j\right) = n_v\left(v_j\right)_{MSMPR} + \left(B\left(v_j\right) - D\left(v_j\right)\right) \cdot t_j \qquad t_j = \frac{\Delta l_j}{G} \tag{3.08}$$

3.3.4 Size-dependent growth rate

A semi-empirical size-dependent growth rate model, equation 3.09, has been obtained from the literature[28] yielding the steady state MSMPR population density distribution given by equation 3.10.

$$G(l) = G_m\left(1 - \exp\left(-a_1\left(l + a_2\right)\right)\right) \tag{3.09}$$

$$n(l) = n(l_0) \cdot \exp(a_1 \cdot l) \cdot \left(\frac{\exp\left(a_1\left(l + a_2\right)\right) - 1}{\exp\left(a_1 \cdot a_2\right) - 1}\right)^{\frac{-1 - a_1 \cdot \bar{t} \cdot G_m}{a_1 \cdot \bar{t} \cdot G_m}} \tag{3.10}$$

This three-parameter, size-dependent growth model has previously been used to describe sodium sulphate decahydrate and potash alum crystallisation.[28] The empirical model parameters affect the size dependence of the growth rate (a_1) and the growth rate at small crystal sizes (a_2). Input to the simulation procedure is the mean residence time ($\bar{t}$), the population density of nuclei ($n(l_0)$), the maximum growth rate (G_m) and estimates of a_1 and a_2. The empirical parameters of the kinetic model (a_1 and a_2) have been estimated by a stepwise

sum of least squares fitting of the PSD and the crystal concentration respectively. The 64-interval discretization is sufficient to obtain convergence of the solution, as it also was seen for the breakage-only and the pilot plant PSD simulations.

3.4. Experimental Setup and Procedure

3.4.1 Description of setup

The wet FGD pilot plant simulates a single vertical channel of the packing zone in a co-current full-scale wet FGD grid absorber. The basic outline of the pilot plant is illustrated in Figure 3.1. A 110 kW natural gas boiler generates a feed flue gas to which pure SO_2 is subsequently added. The flue gas is brought into contact with limestone slurry in the absorber, a 7 m PVC pipe (D_i = 3.3 cm) with multiple sampling sites. The slurry leaving the absorber is collected in a holding tank, D_i = 0.4 m, where air injection and reactant addition take place. The pH of the holding tank is kept constant at 5.4 by an on/off control of the feed stream. A timer-controlled pump removes the slurry that exceeds a given level, ensuring a constant slurry level in the tank. From the holding tank the slurry is recycled to the absorber ensuring a liquid/gas ratio of 13.5-14.0 L m^{-3} (STP). Due to the intensive stirring of the holding tank, and because the residence time in the falling film absorber constitutes less than 10 % of the residence time in the holding tank, the pilot plant is considered well-mixed. Further details concerning the pilot plant can be seen in a previous publication[56], but it should be noted that the absorber length has been increased from 5 to 7 m, since that publication, to obtain higher desulphurisation degrees.

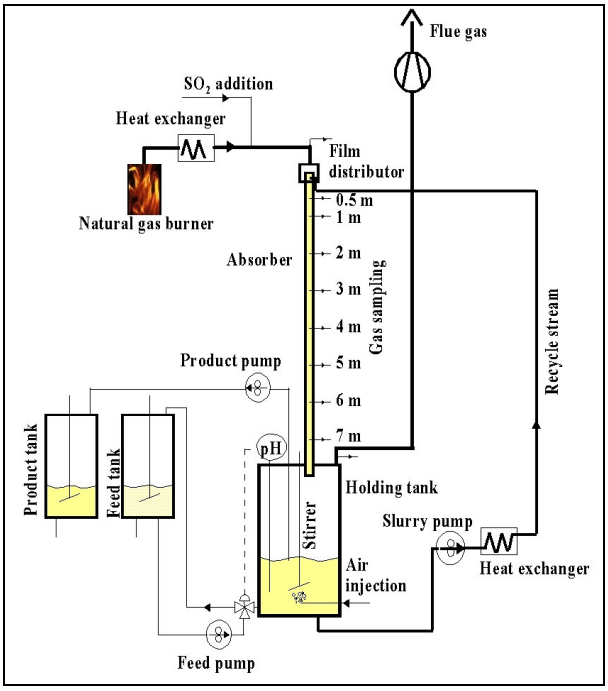

Figure 3.1: Principal diagram of the wet FGD pilot plant.

3.4.2 Experimental procedure

The gypsum slurries used in the breakage experiments have been generated by desulphurisation of a 1000 ppm(v) flue gas stream using a feed stream containing 7.1 wt % Faxe Bryozo limestone and 2.2 wt % (25 g L^{-1}) Cl^-. Calcium chloride ($CaCl_2 \cdot 2H_2O$) is used to simulate the presence of Ca^{2+} and Cl^- ions in full-scale wet FGD plants. The Cl^- ions originate from gaseous HCl absorbed in the slurry.[57] When the steady state gypsum concentration is obtained, the flue gas flow is turned off and the initial PSD measured. The slurry is now subjected to the continued mechanical inputs from stirring, pumping (recirculation) and air injection. The initial PSD as well as the development over time is measured by laser diffraction with a Malvern Mastersizer S long bed. Two individual PSD analyses were performed on each slurry sample, each representing the average of 6 measurements. The measurements performed yield the cumulative volume fraction of 64 particle size intervals ranging from 0.05 to 878.67 μm. Experiments have been performed at crystal concentrations of 144.2 and 75.0 g L_{slurry}^{-1} at a constant suspension volume, in the absence of input/output streams, for 336 hrs and 600 hrs respectively. No particle growth is expected to occur, as no further SO_2 addition takes place after the breakage experiments have been initiated. Selected

process parameters of the breakage experiments can be seen in Table 3.1 and 3.2. The PSD measurement and the crystal concentration can be used to calculate the population densities, equation 3.11 and 3.12.

$$n(l_j) = \frac{M_T \cdot \left(F_v(l_j) - F_v(l_{j-1})\right) / \left(\rho_s \cdot \bar{v}_j\right)}{\Delta l_j} \tag{3.11}$$

$$n_v(v) = n(l) \cdot \frac{dl}{dv} = n(l) \cdot \frac{1}{A_{sur}} \tag{3.12}$$

Table 3.2: Selected process parameters.

Parameter	
Slurry volume in holding tank, absorber and recycle stream.	30 L
Recycle stream from holding tank to absorber	0.078 L s^{-1}
Air injection to holding tank	0.233-0.267 L (STP) s^{-1}
Stirring rate in holding tank	310 RPM

An overview of the changes in PSD as a function of time can be obtained by monitoring the development of a suitable mean diameter. Due to the importance of the dewatering properties of the gypsum the Sauter Mean Diameter (SMD) is chosen as the mean diameter of interest. The SMD describes the diameter of a sphere with the same surface area to volume ratio as the particle investigated and is reported to be the appropriate average particle size in the case of fluid flow through porous media, such as the solid liquid separation in dewatering processes.[58]

3.5 Results and discussion

3.5.1 McCabe analysis

The steady state PSD in the pilot plant is evaluated based on experimental data obtained after 143 hrs of desulphurisation of a 1000 ppm(v) SO_2 flue gas stream at a liquid to gas ratio of 13.8 L Nm^{-3}. The mean slurry residence time ($\bar{t}$) was 28.13 hrs corresponding to operation for 5.1 residence times. A simple mass balance of a well-mixed vessel shows that 5.1 residence times corresponds to 99.3 % of the steady state crystal concentration. Figure 3.2 shows the population density obtained by the use of equation 3.11, assuming spherical particles.

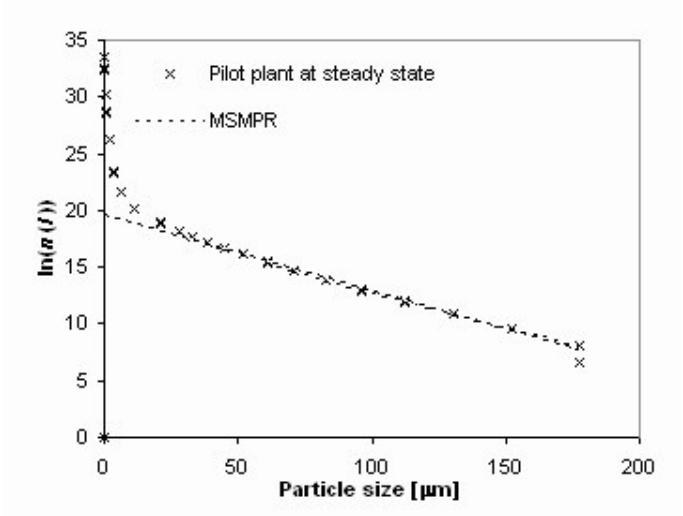

Figure 3.2: Semi logarithmic plot of population density (Experimental and MSMPR-model) versus particle size. Steady state measurements have been performed on the slurry formed by desulphurisation of a 1000 ppm(v) gas stream.

A considerable curvature, compared to the MSMPR model, is observed below particle sizes of 25 µm, as it has also been reported for other crystallising systems.[23,24,25,26,27] As previously mentioned crystal breakage is one of the potential explanations of this phenomenon. Above a particle size of 25 µm the PSD data points show a linear behaviour and apparent growth and nucleation rates can be extracted by McCabe analysis. The mean growth and nucleation rates are presented below alongside the corresponding analytical standard deviations. Because of the population density deviation at the small particle sizes the mass concentration calculated for the MSMPR system will be lower than the experimental measurements. The nucleation rate in a MSMPR system required to obtain the measured crystal concentration of 144.2 g L_{slurry}^{-1} is shown in parenthesis and will be used in the simulations.

- $G = 1.44\ 10^{-4} \pm 0.06 \cdot 10^{-4}$ µm s^{-1}
- $B^0 = 5.44\ 10^4 \pm 0.44 \cdot 10^4$ no. L_{slurry}^{-1} s^{-1} ($6.25\ 10^4$ no. L_{slurry}^{-1} s^{-1})

3.5.2 Breakage modelling

In the breakage experiments performed the changes in PSD of the gypsum slurry has been monitored as a function of the time it has been exposed to the continued mechanical inputs from stirring, pumping (recirculation) and air injection. The changes observed can be used to describe the extent as well as the type of breakage taking place in the pilot plant.

Figure 3.3 shows the volumetric PSD frequency plotted as a continuous curve with a logarithmic scale on the x-axis at three selected times during experiment 1. The frequency curve describes the change in cumulative volume fraction ($F_v(l)$) as a function of the change in logarithmic particle size. This representation is well suited for showing PSDs covering wide size ranges.[59] The changes in the PSD frequency curves show a decrease in the volume fraction of particles above approximately 25 µm and a corresponding increase in the volume fraction of particles below this particle size. This corresponds well with the fact that an increased fraction of this size range is observed at steady state. The size of the new particles varies from the submicron range to particles of several microns. The formation of such a wide range of particle sizes indicates that the breakage mechanism is not the simple breakage of a particle into a few large pieces, such as the 2-piece breakage mechanism mentioned previously. This breakage behaviour is better described by mathematical distribution functions.

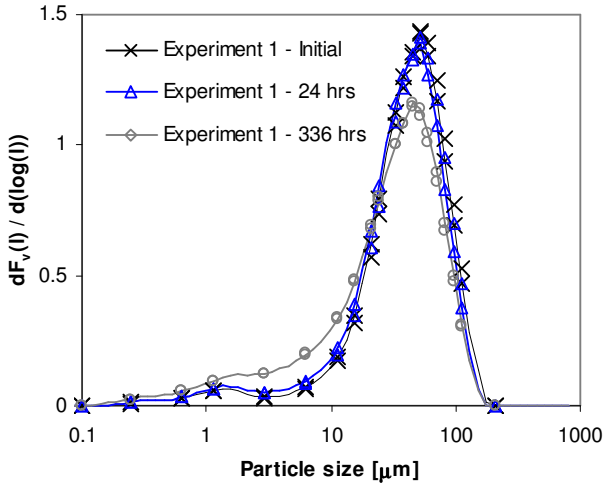

Figure 3.3: Frequency distribution curves at selected times during breakage experiment 1. Experimental conditions are provided in Tables 3.1 and 3.2.
Note that both the points and the continuous curves represent experimental measurements.

The SMD development of both experiments is shown in Figure 3.4. A decreasing trend as a function of time is observed, corresponding to an increase in the fraction of small crystals and thereby a deterioration of the dewatering potential. The observed trend is pronounced during the initial approximately 200 hrs of the experiments and slows down later, most likely as a consequence of the decreased concentration of large particles. The only exception to this decreasing trend is the sudden and unexpected increase in SMD after 24 hrs of mechanical inputs in experiment 2. No particles smaller than 1 µm were present in this sample, indicating that dissolution might have been taking place. The higher particle concentration of experiment 1, and thereby the increased likelihood of particle – particle collisions, causes a steeper initial decrease in the SMD in this experiment.

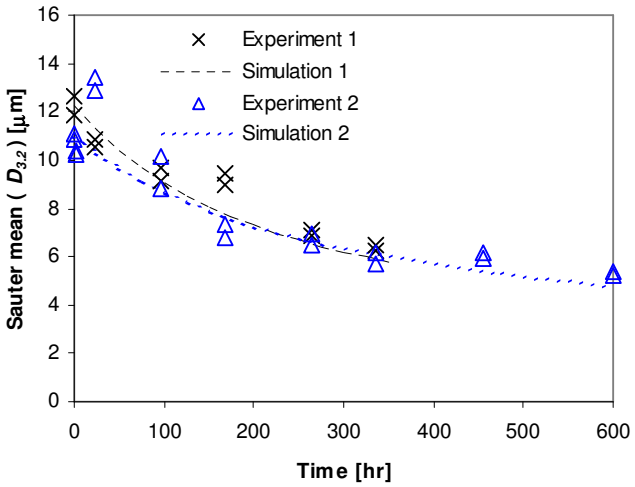

Figure 3.4: Dynamic development of simulated and experimental SMD in breakage experiment 1 (144.2 g L^{-1}) and 2 (75 g L^{-1}). Experimental conditions are provided in Tables 3.1 and 3.2.

Based on the previously described solution procedure two sets of kinetic parameters (k_d, e_5, k_{we}) have been determined by a stepwise iteration of the parameters aiming at a minimization of the sum of least squares of the PSD after 336 hrs of the two breakage experiments.

Experiment 1:

$k_d = 0.094\ L_{slurry}^{0.5} \cdot no^{-0.5} \cdot dm^{-3} \cdot s^{-1}$

$e_5 = 1.55$

$k_{we} = 1.09$

Experiment 2:

$k_d = 0.442\ L_{slurry}^{0.5} \cdot no^{-0.5} \cdot dm^{-3} \cdot s^{-1}$

$e_5 = 1.49$

$k_w = 1.20$

The kinetic parameters obtained show that different combinations of k_d and e_5 are able to describe the experimental data and that a strong dependence on the particle concentration ($e_5 > 1$) exists. No duplicate breakage experiments were performed and so it was not possible to assess parameter uncertainties. However, as it will be shown later, very precise parameter values are not needed because particle breakage is not significant during the slurry residence times used in wet FGD plants. Figure 3.4 shows the simulated development in SMD as well as the experimental measurements. Simulations are in good qualitative agreement with the experimental data and predict the stronger decrease of SMD in experiment 1 compared to experiment 2 as well as the slower decrease of SMD with time. A slight under-prediction of the SMD of both experiments are observed at long exposure times. Figure 3.5 illustrates the simulated and the measured PSD frequency curves at selected points in time during breakage experiment 1. The simulated PSD frequency curves are in good agreement with the experimental ones, showing a similar disappearance of particles above approximately 25 µm and a corresponding increase in particles from about 25 µm down to the submicron range in both experiments.

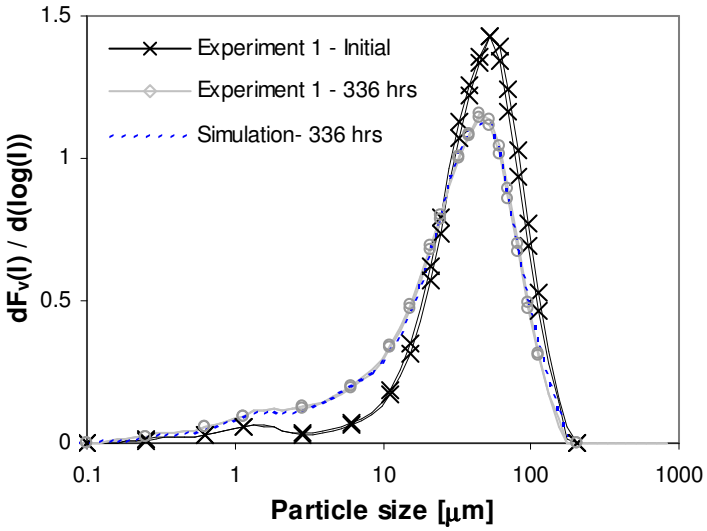

Figure 3.5: Experimental and simulated frequency distribution curves of breakage experiment 1 (0 hrs and 336 hrs), experimental conditions are provided in Tables 3.1 and 3.2.

3.5.3 Pilot plant PSD – Nucleation, growth and breakage

Based on the derived breakage kinetics, the influence of breakage on the steady state PSD of the wet FGD pilot plant has been evaluated. Input to the simulation procedure is the kinetic breakage parameters determined in the transient experiments (k_d, e_5 and k_{we}), the mean residence time ($\bar{t}$) and the crystal growth rate obtained by the McCabe analysis. The nucleation rate has been determined based on a fitting of the particle concentration (144.2 g L_{slurry}^{-1}).

The population density plot obtained, Figure 3.6 (left), show that an increased number of small particles and thereby a curvature of the semi logarithmic population plot. The PSD plot, Figure 3.6 (right), does, however, show that simulated volume fraction of fines is significantly lower than the experimental measurements. This indicates that breakage is not the only source of the increased fraction of small particles in the pilot plant PSD compared to the MSMPR model. A finite growth rate of the fragments would only further increase the disagreement between the simulations and the experimental results.

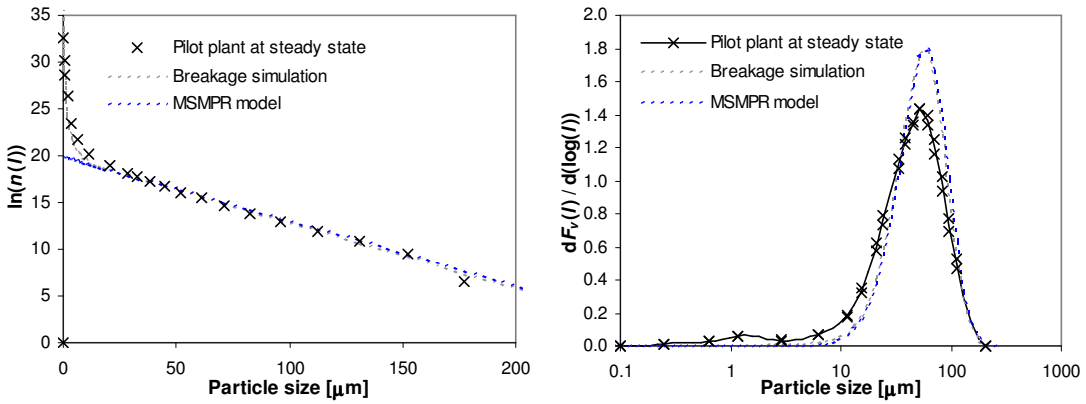

Figure 3.6: Experimental and simulated (growth and breakage) semi logarithmic population density plot (left) and frequency distribution (right). Steady state measurements have been performed on the slurry formed by desulphurisation of a 1000 ppm(v) gas stream. Kinetic parameters: G = 1.44 10^{-4} µm s^{-1}, $\bar{t}$ = 28.13 hrs, B^0 = 6.58 10^4 no. L_{slurry}^{-1} s^{-1}, k_d = 0.094 $L_{slurry}^{0.5}$ $no^{-0.5}$ dm^{-3} s^{-1}, e_5 = 1.55 and k_{we} = 1.09.

3.5.4 Pilot plant PSD and the influence of size dependent growth

The influence of size-dependent growth on the steady state PSD of the wet FGD pilot plant has furthermore been evaluated. Input to the simulation procedure is the mean residence time ($\bar{t}$), the population density of nuclei ($n(l_0)$) (estimated from the experimental data), the maximum growth rate (G_m) from the McCabe analysis and the empirical model parameters (a_1 and a_2) from a stepwise sum of least squares fitting of the PSD and the crystal concentration respectively. The following model parameters were obtained by the sum of least squares fitting procedure (step-size in parenthesis):

- a_1 = 0.057 (0.001) μm^{-1}
- a_2 = 0.039 (0.001) μm

The system shows a strong size-dependence (i.e. a low a_1-value). Figures 3.7 show the obtained population density (left) and PSD (right) plots. The simulations and the experimental results agree well down to a particle size of a few microns. Below this particle size the model is, however, unable to describe the increased levels of fines observed. A considerable measurement uncertainty is, however, also expected at these small particle sizes.

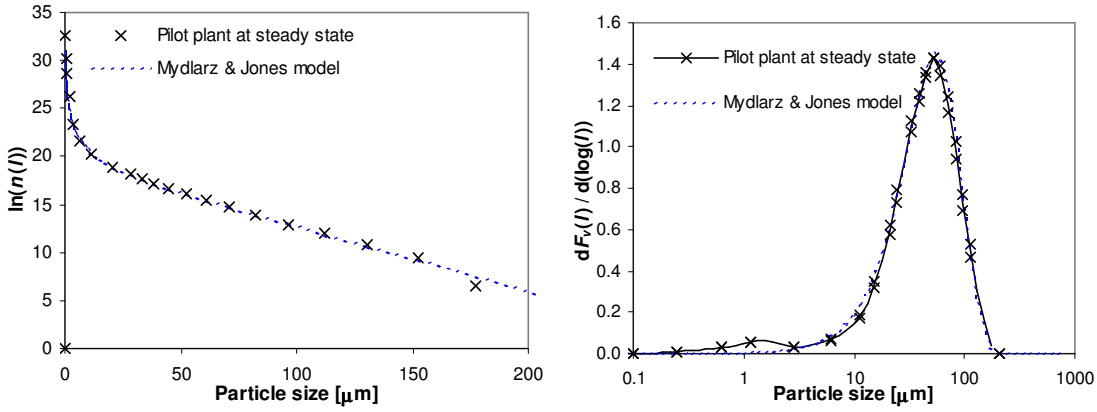

Figure 3.7: Experimental and simulated (size-dependent growth) population density (left) and frequency distribution (curves) curves at steady state desulphurisation of a 1000 ppm(v) gas stream. Kinetic parameters: G_m = 1.44 10^{-4} µm s^{-1}, $\bar{t}$ = 28.13 hrs, $n(l_0)$ = 2.15 10^{14} no. μm^{-1} L_{slurry}^{-1}, a_1 = 0.057 μm^{-1} and a_2 = 0.039 µm.

A size dependent growth rate of particles larger than 100 μm has, in the case of a diffusion controlled reaction, been explained in the literature by the higher particle settling velocity and thereby thinner boundary layers.[15,60] Below a particle size of 50 μm and in well-stirred systems, as in this study, this mechanism is considered unlikely.[27] Crystals smaller than a few microns may have a lower effective growth rate, due to an enhanced dissolution rate, i.e. Gibbs Thomson effect.[55] However in the size range studied, size-dependent surface integration kinetics is considered the most likely explanation. An increasing number of dislocations, and thereby an enhanced surface integration rate, may be present in large crystals due to mechanical stress, impurity incorporation and an increased likelihood of collisions and surface damage.[15,26] However, growth rate dispersion of secondary nuclei, through differences in dislocation concentration (facilitates growth) and integral stress (inhibits growth), may also yield an apparently size-dependent growth rate.[61]

3.6. Conclusion

This investigation of the PSD in a wet FGD pilot plant has demonstrated that increased levels of small particles are present compared to the predictions of the simple MSMPR model by Randolph and Larson.[22] Experiments concerning the breakage process have been carried out and a population balance model describing the redistribution of particles derived. Simulations show that the breakage process is unable to generate the increased levels of fine particles observed in the pilot plant. A three-parameter empirical size dependent growth model is able to describe the experimental data down to a particle size of a few microns. Size-dependent integration kinetics or growth rate dispersion of secondary nuclei, due to dislocations and integral stress, is considered the most likely explanations of the apparently size dependent crystal growth rate.

The influence of breakage on the crystallisation process taking place at full-scale wet FGD plants will be influenced by the mechanical inputs to the system (stirring and pumping) as well as operating conditions such as the solid concentration, residence time and the presence of growth inhibiting species. The optimal operating conditions in terms of gypsum crystallisation will most likely be plant specific and time dependent due to these effects.

Chapter 4

Gypsum crystallisation in full-scale wet FGD-plants

This chapter contains an investigation of the gypsum crystallisation in full-scale wet FGD-plants. The results have been collected in the article "Investigation of the gypsum quality at three full-scale wet Flue Gas Desulphurisation plants", which will be submitted to Fuel. This article was written by Brian Brun Hansen, Søren Kiil and Jan Erik Johnsson (The Department of Chemical and Biochemical Engineering, Technical University of Denmark).

Abstract

In the present study the gypsum quality at three full-scale wet FGD plants were examined and compared to the gypsum from a pilot plant. Gypsum quality can be expressed in terms of moisture content (particle size and morphology dependent) and the concentration of residual limestone and other impurities. The PSD in the holding tanks of the investigated plants were similar, apart from a slightly higher fraction of small particles in the full-scale plants. The highest levels of small particles were present in plants with elevated degrees of gypsum saturation, indicating nucleation, but fly ash accumulation and impurities from the sorbent or process water might also have contributed. The crystal morphology obtained in the pilot plant was columnar with distinct crystal faces as opposed to the amorphous shapes found at the full-scale plants. All the investigated full-scale plants consistently produced gypsum with high levels of purity and low moisture and impurity contents. An episode concerning a sudden deterioration in the gypsum dewatering properties was furthermore investigated, and a change in crystal morphology, as well as an increased impurity content (aluminium, iron and fluoride), was detected.

4.1. Introduction

The wet FGD-process removes SO_2, HCl, hydrofluoric acid (HF) and other acidic compounds from flue gases generated by the combustion of fossil fuels, such as coal and oil.[4,57,62] The majority of the desulphurisation capacity installed worldwide uses the wet FGD process in which the acidic flue gas components are captured by an alkaline slurry in an absorption step.[4] The wet FGD process can be subdivided according to the way the gas-slurry contact is obtained in the absorber. The counter-current spray tower distributes the slurry as droplets by atomising nozzles, the co-current packed tower distribute the slurry as a liquid film over the grid elements in the absorber and in the jet bubbling reactor the flue gas bubbles through the slurry. A slurry holding tank is often an integrated part of the absorber, where the absorbed SO_2 dissociates to HSO_3^- and is further oxidised to sulphate ions (SO_4^{2-}) by injection of air. Calcium ions, from the dissolution of finely ground limestone or chalk, will finally combine with SO_4^{2-} and crystallise as gypsum particles:

$$CaCO_3(s) + SO_2(g) + 2\ H_2O(l) + ½O_2(g) \Leftrightarrow CaSO_4{\cdot}2H_2O(s) + CO_2(g) \qquad (4.01)$$

A purge stream is used to control the concentration of chloride ions, from absorbed HCl, in the slurry. Based on an online measurement of the slurry density, the gypsum produced will be withdrawn when a certain solids level is reached. Hydrocyclones, centrifuges or belt filters are used for the withdrawal, washing and dewatering of the gypsum until a commercial product is obtained. The hydrocyclones selectively removes the larger particles within the absorber (thereby depleting the population of large particles) and generate a concentrated stream containing the larger particles and a dilute stream containing the smaller particles. The concentrated stream undergoes further processing before the final gypsum product is obtained, while the dilute stream is recycled to the absorber or partly used as a purge stream. Specifications with respect to the purity, the moisture content (size and morphology dependent) and the content of different impurities (residual limestone, sulphite (SO_3^{2-})) exist, depending on the subsequent commercial use of the gypsum (wallboards production, cement production or as a soil conditioner). The operation of a power plant, including the wet FGD unit, is dynamic in nature, due to the changing demands of electricity and heat during the days, weeks and seasons of the year.

The literature contains several bench-scale investigations of gypsum crystallisation within industrial processes such as phosphoric acid production[36,41,42] and wet FGD[9,17]. A few articles concerning gypsum quality at full-scale wet FGD plants have furthermore been published in the literature.[63,64]

A deterioration of the gypsum dewatering properties at the German lignite-fired Jänschwalde Power Plant, equipped with the two-stage NOELL/KRC wet FGD process, was linked to a change of particle size and morphology.[63] The volumetric mean particle diameter (D_{50}) decreased from 72 μm to 62 μm and the initially amorphous shaped crystals changed towards more sharp-edged geometrical shapes. During this time the dissolved salt concentration in the slurry increased, thereby increasing the density of the liquid phase. The withdrawal of gypsum was, however, still initiated at the same slurry density level, now corresponding to a lower solids concentration, and thereby a lower solids residence time, yielding smaller crystals. The authors provided no mechanism explaining the morphology changes, but report that a correction of the density set point for slurry withdrawal caused the crystals to return to the initial shape and size.

Another investigation used part of the flue gases (containing fly ash) from two German lignite-fired power plants for desulphurisation in a pilot-scale wet FGD plant.[64] Distinct differences in the gypsum particle size distribution (PSD) and morphology were observed despite operation at similar residence times, temperatures and pH values. The amorphous shaped gypsum crystals from the Neurath Power Plant (D_{50} ~ 30 μm) were larger than the crystal from the Niederaußem Power Plant (D_{50} ~ 20 μm), which furthermore resembled distorted plates. Experiments with increased degrees of stirring and prolonged residence times excluded mechanical attrition as the source of the differences in the gypsum quality. Increasing levels of chloride and fines (particle size range not defined by the authors) were subsequently identified as the source of the differences in particle size and morphology. It was not determined whether any kind of fines could trigger such morphology changes or if fines of a specific origin (i.e. fly ash, reactant impurities etc.) were required.

More than 99 % of the gypsum produced by the Danish power plants pass the gypsum quality specifications, established by the wallboard and cement industry, but issues such as a decreased dewatering rate (an increased moisture content of the final gypsum product), a discolouring of the gypsum, and increased impurity levels has been encountered. Several

hundred tons of such off-spec gypsum may be produced annually causing expenses for disposal. An increased understanding of the gypsum crystallisation process could ensure a more consistent gypsum quality and thereby facilitate a more efficient resource management and provide the power plant industry with an income as opposed to the expenses associated with disposal. This issue will continue to be of importance because the combustion of fossil fuels is expected to continue to supply a substantial part of the world's energy demand in the coming years.[1]

4.2. Crystallisation theory relevant to investigation

The crystallisation process encompasses the formation (nucleation) and growth of solid crystals from a supersaturated solution. Nucleation mechanisms include the formation of new particles from the super saturated solution (homogenous nucleation), precipitation on foreign particles (heterogeneous nucleation) and mechanical attrition of existing crystals (secondary nucleation).[9,16] The extent of nucleation in an industrial crystalliser will therefore depend on the saturation of the liquid phase as shown in Equation 4.02, the properties of any particles present and the mechanical inputs to the system.

$$S = \frac{a_{Ca^{2+}} \cdot a_{SO_4^{2-}} \cdot a_{H_2O}^2}{K_{so,CaSO_4 \cdot 2H_2O}} = \frac{\gamma_{Ca^{2+}} \cdot c_{Ca^{2+}} \cdot \gamma_{SO_4^{2-}} \cdot c_{SO_4^{2-}} \cdot \left(\gamma_{H_2O} \cdot c_{H_2O}\right)^2}{K_{so,CaSO_4 \cdot 2H_2O}} \quad (4.02)$$

The subsequent crystal growth is facilitated by the diffusion of solute molecules to the crystal surface, where integration into the crystal lattice takes place.[18] The crystal growth rate depends on the availability of ions, expressed as the degree of saturation, as well as the relative concentrations and characteristics of the lattice ions due to differences in their size and degree of hydration.[19] A decreasing Ca^{2+}/SO_4^{2-} concentration ratio increases the growth rates in the case of gypsum crystallisation,[18,36] indicating that the diffusion and integration of SO_4^{2-} is the growth-limiting step. The crystal growth rate of the various crystal faces as well as the operating conditions determine the obtained crystal morphology, size and impurity content.

The topography of the crystal surface offers a range of different binding sites, where the most favourable ones constitute only a small fraction of the total number of sites.[16] Even a small amount of a foreign species preferably adsorbed onto these "active" sites may therefore have a significant effect on the rate of ion incorporation (crystal growth) and the resulting crystal morphology. Even in the absence of foreign species, different crystal morphologies may be encountered, due to differences in the supersaturation of the liquid phase. Gypsum crystals have been reported to exhibit thick plate or rod-like shapes at low degrees of saturation ($1.0 \leq S \leq 1.2$), while longer and thinner needle-like crystals are formed at higher super saturations.[19,36]

4.3. Strategy of investigation

The operating conditions and the resulting gypsum quality at three full-scale FGD plants and one pilot plant (listed in Table 4.1) were investigated during this campaign. Slurry samples were withdrawn and analysed in terms of PSD, morphology and liquid phase composition, while the process monitoring equipment provided data on the flue gas flow, temperature, SO_2 concentration and slurry pH. Information on the purity, moisture content and residual limestone content of the gypsum product was furthermore provided by the involved power plant companies (DONG Energy A/S and Vattenfall A/S). As previously mentioned the changing demands of electricity makes the operation of a wet FGD plant dynamic in nature. This aspect was investigated by following the operation of Amager Power Plants unit 3 (APP3) for 3 weeks while withdrawing samples every 2-3 days. The investigations at Nordjyllands Power Plants unit 3 (NPP3) and Esbjerg Power Plants unit 3 (EPP3) were of shorter duration (4 days and 1 day respectively) and were used for a comparison of the obtainable gypsum properties at FGD plants of similar design. At NPP3 wastewater containing Na^+ and SO_4^{2-} from the flue gas cleaning at a waste incineration plant was added to the slurry in the days preceding the investigation. Bituminous coals (no. 1 to 5 in Table 4.2) with low levels of sulphur ($\leq$ 1.0 % w/w) and low to medium ash contents (SiO_2/Al_2O_3 rich) were combusted at the investigated plants. The high degree of control of the experimental conditions in the investigated pilot plant enables the development of a steady state at which samples were withdrawn. These samples were used to investigate to which extent pilot-scale experiments could be transferred to full-scale conditions.

An episode concerning a sudden increase in the moisture content of the gypsum produced at APP3 was furthermore investigated through microscopy and elemental analysis. The bituminous coals (no. 1, 4, 6, 7 in Table 4.2) combusted during this time were similar to the ones used at the other plants of this investigation.

Table 4.1: Overview of investigated wet FGD-plants

Power plant	**Amager**	**Nordjylland**	**Esbjerg**	**Pilot plant**
Unit	3 (APP3)	3 (NPP3)	3 (EPP3)	-
	250 MW_e	385 MW_e	370 MW_e	0.1 MW_e
Absorber type	Spray tower	Packed tower		Falling film[a]
Manufacturer	Deutche Babcock	Mitsubishi heavy industries		
Holding tank [m^3]	1700	1500	2000	0.03
Liquid/Gas ratio [L m^{-3}]	~ 20	~ 25	~ 19	~ 14
Fuel	Bituminous coal 1 & 2	Bituminous coal 1,4 & 5	Bituminous coal 1 & 3	Natural gas + SO_2
Reactant	Limestone	TASP[b] and chalk	TASP[b] and Chalk	Limestone
Duration of campaign	502 hrs	97 hrs	Single sample	Steady state
Samples (unfiltrated/filtrated)	9/10	12/3	2/2	1 /1
Multiple samples[c] (unfiltrated/filtrated)	None/Once	Six times/Once	Once/Once	

[a] Downscaled packed tower.

[b] The by-product from the spray-dry scrubbing FGD process.

[c] Withdrawal of two samples in sequence in order to evaluate the uncertainties of the sampling and analytical procedures.

Table 4.2: Heat of combustion, sulphur content, ash content and ash composition of coal types encountered during the investigation. Information supplied by Dong Energy A/S and Vattenfall A/S.

Bituminous coal nr		**1**	**2**	**3**	**4**	**5**	**6**	**7**
Heat of combustion	MJ kg^{-1}	25.3	25.0	28.3	24.3	25.3	24.9	25.9
Sulphur content	wt. %	0.41	0.71	1.0	0.90	0.78	0.63	0.30
Ash content	wt. %	12.0	5.5	9.7	12.0	15.3	8.4	12.4
Ash composition								
SiO_2	wt. %	57.0	52.7	34.0	53.0	69.0	61.0	48.0
Al_2O_3	wt. %	21.0	23.5	16.0	31.0	21.0	20.5	21.0
TiO_2	wt. %	0.80	1.16	0.83	2.10	1.10	0.80	0.74
P_2O_5	wt. %	0.50	0.34	0.94	0.18	0.29	0.17	0.34
SO_3	wt. %	3.50	4.50	15.0	1.30	0.77	1.80	6.20
Fe_2O_3	wt. %	6.30	10.0	11.0	7.80	3.20	8.30	8.70
CaO	wt. %	4.5	2.7	14.0	2.2	1.1	2.0	10.0
MgO	wt. %	2.10	2.44	3.60	0.48	0.65	2.20	1.80
Na_2O	wt. %	1.30	0.56	3.00	0.15	0.28	0.90	0.68
K_2O	wt. %	2.50	2.43	1.40	0.74	0.60	2.10	1.30

4.4. Experimental procedure

4.4.1 Measuring campaign

Slurry samples were withdrawn from either the holding tank of the pilot plant or the stream connecting the holding tank and the hydrocyclones at the full-scale plants and were stored in high-density Polyethylen (HDPE) bottles. The stirring, air injection and pumping (recirculation) ensured a well-mixed holding tank and thereby representative samples.

The samples for analysis of the ionic liquid composition were passed through a 0.45 μm filter and diluted 1:10 with laboratory grade pure water to prevent further precipitation. Two analytical laboratories were used to determine the samples ionic composition. The analytical laboratory at Amager Power Plant used a Dr. Lange test kit and a XION 500 spectrophotometer for chlorine analysis, while calcium, sodium, magnesium and sulphur were measured with a Perkin Elmer Optima 3300DV by a axial ICP-OES (Inductive Coupled Plasma Optical Emission Spectroscopy). The analytical laboratory at Ensted Power Plant (ENPP) used axial ICP-OES (Spectro Ciros-CCD) to measure sulphur and chlorine, while calcium, sodium, magnesium were measured by radial ICP-OES (Perkin Elmer Optima 3000).

The slurry samples for PSD and morphology analysis did not undergo any treatment during their withdrawal and were stored for up to a few weeks at room temperature before analysis. The limited solubility of gypsum (~ 2 g L^{-1}), compared to the slurry concentration (> 100 g L^{-1}), and its invariability with temperature[65] ensured that no major changes in PSD took place during storage, as it has been verified previously.[66] The PSD analysis was performed by laser diffraction (Malvern Mastersizer S longbed) on an ethanol/slurry dispersion. The crystal morphology was investigated by Environmental Scanning Electron Microscopy (ESEM, FEI Quanta 200) at the department of civil Engineering DTU-BYG. The crystals for morphology studies were collected on a 0.45 μm filter and subsequently dried at 30 ^{o}C.

4.4.2 Decreased dewatering properties at APP3

Powder samples of the final processed gypsum product were collected from the belt filter at APP3. The collected powder samples were dried at 30 ^{o}C in a "WTC binder" oven and then stored in sealed polyethylene (PE) bags. The chemical compositions of the powder samples were measured at the ENPP analytical laboratory. The concentration of foreign cations in the crystal lattice were determined by dissolving the samples in a warm mixture of acids (HF and HNO_3) in a microwave oven (Ethos 1/1600, Milestone), followed by H_3BO_3 neutralisation and analysis by a radial ICP-OES (Perkin Elmer Optima 3000). The concentration of foreign anions in the crystal lattice were determined by dissolving 0.05 g sample in 250 ml ultra pure water, followed by analysis with a Dionex Ionic ICS 2000 chromatograph (AG/AS18-column). The crystal morphology was investigated by Scanning Electron Microscopy (SEM, Zeiss 1540 EsB) at the Danish Technological Institute.

4.5. Results and discussion

4.5.1. Operating conditions

The operation of a wet FGD plant is, as previously mentioned, dynamic in nature because of the changing electricity and heat consumption during the days, weeks and seasons of the year. The flue gas flow, Q_g, the SO_2 volume fraction, ϕ_{SO_2}, and the desulphurization degree, η, determines the amount of gypsum produced, while the amount of gypsum accumulated in the plant is calculated from the slurry volume, V_{sl}, and the gypsum volume fraction, ϕ_{Gy}. The average solid residence time, equation 4.03, combines these aspects and can consequently be used for an evaluation of the changes in operational conditions.

$$\bar{t}_S = \frac{V_{sl} \cdot \varphi_{gy} \cdot \rho_{gy}}{Q_g \cdot \varphi_{SO_2} \cdot \eta \cdot M_{gy} / V_M} = \frac{V_{sl} \cdot \left(\frac{\rho_{sl} - \rho_{wa}}{\rho_{gy} - \rho_{wa}} \right) \cdot \rho_{gy}}{Q_g \cdot \varphi_{SO_2} \cdot \eta \cdot M_{gy} / V_M} \qquad (4.03)$$

Figure 4.1 shows the development in flue gas flow rate and solid residence time at APP3 during this investigation, thereby illustrating the changing operating conditions at full-scale wet FGD plants compared to the well-controlled conditions at bench or pilot-scale. The density of the aqueous electrolyte solution, ρ_{wa}, was estimated based on the temperature (Table 4.3) and the electrolyte concentration (assumed to consist solely of $CaCl_2$).[65] The peaks in solid residence time was associated with a decrease in the flue gas flow rate, but the intermediate development of the solid residence time shows that changes in other operational parameters, such as $V_{sl,}$ ϕ_{SO_2} and ϕ_{Gy} (due to a discontinuous withdrawal of gypsum) also had an effect.

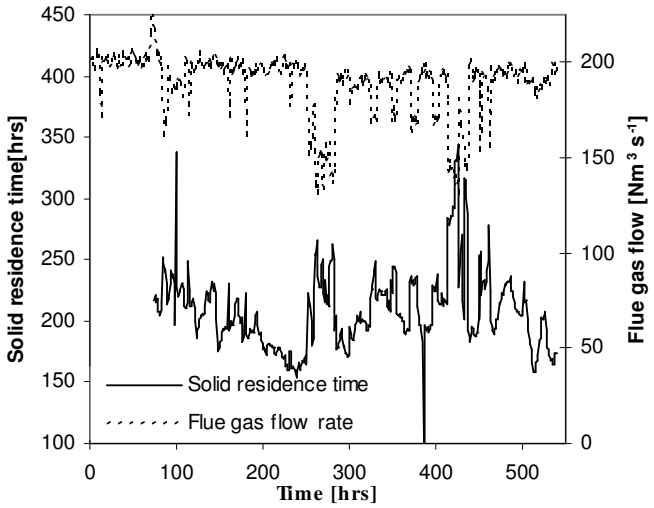

Figure 4.1: Development in flue gas flow rate and solid residence time at APP3 (The initial 78 hrs of the solid residence time curve has been excluded due to erroneous density measurements).

Table 4.3 provides a comparison of the average operating conditions at the investigated wet FGD plants. Similar operating temperatures and pH values were present at all the four investigated wet FGD plants. The full-scale FGD plants were designed for the combustion of coals with higher sulphur contents than the coals used during this investigation, yielding relative long solids residence times. This was especially the case at APP3, because the plant was running at low load and thereby a low flue gas flow rate. The calcium to sulphur molar ratios at the three full-scale plants were favorable in terms of gypsum crystal growth,[18,36] while the high degree of saturation at EPP3 and NPP3 could be associated with excessive

nucleation. The degrees of saturation in the pilot plant and at APP3 were quite similar, despite considerable differences in ionic slurry composition (see section 4.5.2).

Table 4.3: Average operating conditions of the investigated wet FGD plants

Power plant		Amager	Nordjylland	Esbjerg	Pilot plant
Unit		APP3	NPP3	EPP3	-
Flue gas flow rate	$Nm^3\ s^{-1}$	189	315	305	0.0057
SO_2 concentration	ppm	250	530	350	990
Solids residence time	hrs	210	44	110	28
PH		5.3	5.4	5.9	5.4
Slurry temperature	°C	51[d]	52[d]	49[d]	50
Calcium/sulphur molar ratio[e]		0.55	0.25	0.92	24
Saturation[e] – eq. 4.02		1.22	2.32	4.12	1.24

[d] The temperature of the flue gas leaving the FGD plant is used as an approximation.

[e] For further details see section 4.5.2.

4.5.2 Liquid phase composition

The data obtained from the analysis of the elemental liquid phase composition can be seen in Table 4.4. The charge balance error (CBE, equation 4.04) evaluates the performed analysis in terms of deviations from an electrically neutral solution. Considerable deviations from electrical neutrality may arise if an important ionic species have been overlooked or because of systematic sampling/analytical errors.

$$CBE = \frac{\sum c_{cat} \cdot z_{cat} - \sum c_{an} \cdot |z_{an}|}{\sum c_{cat} \cdot z_{cat} + \sum c_{an} \cdot |z_{an}|} \qquad (4.04)$$

Analyses from APP analytical laboratory were associated with a considerable excess of anions (CBE's > -10 %). Additional analyses performed at the ENPP analytical laboratory yielded significantly lower chloride levels and correspondingly improved CBE's. Trace amount of additional cations may very well be present in the complex slurry mixture thereby ensuring electrical neutrality (Potassium and Manganese were detected – improving the CBE with ≤ 1.4 %).

Table 4.4: Liquid phase composition (standard deviation in parenthesis in the case of multiple samples)

Plant		Analytical laboratory	Ca [mg L^{-1}]	Mg [mg L^{-1}]	Na [mg L^{-1}]	S [mg L^{-1}]	Cl [mg L^{-1}]	CBE[f] [%]
APP	0 hrs	APP[g]	1134	1169	2339	1726	7250	-10.2
APP	46 hrs	APP[g]	1104	1118	2177	1758	5780	-6.00
APP	93 hrs	APP[g]	1051	1024	1936	1683	6720	-14.3
APP	93 hrs	ENPP[h]	1095 (±7)	1085 (±5)	1937 (±19)	1585 (±7)	5525 (±7)	-5.51 (±0.39)
APP	167 hrs	APP[g]	881	759	1385	1445	4590	-13.7
APP	214 hrs	APP[g]	876	783	1440	1560	4400	-12.9
APP	333 hrs	APP[g]	835	889	1790	1766	5020	-13.3
APP	382 hrs	APP[g]	874	901	1788	1813	5030	-13.2
APP	430 hrs	APP[g]	805	835	1626	1694	4590	-13.4
APP	502 hrs	APP[g]	785	744	1376	1591	4070	-14.4
NPP	24 hrs	ENPP[h]	2101 (±7)	3014 (±40)	14090 (±198)	6805 (±49)	25325 (±64)	-8.22 (±0.57)
NPP	24 hrs	APP[g]	2075 (±7)	2900 (±0)	14675 (±35)	6965 (±92)	30260 (±28)	-13.55 (±0.15)
NPP	94 hrs	APP[g]	2350	3160	16200	7400	32800	-12.3
EPP		ENPP[h]	3625 (±11)	1689 (±4)	1741 (±6)	3150 (±5)	9652 (±12)	-8.46 (±0.15)
Pilot plant		ENPP[h]	10900			380	19200[i]	-1.93

[f] Assuming that sulphur is present as SO_4^{2-} due to forced oxidation.

[g] Amager Power Plant

[h] Ensted Power Plant

[i] Based on an estimated feed concentration.

Figure 4.2 shows the liquid phase elemental charge distribution from the investigated wet FGD plants. The ionic composition of the pilot plant was dominated by calcium and chloride, while only a low level of sulphur was present. $CaCl_2$ was added to the pilot plant slurry, in order to simulate the absorption of HCl taking place in full-scale plants, thereby increasing the Ca^{2+} and Cl^- concentration. The full-scale wet FGD plants furthermore contained considerable fractions of magnesium (Mg^{2+}) and sodium ions (Na^+) from dissolved fly ash and reactant impurities. The high levels of Na^+ and SO_4^{2-} at NPP3 originate from the addition of wastewater from flue gas cleaning at a nearby waste incineration plant. This flue gas cleaning process captures and oxidises SO_2 to SO_4^{2-} using sodium hydroxide (NaOH) as reactant.

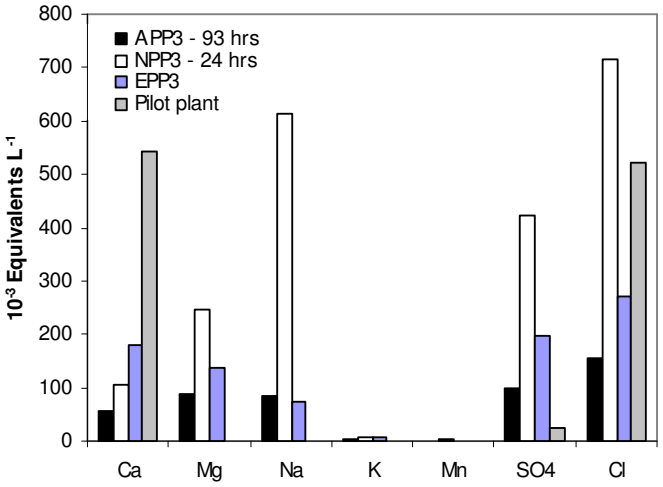

Figure 4.2: Charge distribution of the investigated wet FGD slurries.

Based on the slurry temperature (Table 4.3) and elemental composition (Table 4.4), stated as $CaSO_4$, $CaCl_2$, NaCl and $MgCl_2$ concentrations, the degree of gypsum saturation was simulated by a fortran program using the extended UNIQUAC model.[67] In order to obtain an electrical neutral solution, 50 % of the CBE was closed by increasing the cationic concentrations, while the remaining CBE was eliminated be decreasing the anionic concentrations. The obtained degrees of gypsum saturation are shown in Table 4.3.

4.5.3 Gypsum quality parameters

The gypsum produced by the wet FGD process must comply with certain quality specifications, in order to be used commercially within the wallboard or cement industry. The gypsum quality in terms of particle size (dewatering properties), morphology (dewatering properties), purity, moisture content and residual limestone content was investigated in this study.

Particle size, purity, moisture content and content of residual limestone

The PSD of the solids (gypsum and fly ash) in the holding tanks of the investigated plants, Figure 4.3, were of a similar size range. The slurry samples from NPP3 and EPP3 contained higher fractions of small particles and showed a distinct separation into two different solid phases, a gypsum phase and a phase consisting of fines on top of the former. Potential sources of fines include residual reactant, reactant impurities, fly ash from the flue gas, impurities in

the process water and an increased nucleation rate, the latter explanation was supported by the elevated degrees of saturation at EPP3 and NPP3. The lower maximal particle size present in the three full-scale plants, compared to the pilot plant, is a consequence of selective removal of large particles performed by the hydrocyclones at these plants. Despite the low degree of saturation in the pilot plant and the short solid residence time, the crystals formed were of a comparable size to the ones from the full-scale plants. This may be due to either particle attrition/breakage taking place in the full-scale plants or an enhanced crystal growth rate in the pilot plant due to the absence of growth-inhibiting impurities.

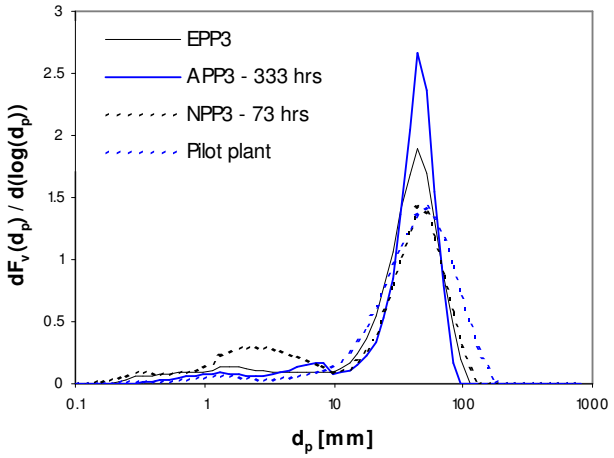

Figure 4.3: PSD of the solids in the holding tanks of the investigated wet FGD plants.

Table 4.5 presents a number of gypsum quality parameters as well as the holding tank PSD quantiles from the investigated plants, while Figure 4.4 shows the temporal development at APP3. The gypsum quality at the three investigated full-scale plants were comparable to each other, while a higher content of residual limestone was present in the pilot plant gypsum, due to a shorter residence time and the absence of a selective product withdrawal. The long solids residence time, ~ 200 hrs, at APP3 dampened temporal variations in gypsum quality and ensured a consistent high quality during the 502 hrs investigation. The PSD of the holding tank solids did, however, show some variations, because of the discontinuous gypsum withdrawal.

Table 4.5: Gypsum quality parameters and holding tank PSD quantiles.

Plant	APP3 – 333 hrs	NPP3 – 73 hrs	EPP3	Pilot plant
D_{10} [µm][j]	6.9 (0.5)	1.6 (0.2)	2.7 (0.2)	12.9
D_{50} [µm][j]	41.2 (0.4)	34.9 (2.1)	37.9 (0.5)	42.8
D_{90} [µm][j]	61.6 (0.1)	72.9 (5.3)	64.1 (2.2)	90.4
Gypsum purity[k] [%]	98.7 (0.3)	98.7	98.6	-
Moisture content[k] [%]	7.1 (0.9)	7.4 (0.9)	11.3	-
Residual limestone[k] [wt %]	0.3 (0.1)	0.8 (0.1)	0.7	2.3

[j] Standard deviation of the sampling and analytical procedure in parenthesis

[k] Data from the standard gypsum quality analysis (thermo gravimetric analysis - TGA) performed at the power plant every 2-3 days. Temporal standard deviation in parenthesis

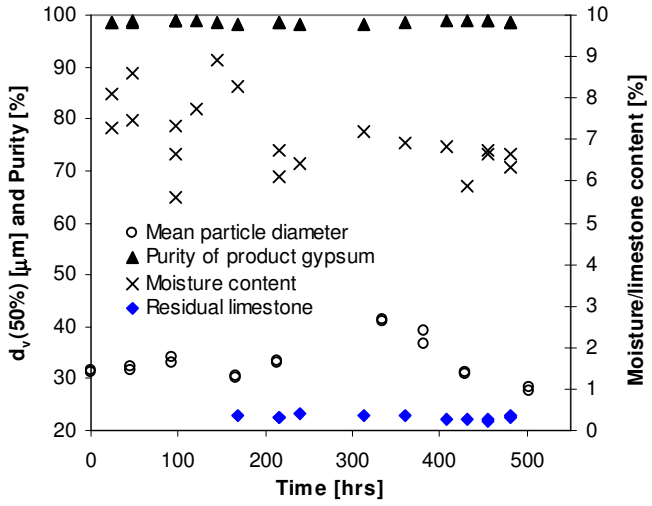

Figure 4.4: Development of gypsum quality parameters at APP3.

Morphology

The columnar or columnar-stump shaped gypsum crystals from the pilot plant (Figure 4.5) had distinct crystal faces but showed some minor signs of attrition along the edges of the crystals. The full-scale gypsum crystals (Figure 4.6) had amorphous shapes and showed few or no distinct crystal faces. The APP3 crystals were more flat in nature than the crystals from the two other full-scale plants. Rapid crystallisation processes (i.e. high super saturations) have in the literature been associated with amorphous-appearing crystals, which still retain an internal crystalline structure.[21] The high supersaturations at NPP3 and EPP3 support this explanation, but the low supersaturation at APP3 also points towards another explanation. The long solid residence time at this plant may have facilitated breakage and attrition of the crystals due to the mechanical stresses induced by stirrers and pumps.

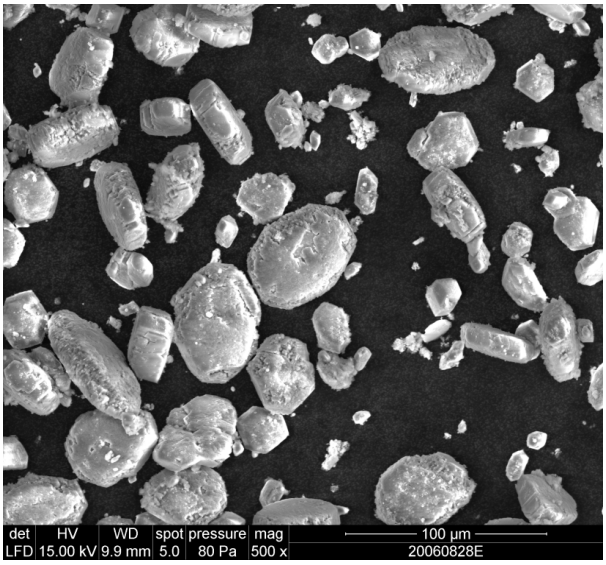

Figure 4.5: ESEM picture of APP3 crystals – plant details and operating conditions can be seen in Tables 4.1 & 4.3.

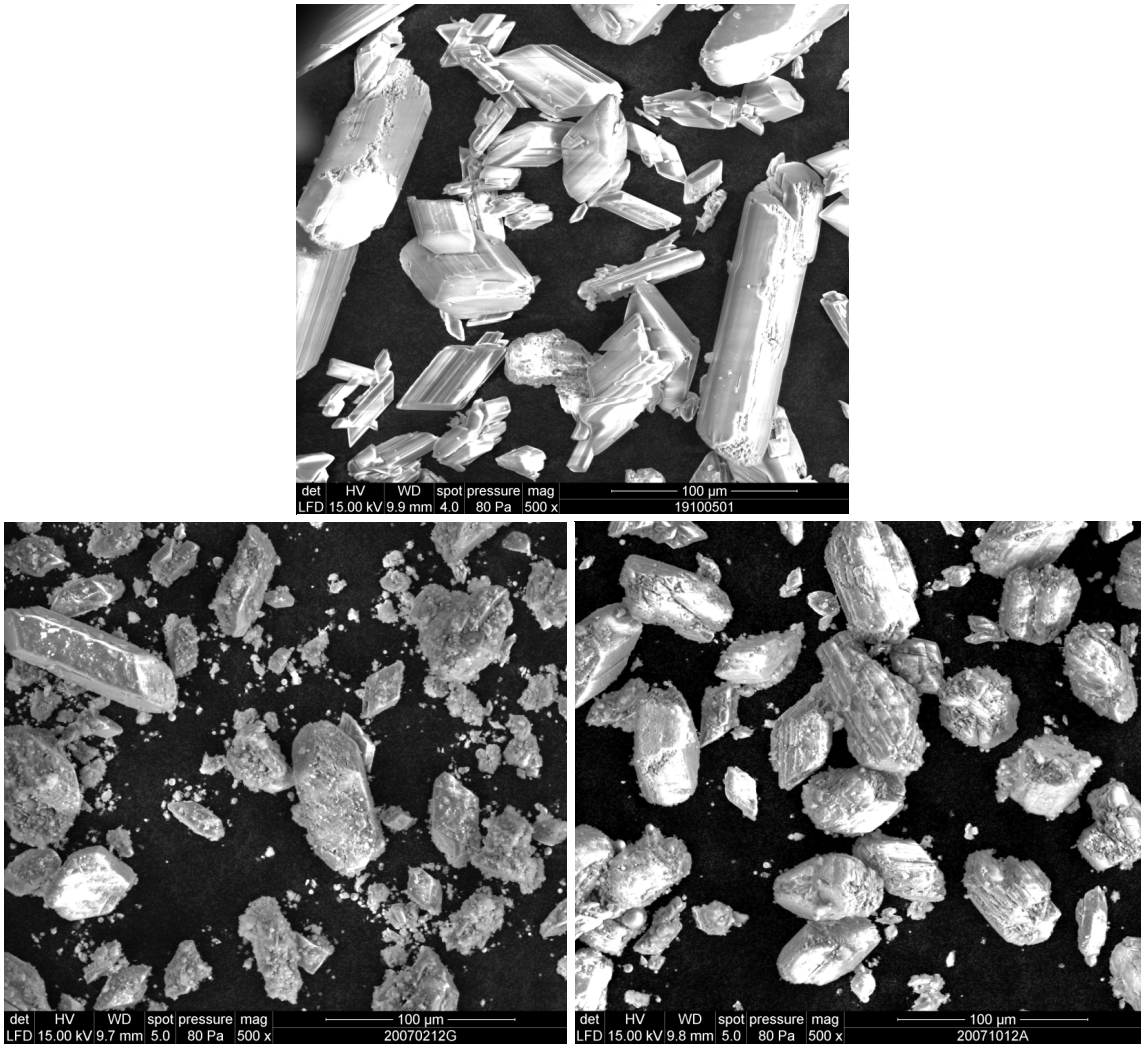

Figure 4.6: ESEM picture of pilot plant crystals (top), NPP3 crystals (lower-left hand-corner) and EPP3 crystals (lower-right hand-corner) - plant details and operating conditions can be seen in Table 4.1 & 4.3.

4.5.4. Episode concerning decreased dewatering properties

During the start-up of APP3 after a revision, a sudden increase in the moisture content of the gypsum product (Figure 4.7) was experienced and caused the gypsum product to fail the quality specifications.

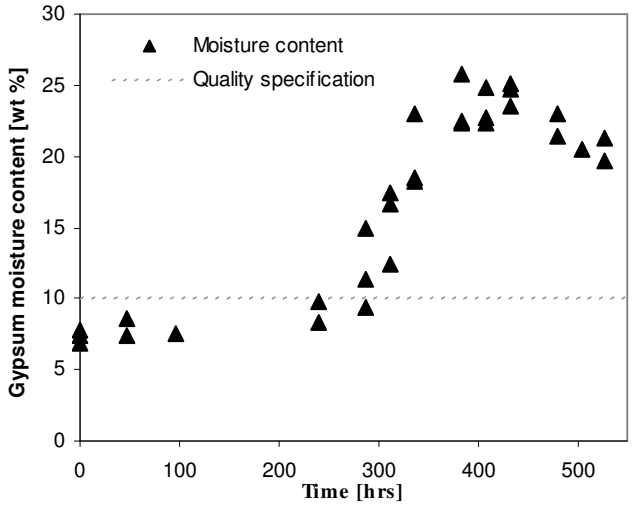

Figure 4.7: Development in the moisture content of the washed and dewatered gypsum product at APP3 during start-up.
Plant details and operating conditions can be seen in Tables 4.1 & 4.6.

The start-up was associated with a decreased flow rate of the purge stream, due to plugged pipes, thereby accumulating electrolytes and fines in the system. Increased amounts of fly ash were furthermore escaping the electrostatic precipitator, thereby ending up in the wet FGD absorber. The average operating conditions are shown in Table 4.6 and the development in slurry density and flue gas flow rate is shown in Figure 4.8. In the days preceding the increased gypsum moisture content, foaming was interfering with the online density measurement and no gypsum was withdrawn for several days (from 130 hrs to 240 hrs) yielding a density ~ 1200 kg m^{-3}. The increased solid concentration (density) and the decreasing flue gas flow rate caused the average solid residence time to increase from ~ 200 hrs to > 500 hrs hrs.

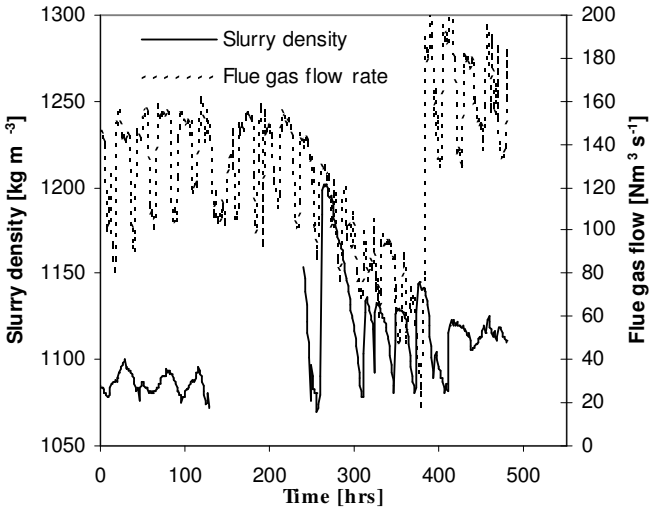

Figure 4.8: Development in slurry density and flue gas flow rate at APP3 during start-up.

Table 4.6: Average operating conditions at APP3 during start-up.

Operating parameter		
SO_2 concentration	360	ppm_v
Solid residence time - before density increase	201	hrs
Solid residence time - during episode	535	hrs
PH	5.4	
Slurry temperature	51[1]	^oC

[1] The temperature of the flue gas leaving the FGD plant is used as an approximation of the slurry temperature.

Microscopy of the gypsum product before and during the increase in moisture content, Figures 4.9, showed a distinct shift from amorphous shaped crystals towards thin plates. This change in crystal morphology enabled a closer packing of the crystals and consequently decreased dewatering properties. The morphology change was furthermore associated with higher impurity levels (aluminium, fluoride and iron) in the crystals, Table 4.7. Aluminium and iron originate from fly ash escaping the electrostatic precipitator as well as corrosion within the plant, while the absorption of the acidic gaseous HF transfer fluoride to the FGD plant.

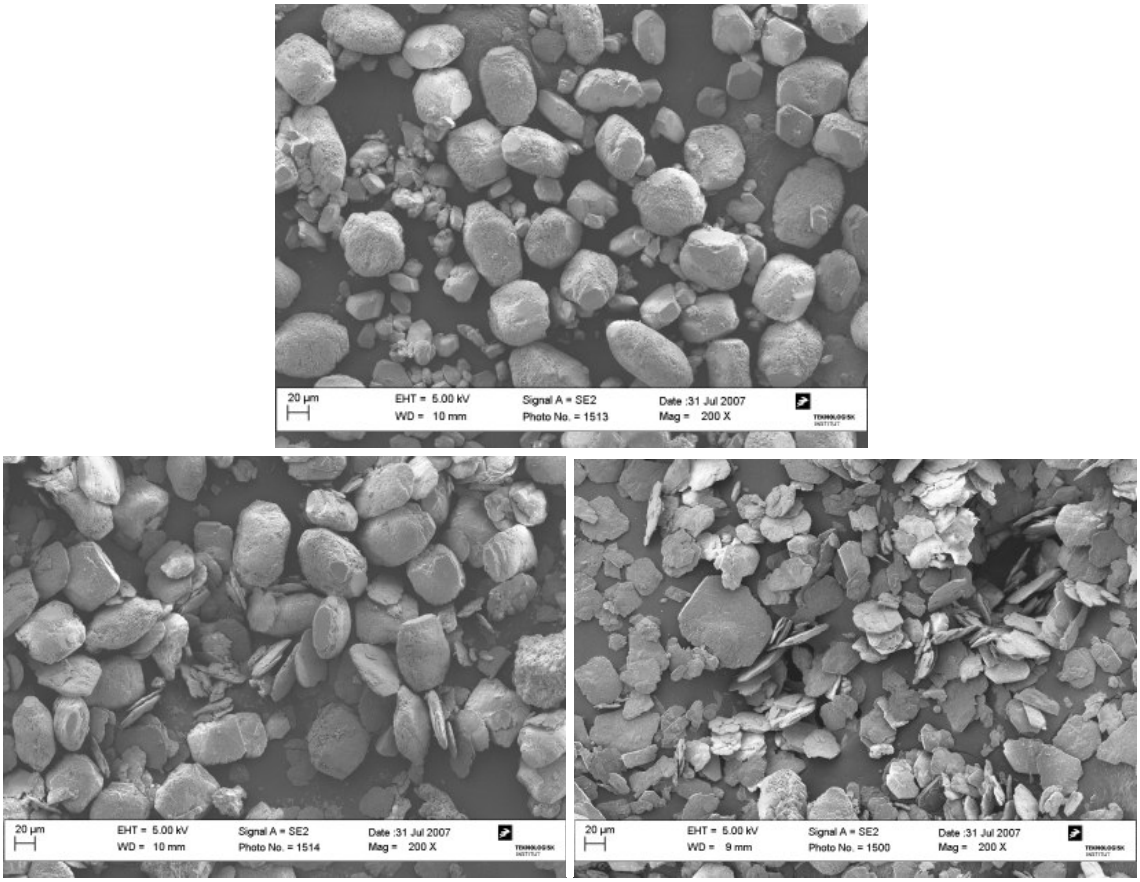

Figure 4.9: ESEM picture of APP3 crystals twelve days before (top), two days before (lower-left hand-corner) and eight days after (lower-right hand-corner) peak in density. Reproduced with the permission of Vattenfall A/S.

Table 4.7: Content of impurities in the gypsum product during start-up at APP3.

Element	**Amorphous morphology**		**Plate morphology**	
	[wt %]	[mmol kg^{-1}]	[wt %]	[mmol kg^{-1}]
Aluminium	0.082	30.4	0.14	51.9
Iron	0.042	7.5	0.069	12.4
Fluoride	0.11	57.9	0.15	78.9

A similar shift in morphology and an increased aluminium and fluoride uptake has been reported for gypsum formed during wet phosphoric acid production (phosphogypsum).[41,42] This process consist of the digestion of phosphate rocks by concentrated sulphuric acid and it involves mineral impurities similar to the ones present in the various coal types combusted at the power plants. The morphology changes of the phosphogypsum were facilitated by the substitution of SO_4^{2-} ions at the {011} and $\{\bar{1}11\}$ crystal faces by growth inhibiting aluminium fluoride complexes (AlF^{2+} to AlF_6^{3-}), as illustrated by Figure 4.10.

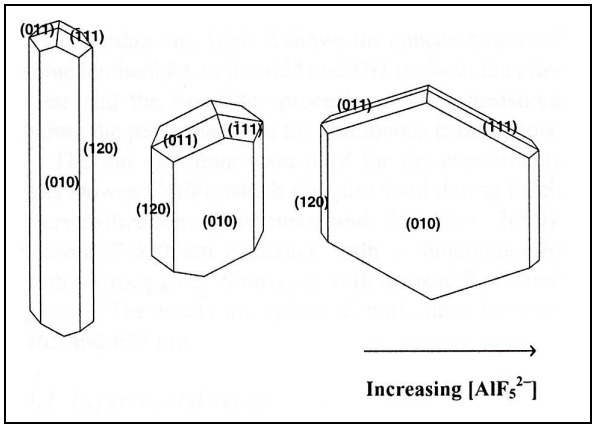

Figure 4.10: Changes in morphology as a function of AlF_5^{2-}-concentration.[41,42] Reproduced with permission of Delft University of Technology and Elsevier.

The aluminium concentration of the FGD gypsum and the phosphogypsum were similar (30-60 mmol kg^{-1}), while the fluoride to aluminium ratios were quite different (2:1 vs. 5:1).[39] The differences in the operating conditions of the two processes may, however, favour the formation and adsorption of different growth retarding aluminium fluoride complexes. Another possible explanation is crystal breakage along characteristic mineral planes facilitated by the increased crystal concentration and thereby an increased crystal collision frequency.[68]

4.6. Conclusions

This investigation of the gypsum quality at full-scale wet FGD plants has demonstrated that even though the PSD and morphology can remain relatively unchanged for prolonged periods of time, distinct changes in crystal morphology may take place within a few days. The crystal morphology at the three full-scale plants investigated all had amorphous shapes with few or no distinct crystal faces as opposed to the columnar pilot plant crystals with distinct crystal faces. A deterioration of the gypsum dewatering properties at APP3 was linked to a change in crystal morphology, thin plate shaped crystals, and an increased content of iron, aluminium and fluoride.

Unacceptable moisture contents in the final gypsum product may be a consequence of both the gypsum PSD and morphology. An increased processing time may to some extent overcome this, but efforts to change the PSD or morphology should also be considered. The presence of growth retarding species may influence the gypsum PSD and morphology. This effect may be reduced by an increased wastewater withdrawal, optimisation of the preceding particulate control device and a change of fuel/limestone. The supersaturation may furthermore influence the growth rate, the nucleation rate and the crystal morphology. The supersaturation in a wet FGD plant is influenced by the sulphur content of the fuel used, the desulphurisation degree as well as the total crystal area available for growth. Finally an increased slurry volume or solids concentration can provide a longer solid residence time, thereby yielding larger particles.

Chapter 5

Foaming in wet Flue Gas Desulphurisation plants

This chapter contains an investigation of the occurrence of foaming in wet FGD-plants. The results have been collected in the article "Foaming in Wet Flue Gas Desulfurization Plants: The Influence of Particles, Electrolytes, and Buffers", which has been published in *Industrial & Engineering Chemistry Research* **2008**, 47(9), 3239-3246. This article was written by Brian Brun Hansen, Søren Kiil, Jan Erik Johnsson and Klaus Bloksgaard Sønder (The Department of Chemical and Biochemical Engineering, Technical University of Denmark). The article is presented in the same form as it was printed, with only minor layout changes and a slight editing to avoid repetitions.

Abstract

The objective of this work is to study the influence of particles, electrolytes, and buffers on the foaming ability of wet FGD-slurries. Foaming within this industrial process has been associated with a range of operational problems, as well as an increased degree of absorption. The foaminess of selected process parameters has been assessed, systematically, using laboratory-scale Bikerman experiments. Adipic acid alone, as well as a combination of small particles and an electrolyte, have been demonstrated to generate weak transient foams (with a Bikerman coefficient (Σ) of $\leq$ 7 s), that potentially can interfere with process monitoring equipment. Additional experiments with a wet FGD pilot plant showed an increased absorption efficiency of sulphur dioxide (SO_2) by a tap water solution with small quartz particles and calcium chloride ($CaCl_2$), compared to a solution of pure tap water.

5.1 Introduction

A wide range of products contains a foam structure. Examples include fire fighting chemicals, polymeric insulation materials, shaving cream, and meringues/cakes. The presence of foam may also affect the customer's perception of the efficiency of a product, such as in the case of detergents, or provide an aesthetic appeal, such as in the case of personal care products and beer. Within industrial processes, foaming can be both beneficial and harmful. It can provide an increased interfacial area for absorption, protect melts from the atmosphere, or provide separation of different minerals by flotation. In other cases, foaming is associated with problems such as overflow to subsequent piping/reactors. Foaming within industrial processes can be identified by sight glasses, the withdrawal of samples, or via density measurements (radioactive scanning).[69]

One such industrial process is the wet FGD-process, in which SO_2 and other acidic compounds are removed from flue gases generated by fossil fuel (coal and oil) combustion. A range of different desulphurisation technologies exists, but the wet FGD-process covers the majority of the installed capacity worldwide.[4] The wet FGD-process consists of an absorber that brings a flue gas that contains acidic species (SO_2 and HCl) into contact with an alkaline slurry. The mass transfer of SO_2, and thereby the degree of desulphurisation, may be influenced by both gas-film resistance and liquid-film resistance, depending on the SO_2-concentration in the flue gas, the ratio of liquid to gas, and the reactant used. The influence of the liquid-film diffusion can be reduced by the presence of organic buffers in the slurry. The slurry leaving the absorber is collected in a holding/reaction tank, which often is an integrated part of the absorber. The wet FGD-process can be subdivided according to the way the gas-slurry contact is obtained. In the JBR absorber-design, the flue gas is bubbled through a tank that contains the slurry, while the counter-current spray tower and the co-current packed tower distribute the slurry as droplets, using atomising nozzles, or as a liquid film across the grid elements. In the two latter cases, the oxidation air will be bubbled through the liquid phase and stirrers will be present to keep the slurry well-mixed. Because of this difference in design, the superficial gas velocity of the gas phase that is passing through the slurry will be of a magnitude of 1 m s^{-1} in a JBR absorber, compared to 0.01 m s^{-1} in the other two designs. The stirring in the holding tank, as well as the splash from the falling slurry, will provide an additional incentive for foaming in the two latter cases.

Within the Danish power-plant sector, foaming in wet FGD-plants has been linked to problems such as interference with the online density and slurry level measurements, gypsum scaling in the demister, cavitation in recycle pumps, and overflow of the slurry tank. However, foaming may also provide an increased interfacial area for absorption of SO_2. The higher gas flow through the slurry in the JBR design generates a pronounced foaming. An increased degree of desulphurisation is observed when the flue gas stream passes through the foam layer on top of the slurry.[70]

The literature contains a few observations of foaming during wet FGD experiments,[62,70] but no systematic investigation of its source has been reported. However, a systematic investigation of foaming within another industrial process (sour water stripping) has been reported.[46] Foaming in the presence of 25 g $Cl^- L^{-1}$ has been reported for wet FGD pilot scale experiments with a falling-film column[62] as well as the JBR[70] design. The falling-film experiments showed a minor increase in the degree of desulphurisation (from 80% to 83%), whereas a significant increase was observed in the JBR experiments (from 80% to >99%). Foaming was observed in falling-film column experiments with $0.5 \cdot 10^{-2}$ and 10^{-2} M adipic acid but not in the presence of 10^{-2} M citric acid.[62] These organic acids provide an increased degree of desulphurisation (from 83 % to 90-92 %), because of their pH buffering effect; however, the slight difference in the degree of desulphurisation in the presence of 10^{-2} M adipic acid (92 %) and 10^{-2} M citric acid (90 %) may be the result of the observed foaming. An investigation of foaming in a packed tower for sour water stripping, which is classified as a heavy foaming system,[71] has furthermore been reported in the literature.[46] Based on Bikerman experiments and gas chromatography-mass spectroscopy (GC-MS) measurements, the foaming compounds were identified as impurities (phenol and p-cresol) that were present in the feed, which were further enriched within the packed tower. These impurities contained both hydrophilic and hydrophobic parts, making them surface-active.

This work will focus on the foaming problems that occasionally occur in wet FGD-plants. Because the combustion of fossil fuels supplies a substantial part of the world's present energy demand, and is expected to continue to do so in the coming years,[1] an increased understanding of the various aspects of the FGD-technologies is important to the power-plant industry.

5.2 Foaming theory

Bubbles in a liquid may form as a result of injected air, stirring, or the flow conditions that are present. The balance between the arrival of new bubbles to the surface and their persistence (lifetime) determines if an accumulation of bubbles, and thereby foam formation, will occur. Kitchener classified foams into the following three categories, according to their persistence and composition:[72]

(1) Temporary dispersions, which involve spherical bubbles in a foam layer with an air content of < 74%.

(2) Transient foams, which involve polyhedron bubbles in a foam layer with a short average bubble lifetime.

(3) Persistent foams, which involve polyhedron bubbles in a foam layer with a considerable average bubble lifetime.

The persistence of a foam will be influenced by gravity-induced drainage of the bubble walls (lamella), gas diffusion between the bubbles, attractive/repulsive forces of the approaching surfaces, and capillary flow toward the plateau border that is induced by the lower pressure above a curved surface (see Figure 5.1). Foaming agents that provide increased bubble persistence include surfactants, macromolecules (such as polymers or proteins), or finely dispersed solids.[46]

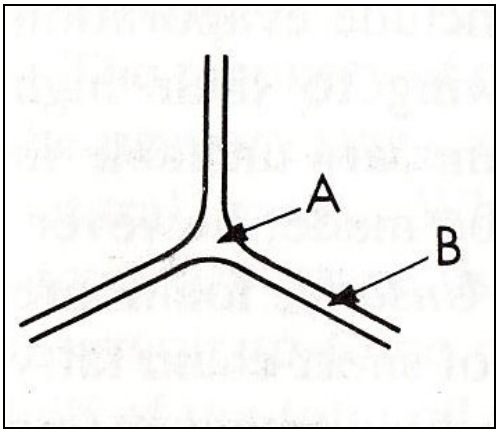

Figure 5.1: Plateau border at the intersection of three bubbles; the curvature at point A causes a lower pressure of the liquid than that at point B, thereby inducing capillary flow toward the Plateau border.[45] Reprinted with permission of Elsevier.

Surfactants and macromolecules preferably arrange themselves at the liquid/gas interface, thereby reducing the surface tension of the solution and the additional energy required to generate the increased surface area present in foams. Furthermore, the lamella will have an increased elasticity/resistance to local film thinning, because of the Marangoni effect, i.e., the restoring liquid flow induced by the decreased surfactant concentration at the thinned region (increased surface area). Furthermore, the foam stability may benefit from an increased viscosity and the sterical/electrostatic double-layer interaction when two bubble surfaces come within 100 nm of each other.[47]

Foaming systems in which solid particles are present are often called froths. Particles adhering at the gas/liquid interface can be envisioned as an armoured layer around the bubbles, which increases the strength of the froth and decreases the drainage rate of the lamella.[47] Increasing the particle hydrophobicity will promote the adhesion process; however, if this property becomes too pronounced (with a contact angle of >90°), the particles may act as air bridges through the lamella,[47] thereby destabilising the froth. The stabilising effect of particles, consequently, will be dependent on their size, shape, and hydrophobicity/wettability.[47,48] Electrolytes may promote the adhesion of particles to the gas/liquid interface, through a reduction of the electrostatic repulsion between the particles and the bubbles (a thinner electrostatic double layer) and interactions that increase the hydrophobicity of the particle surface.[47,48] A thinner electrostatic double layer may also destabilise the dispersion and lead to particle flocculation. The thickness of the electrostatic double layer (κ^{-1}), as expressed by equation 5.01, will be dependent on the type, charge, and concentration of the electrolyte.

$$\kappa^{-1} = \sqrt{\frac{\varepsilon_0 \cdot \varepsilon_r \cdot k_b \cdot T}{N_a \cdot q^2 \cdot \sum_i C_{i,b} \cdot z_i^2}} \qquad (5.01)$$

5.3 Strategy of Investigation

This investigation of the occurrence of foaming in wet FGD-plants consists of laboratory as well as pilot-scale experiments. The purpose is to explore, systematically, the effect on foaming for several relevant compounds present in FGD-slurries. These compounds, which are presented in Table 5.1, have been selected based on knowledge of the wet FGD-process as well as the overview provided in the Introduction. The concentration ranges provided represent realistic conditions that prevail in full-scale wet FGD-plants. $CaCl_2 \cdot 2H_2O$ is used to simulate the presence of Ca^{2+} and Cl^- ions in full-scale wet FGD-plants. The Cl^- ions originate from gaseous HCl that has been absorbed in the slurry.[57]

Table 5.1: Parameters Selected for Further Investigation.

Parameters	Concentration	Chemical
Additives		
Adipic acid	10^{-2} M	Adipic acid
Ions		
Sulphate	1.2 g L^{-1}	Sodium sulphate (Na_2SO_4)
Chloride	25 g L^{-1}	Calcium chloride ($CaCl_2 \cdot 2H_2O$)
Particles		
Limestone	30 g L^{-1}	Faxe foderkalk
Gypsum	300-380 g L^{-1}	FGD gypsum, with a few wt. % limestone

In addition to additives, ions, and particles, the microbiology present within full-scale wet FGD-plants may also be a potential source of foaming. The carboxylic acids used as organic buffers within a wet FGD-plant may provide a carbon source for bacteria present in the warm (~50 °C) slurry.[73] This biomass will release macromolecules and proteins during its degradation, thereby introducing foaming agents to the system. Foaming, as seen along the shores of lakes and oceans during autumn, may be the consequence. However, this aspect will not be addressed in this investigation because of the absence of microbiological activity in the pilot plant.

A Bikerman column has been used for the initial laboratory-scale screening of the different parameters in solutions of demineralised water at room temperature. Based on the results of this screening, further experiments and surface tension measurements (using a Wilhelmy plate) have been performed to identify the mechanisms that cause foam and their concentration dependence. Selected foaming mixtures have then been used in a falling-film

pilot plant to investigate the influence of foaming on SO_2 absorption. Finally, considerations regarding the transfer of the result to industrial scale have been performed.

5.4 Experimental Setup and Procedure

5.4.1 The Bikerman Method

The Bikerman method belongs to the dynamic type of foam measurement techniques, in which the foam height is determined by a dynamic equilibrium between the rate of bubble formation and the rate of bubble collapse. This type of technique is especially useful in the case of solutions with a low foamability.[46]

The experimental setup consists of a glass column (with an inner diameter of D_i = 0.07 m) that has been equipped with a porous glass disc in the bottom. Bubbles are generated by a flow of nitrogen through the porous glass disc. The experiments were performed at room temperature using 0.1 L of the different solutions. The foam height (h), as a function of gas flow rate (u_{su}), is recorded and used to calculate Bikerman/foaminess coefficients of the solution (Σ):

$$\Sigma = \frac{h}{u_{su}} \tag{5.2}$$

This coefficient expresses the average bubble lifetime in the foam before it bursts. Σ is reported to be independent of gas flow rate, the shape, and dimensions of the column and the amount of solution present, provided that evaporation (low gas velocities) or rupture of the lamella (high gas velocities) is not significant.[74]

5.4.2 SO_2 absorption in a wet FGD Pilot Plant

A detailed introduction for the wet FGD pilot plant has previously been given in section 3.4.1. During normal desulphurisation operation, the additives, ions, and particles mentioned in Table 5.1 will be present simultaneously. To investigate the influence of individual parameters, the degree of absorption will be investigated by absorbing SO_2 from a 500 ppm(v)

flue gas stream, using tap water solutions of salts and/or particles at a liquid to gas ratio of 13.1-13.5 L m^{-3} (at 273.15 K and 101.3 kPa). Before an experiment was started, the holding tank was filled with a 30-L batch of tap water (Eastern Zealand-Denmark) that contained a carbonate buffer. During the experiments, neither the addition of an alkaline feed stream nor the withdrawal of a product stream was performed. As the buffering effect from the bicarbonate (HCO_3^-)/carbonic acid (H_2CO_3) equilibrium is being used up by the SO_2 that is absorbed, the pH of the holding tank will decline from ~7 until the experiment is stopped at pH 6.2, after ~20-30 min. In this pH range, the buffering effect from the carbonate/ bicarbonate (CO_3^{2-}/HCO_3^-) equilibrium will be negligible (pK_a = 10.33).[65] Based on the amount of SO_2 supplied (equation 5.03) and the amount that absorbs and reacts with bicarbonate (equations 5.04-5.07), the average absorption efficiency can be calculated (equation 5.08).

$$n_{SO_2 in} = \frac{\Delta t \cdot Q_g \cdot \Phi_{SO_2,in}}{V_{m,SO_2}} \tag{5.03}$$

$$n_{SO_2,ab} = V \cdot \Delta C_{HCO_3^-} \tag{5.04}$$

$$pH = pK_a + \log \frac{C_{HCO_3^-}}{C_{H_2CO_3}} \tag{5.05}$$

Rearranging leads to

$$\rightarrow \frac{C_{HCO_3^-}}{C_{HCO_3^-} + C_{H_2CO_3}} = \frac{10^{pH-pK_a}}{1+10^{pH-pK_a}} \tag{5.06}$$

$$\Delta C_{HCO_3^-} = C_{HCO_3^-,in}\left(\left(\frac{10^{pH_{in}-pK_a}}{1+10^{pH_{in}-pK_a}}\right)-\left(\frac{10^{pH_f-pK_a}}{1+10^{pH_f-pK_a}}\right)\right) \tag{5.07}$$

$$\eta_a = \frac{n_{SO_2,ab}}{n_{so_2,in}} \cdot 100 \tag{5.08}$$

Foaming within the pilot plant may be initiated by the oxidation air that is introduced (u_{su} = 0.002 m s^-), from the stirring and from the splash caused by the falling film onto the slurry surface in the holding tank. The degree of hardness of the tap water used (19°dH) corresponds to a HCO_3^--concentration of $6.78 \cdot 10^{-3}$ M.[75]

5.5 Results and Discussion

5.5.1 Initial Bikerman Screening

The foamability of the selected process parameters will be evaluated based on the additional height (Δh) that a foaming solution generates, compared to the foaming height of demineralised water.

$$\Delta h = h_{fo} - h_{wa} \tag{5.09}$$

This quantity will be investigated for superficial gas velocities, u_{su} , in the range of 0.002-0.070 m s^{-1}, thereby covering the average superficial gas velocity of oxidation air (0.01 m s^{-1}) in gypsum-producing wet FGD-plants. Furthermore, it will be noted whether a given solution generates a foam layer or not. However, a non-foaming solution may still generate a small transition zone where individual bubbles burst. The difference, in terms of bubble size and structure, between a foaming and a non-foaming solution is illustrated by Figure 5.2.

Figure 5.2: Foaming behaviour illustrated by 10^{-2} M adipic acid solution (left) and the bubble transition layer formed in the absence of foaming illustrated by demineralised water (right). Both have a velocity of u_{su} = 0.01 m s^{-1}.

Figures 5.3 show the foam height, as a function of superficial gas velocity, of single-process-parameter solutions and particle mixtures. Furthermore, Table 5.2 summarises the outcome of the Bikerman experiments, in terms of whether a foam layer is formed or not and the corresponding Bikerman coefficient, in the case of foaming mixtures.

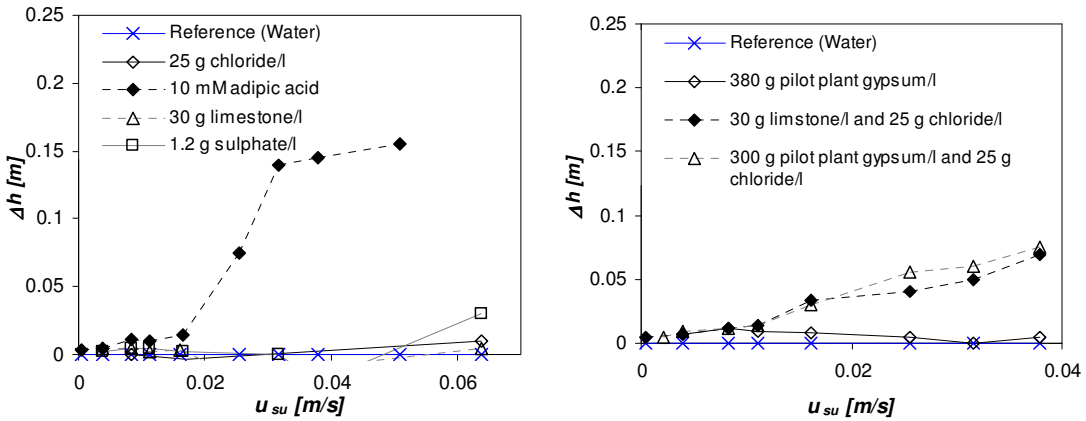

Figure 5.3: Foam layer height (h) of single parameters (left) and particle mixtures (right), as a function of the superficial gas velocity (u_{su}).

Table 5.2: Foamability of the Examined Process Parameters.

Single component mixtures	**Multiple component mixtures**
Non-foaming	
demineralised water	adipic acid + limestone
limestone	gypsum (~5wt% limestone)
sulphate	chloride + sulphate
gypsum	sulphate + limestone
chloride	
Foaming [a]	
adipic acid: Σ = 6.0 s	adipic acid + sulphate: Σ = 7.0 s
	adipic acid + chloride: Σ = 6.0 s
	chloride + limestone: Σ = 3.2 s
	chloride + gypsum: Σ = 3.5 s

[a] Σ [s] at u_{su} = 0.032 m s^{-1}

The only single parameter that caused foaming was the 10^{-2} M adipic acid solution; no foaming was observed in the solutions that contained only limestone, Na_2SO_4, gypsum, or $CaCl_2$. The mixtures that contained adipic acid and Na_2SO_4/$CaCl_2$ caused foaming to an extent similar to that generated by adipic acid itself (Σ = 6-7 s). Particle mixtures (limestone and gypsum) that contained a high electrolyte concentration (25 g Cl^- L^{-1}) also generated foaming, but to a lesser extent than observed with the adipic acid foams. The Bikerman coefficient of the adipic acid solution was slightly higher (Σ = 6.0-7.0 s) than that for the particle mixtures (Σ = 3.2-3.5 s), but both cases must be classified as relatively weak transient foams. The foaming solutions all began foaming above a superficial gas velocity of 0.01-0.02 m s^{-1}. No foaming was observed for mixtures of adipic acid and limestone, gypsum and limestone, $CaCl_2$ and Na_2SO_4, and limestone and Na_2SO_4. The absence of foaming by the adipic acid and limestone mixture is surprising, but it may be related to the fact that an excess of limestone is present. The limestone can react with the adipic acid, yielding its conjugated base, which apparently may remain in solution instead of orienting itself toward the gas/liquid interface.

Figure 5.4 shows the foam height of multiple experiments with gypsum and Cl^- mixtures, demonstrating a good repeatability between the individual experiments.

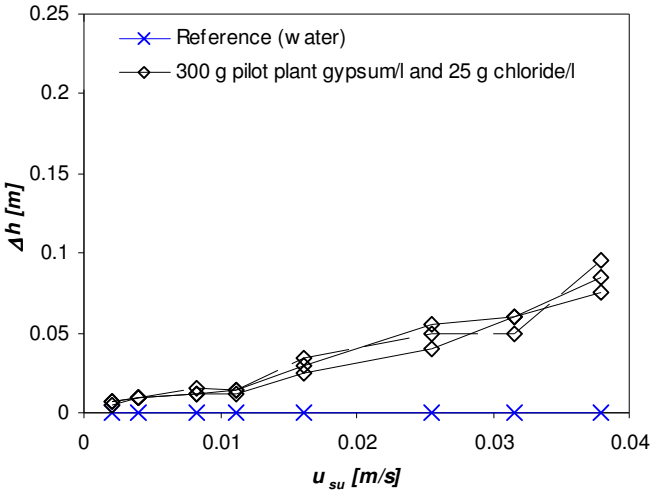

Figure 5.4: Repeatability of the observed foam layer height (h), illustrated here with three gypsum and 25 g Cl^- L^{-1} experiments.

5.5.2 Adipic Acid Mechanism

Adipic acid (HOOC-$(CH_2)_4$-COOH) consists of both hydrophilic (two acid groups) and hydrophobic parts (a hydrocarbon backbone), so its behaviour, in terms of foaming, is expected to be similar to that of simple carboxylic acids. In an overview of the foaming behaviour of different compounds, Bikerman has presented dynamic as well as static data for the foamability of several monoprotic carboxylic acids.[74] The maximal foaminess coefficient of a given solution (equation 5.02) increased from formic acid (2.9 s) to hexanoic acid (37 s), whereas the concentration (mass percentage), at which this occurred, decreased from 8.8% to 0.035%. The time of collapse of a foam after shaking (static method) showed a similar behaviour through the series of formic acid to heptanoic acid, after which it declined. Note that the foaminess of fatty acids is dependent on their ionisation and, thereby, the pH. The maximal foamability is obtained at high pH values, but even below the pK_a, some foamability may remain, as in the case of heptanoic acid.[76] The foaminess coefficient obtained for adipic acid in this investigation (Σ = 6.0 s at 1460 ppm) is somewhat less than the value reported for its monoprotic counterpart, hexanoic acid: Σ = 37 s at 350 ppm. This difference is expected because of the difference in concentration and hydrophobicity of the two compounds.

If the adipic acid is positioning itself at the interface between air and water, as a surfactant, a decrease in surface tension is expected. Typical surfactants can form micelles and consist of a long hydrocarbon tail, as opposed to the short hydrocarbon backbone (four carbon atoms) of adipic acid. To verify if this positioning was occurring, surface tension measurements using the Wilhelmy plate method were performed for the particle-free mixtures. The results obtained are presented in Table 5.3. However, no significant difference in surface tension could be detected in any of the samples. An additional Bikerman experiment with 10^{-2} M citric acid (a triprotic carboxylic acid) did not generate any foaming. This indicates that differences in hydrophility influence foaming, possibly because of differences in the affinity for positioning at the air/water interface.

Table 5.3: Surface tension of solutions

Parameter	Concentration	Average surface tension[b] (mN/m)
Demineralised water		72.8[c]
Adipic acid	10^{-2} M	71.7 (0.9)
Sulphate	1.2 g L^{-1}	70.7 (0.8)
Chloride	25 g L^{-1}	72.0 (1.2)

[b] Standard deviation given in parenthesis.

[c] Reference value taken from the literature.[65]

To investigate whether the absence of a decrease in surface tension was due to the limitations of the measuring technique, additional surface tension measurements (Table 5.4), as well as Bikerman experiments (Figure 5.5), have been performed for solutions of sodium dodecyl sulphate (SDS), which is a classical anionic surfactant.

Table 5.4: Surface tension and Bikerman index of SDS solutions[d]

SDS-Concentration [M]	Average surface tension [mN m^{-1}] [e]	Σ [s][f]
10^{-2}	32.3 (0.3)	[g]
$5 \cdot 10^{-3}$	28.1 (0.8)	[g]
$2 \cdot 10^{-3}$	36.4 (2.3)	[g]
10^{-3}	43.6 (0.5)	[g]
$5 \cdot 10^{-4}$	55.1 (0.3)	[g]
$3 \cdot 10^{-4}$	62.3 (0.7)	4.7
10^{-4}	68.5 (1.1)	3.8
$7 \cdot 10^{-5}$	71.6 (0.8)	1.3

[d] All concentration levels resulted in foaming.

[e] Standard deviation given in parenthesis.

[f] at u_{su} = 0.032 m/s.

[g] No Bikerman coefficient determined.

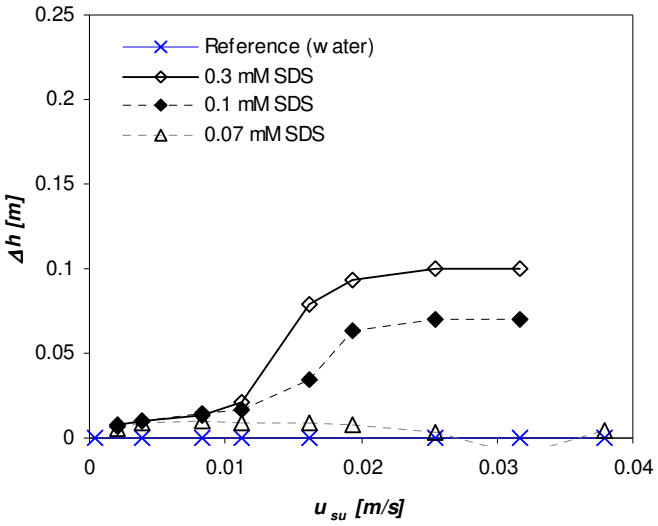

Figure 5.5: Foam layer height (h) for different Sodium dodecyl sulphate solutions, as a function of the superficial gas velocity (u_{su}).

The surface tension of a $7 \cdot 10^{-5}$ M solution of SDS surfactant could not be distinguished from that of pure water, despite the fact that the solution did generate a foam layer of limited average bubble lifetime (Σ = 1.3 s), compared to the more-concentrated (10^{-2} M) adipic acid solution (Σ = 6.0 s). The 10^{-4} M SDS solution produced a significant foam layer (Σ = 3.8 s) and did show a decrease in surface tension. Therefore, changes in surface tension that were too small to be detected by the Wilhelmy plate setup may still facilitate foaming. The foaming potential of adipic acid may consequently be the result of a surfactant-like behaviour of the adipic acid molecules, causing a small decrease in surface tension, an increased elasticity of the lamella, and/or an increased interfacial viscosity.

5.5.3 Particle and Electrolyte Mechanism

The foaming mechanism for the Cl^- and particle mixtures (limestone and gypsum) has been investigated by additional Bikerman experiments, using two different sizes of quartz particles and various electrolytes. Because quartz has been reported to be a strongly hydrophilic mineral,[45] which is completely wettable by water, no foamability is expected from the particles themselves. This was confirmed by experiments with quartz particles in demineralised water. Figure 5.6 shows a comparison of the particle size distributions of the two types of quartz particles, as well as the limestone and the FGD gypsum.

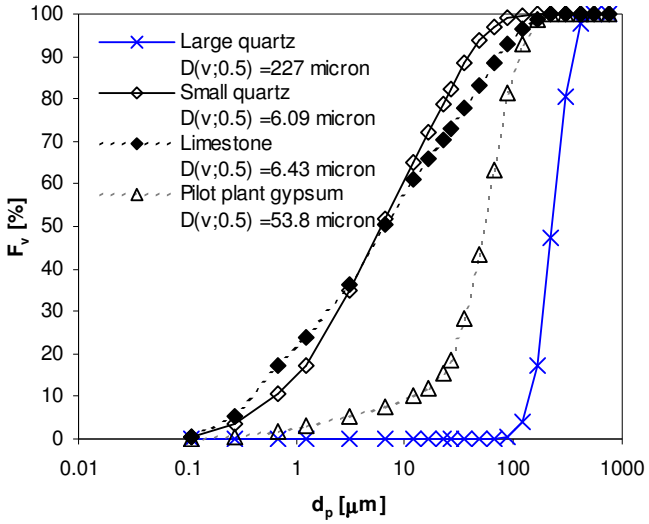

Figure 5.6: Cumulative volumetric particle size distribution of quartz, limestone, and gypsum.

The measured foam height of quartz and electrolyte mixtures, as illustrated by Figure 5.07, shows the importance of particle size on the foaming ability of a solution. Although the small quartz particles in the presence of an electrolyte are able to produce a weak transient foam layer, the corresponding large particles are unable to generate foam. The concentration ranges used for the two quartz types have been selected to simulate the concentration ranges of limestone and gypsum particles in wet FGD-plants, respectively. This is in agreement with the literature, which states that the stabilising effect of particles will increase as the particle size decreases, among other factors.[47] Table 5.5 summarises the foaming behaviour for a range of small-quartz-particle slurries in the presence of different electrolytes.

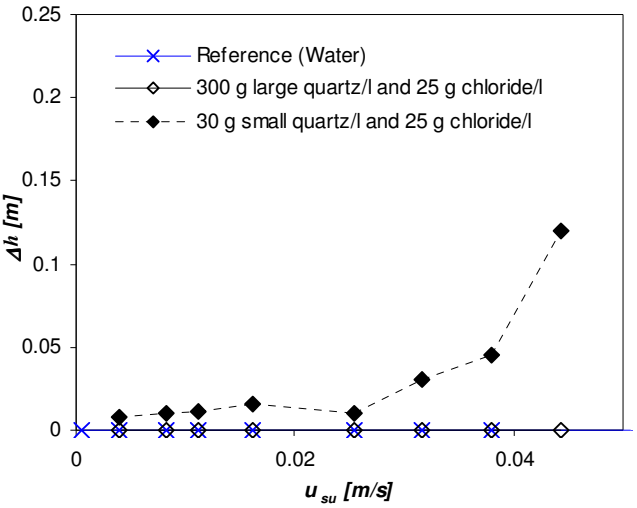

Figure 5.7: Foam layer height (h), for quartz mixtures, as a function of the superficial gas velocity (u_{su}).

Table 5.5: Influence of Selected Electrolytes on the Foamability of Small Quartz Particles

Concentration [g L^{-1}]	**Electrolyte**	**Foam**?	Σ^{h} [s]
	Small Quartz Particles		
30g L^{-1}		no	
	Small Quartz Particles + Chloride		
30g/l + 25g Cl^{-} L^{-1}	$CaCl_2$	yes	2.5
30g/l + 25g Cl^{-} L^{-1}	KCl	yes	1.6
30g/l + 25g Cl^{-} L^{-1}	$BaCl_2$	yes	2.8
30g/l + 25g Cl^{-} L^{-1}	HCl	no	
	Small Quartz Particles + Bromide		
30g/l + 25g Br^{-} L^{-1}	$CaBr_2$	yes	1.3

h Σ [s] at u_{su} = 0.032 m s^{-1}

The hydrophilic quartz particles do not show any foaming behaviour by themselves; however, in the presence of the various electrolytes, a weak transient foam (Σ = 1.3-2.8 s) was observed. The only notable exception to this is the absence of foaming in the presence of HCl. The foaming is believed to be the result of a reduction of the electrostatic repulsion between particles and bubbles (a thinner electrostatic double layer), as well as surface modifications, facilitated by the electrolytes, which generates more hydrophobic particles, as it has been

reported in the literature for experiments that involve modified silica particles.[48] The particles can then adsorb at the liquid/air interface, because of their increased hydrophobicity, and thereby provide a strengthening effect to the bubbles as well as a decreased drainage rate. A reduced foamability in the presence of HCl (pH 2-3) has been reported in the literature for experiments that involve modified anatase (titanium dioxide) particles.[77] Particle flocculation that is due to a weaker surface charge and a thinner electrostatic double layer is used to explain the decrease in foamability. Therefore, the absence of foaming in the quartz and HCl experiment may be the consequence of the flocculation of particles that is due to a weaker surface charge and a thinner electrostatic double layer at the low pH of the solution.

5.5.4 Influence of Particle and Electrolyte Concentration

A parameter analysis of the influence of the particle and electrolyte concentrations on the foamability has been performed using a series of Bikerman experiments. Figure 5.8 shows the foam height h, as a function of quartz and Cl^--concentration (u_{su} = 0.010-0.044 m s^{-1}), and Tables 5.6 and 5.7 summarise whether foaming was observed, as well as the corresponding Bikerman coefficient (u_{su} = 0.032 m s^{-1}). Only marginal or no foaming was observed below a particle concentration of 5 g L^{-1} and a Cl^--concentration of 5 g L^{-1}. The effect of the particle and Cl^--concentration was most pronounced at the highest superficial gas velocities. Above a Cl^--concentration of 10 g L^{-1}, no additional positive effect on the foam height was observed.

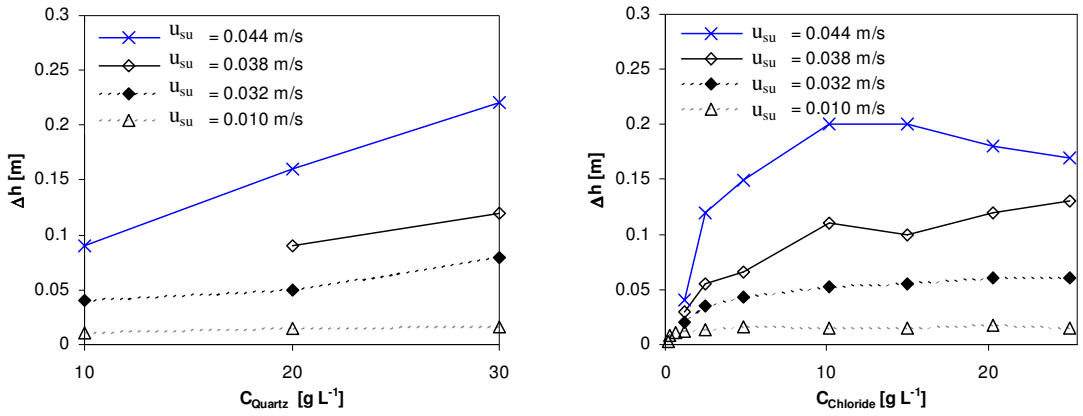

Figure 5.8: Foam layer height (h), as a function of quartz concentration using 25 g Cl^- L^{-1} (left) and as a function of Cl^--concentration using a small quartz concentration of 30 g L^{-1} (right).

Table 5.6: Effect of Quartz Concentration (Small Particles) on the Foamability

Quartz concentration [g L^{-1}]	**Chloride concentration** [g L^{-1}]	**Foam?**	Σ^{i} [s]
30	25	yes	2.5
20	25	yes	1.6
10	25	yes	1.3
5	25	no	

[i] at u_{su} = 0.032 m s^{-1}

Table 5.7: Effect of Cl^--Concentration on the Foamability

Quartz concentration [g L^{-1}]	**Chloride concentration** [g L^{-1}]	**Foam?**	Σ^{j} [s]
30	25	yes	1.9
30	20	yes	1.9
30	15	yes	1.7
30	10	yes	1.7
30	5	yes	1.4
30	2.5	yes	1.1
30	1.2	yes	0.6
30	0.15	no	

[j] at u_{su} = 0.032 m s^{-1}

5.5.5 Pilot Plant Experiments

To investigate the influence of foaming on the SO_2 absorption in tap water, experiments with a foaming mixture of small quartz particles and $CaCl_2$ have been performed in the pilot plant. Figure 5.9 shows the pilot-plant SO_2 absorption efficiencies of tap water in the presence of quartz particles and an electrolyte, calculated based on the observed rate of pH decline.

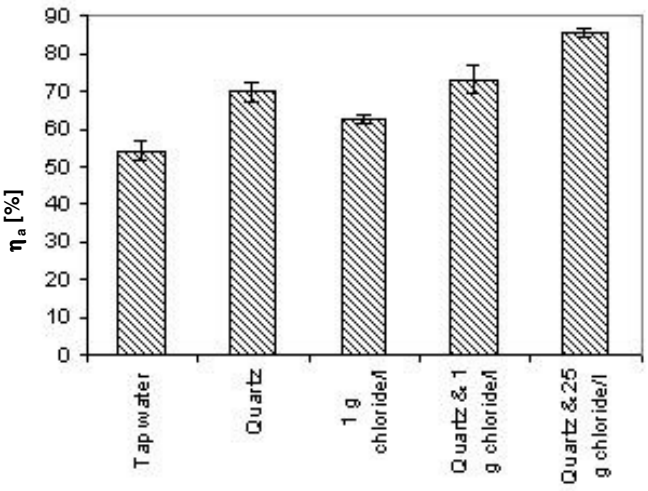

Figure 5.9: Average absorption efficiency in the wet FGD pilot plant (Standard deviation indicated by error bars). Quartz experiments have been performed with the small quartz particles using a concentration of 30 g L^{-1}.

An enhanced mass transfer is obtained in the presence of either small quartz particles (at a concentration of 30 g L^{-1}) or Cl^- (at a concentration of 1 g L^{-1}); however, no additional effect is observed for a mixture of these components. This corresponds well with the fact that only a marginal foaming has been observed for this mixture in the Bikerman column. The higher absorption efficiency of the particle solution may be the consequence of an increased gas/liquid interfacial area of the falling film, as has been reported for gas-liquid slurry reactors.[78] The slightly increased absorption efficiency in the presence of the electrolyte (1 g Cl^- L^{-1}) is rather surprising, because neither the activity coefficients nor the SO_2 solubility are expected to change significantly.[79] It has not been possible to find an explanation for this observation. In the case of small quartz particles and 30 g Cl^- L^{-1}, foaming occurred in the Bikerman column and an increased average absorption degree was observed in the pilot plant, possibly because of foaming.

5.5.6 Discussion

The Bikerman screening showed that solutions of adipic acid or a combination of small particles and an electrolyte are able to generate weak transient foams (Σ = 1.0-7.0 s). The adipic acid may adhere at the gas/liquid interface that surrounds the bubbles, because of the presence of both hydrophobic and hydrophilic parts within the molecule. Adhesion at the gas/liquid interface can provide a slight reduction in the surface tension, as well as increased elasticity of the lamella, thereby providing a stabilising effect on the foam. However, surface tension measurements were unable to confirm this theory. The foamability of adipic acid under industrial conditions may be somewhat lower than the result in this investigation, because of the operation at pH values close to the pK_a of adipic acid (5.41 and 4.41).[65] The foaming in the presence of small particles and electrolytes is believed to originate from the adhesion of particles at the liquid/air interface, where they provide a strengthening effect, as well as a decreased drainage rate. The adhesion can be facilitated by an increased hydrophobicity of the particles, through an increased screening of the electrostatic repulsion between particles, as well as modifications of the particle surface, by electrolytes present in the solution.

Foaming has been observed at and above superficial gas velocities of 0.01 m s^{-1}. This corresponds to the average superficial gas velocity of oxidation air in forced-oxidation wet FGD-plants. Depending on the design and the operating conditions of the plant, however, higher superficial gas velocities may be present, thereby providing an increased foaming potential. The observed weak transient foams might very well interfere with the on-line density and slurry-level measurements within a full-scale wet FGD-plant. More persistent foams, which cause the overflow of storage tanks and scaling at the demister, are more likely to originate from microbiology within the plant, rather than particles, electrolytes, or buffers.

5.6 Conclusions

This systematic investigation of foaming in wet FGD-plants has demonstrated that solutions of adipic acid, or a combination of small particles and an electrolyte, are able to generate weak transient foams (with a Bikerman coefficient of Σ = 1.0-7.0 s). The foaming has been observed at an adipic acid concentration of 10^{-2} M, particle concentrations of $\geq$ 5 g L^{-1}, and electrolyte concentrations of $\geq$ 5 g Cl^{-} L^{-1}. These two foaming mechanisms might explain the pilot-plant observations of foaming that have been reported in the literature.[62,70]

Foaming in a full-scale wet FGD-plant may be caused by the two described mechanisms, as well as microbiology. All three possible mechanisms must be considered when a foaming problem is encountered. Apart from the addition of foam breakers, such as oils, the operator should consider whether the level of organic buffers, small particles, or electrolytes could be changed. A decrease in the level of organic buffers would, apart from the reduced foamability, also decrease the carbon source available to any microbiology present. The level of small particles could be decreased by an increased performance of the preceding particulate control device, as well as the withdrawal of fly ash and other small particles from the plant. An increased withdrawal of wastewater can be used to decrease the electrolyte concentration in a plant, but one should be aware that a decreasing Cl^{-}-concentration could enhance microbiological growth.

Weak transient foams, such as the two mechanisms observed in this investigation, can provide an increased surface area for absorption processes, thereby improving their overall performance. A foaming solution of small quartz particles and $CaCl_2$ showed an increased absorption efficiency of SO_2 during wet FGD pilot-scale experiments with tap water. This may be of interest to industrial absorption processes other than the wet FGD-process.

Chapter 6

Conclusions and suggestions for further work

This chapter summarises the overall conclusions of the work, concerning gypsum crystallisation and foaming in wet FGD-plants, presented in the preceding chapters and subsequently highlight aspects, which may benefit from further attention.

6.1 Conclusions

The combustion of fossil fuels, such as coal and oil, plays a significant role in the global energy supply and is expected to continue to do so in the coming years. The limestone-based wet flue gas desulphurisation process removes SO_2 from the flue gas, thereby abating the detrimental effects known as "acid rain". A commercial product (i.e. gypsum) is furthermore obtained by crystallisation. The performance of wet FGD-plants may be severely affected by poor gypsum dewatering properties and the unexpected and unwanted occurrence of foaming.

The crystallisation process determines the quality and sales potential of the produced gypsum in terms of dewatering properties (i.e. PSD and morphology), impurity content and colour. The incorporation of impurities into the gypsum crystal lattice may have a distinct effect on the growth rate of the individual crystal faces and thereby the obtained morphology. A deterioration of the gypsum dewatering properties at unit 3 of Amager power plant have been linked to a distinct change in morphology and an increased incorporation of aluminium fluoride into the crystal lattice. The PSD obtained in a crystalliser, such as a wet FGD-plant, will depend on the nucleation rate, the subsequent crystal growth rate and breakage/attrition. The extent of breakage/attrition at pilot-scale conditions has been quantified based on transient experiments and population balance modelling.

A minor increase in the fraction of small particles during desulphurisation was predicted, but not to an extent significantly affecting the overall PSD. The rounded crystal shapes and the lack of distinct crystal faces, observed at full-scale conditions might, however, indicate that breakage/attrition is of importance in full-scale wet FGD-plants. The gypsum PSD obtained during desulphurisation in the pilot plant was found to be similar to the PSD observed at the three investigated full-scale wet FGD-plants. A three-parameter, size-dependent growth model, previously used in the literature to describe $Na_2SO_4 \cdot 10H_2O$ and $KAl(SO_4)_2 \cdot 12H_2O$ crystallisation, has been shown to describe the PSD obtained in the pilot plant. Size-dependent integration kinetics, due to dislocations, impurities and collisions are considered the most likely explanation for the observed size-dependence of the crystal growth rate.

A practical implication of these findings is that the slower growth rate of small crystals, favour crystallisers with selective removal of large particles, leaving the small crystals in the crystalliser for further growth. This is, to some extent, being done at full-scale wet FGD-plants by the hydro-cyclones used to decrease the water content of the product stream, thereby generating a lean stream, containing the small particles, for recirculation to the holding tank. It should furthermore be noted that changes in both gypsum PSD and morphology might cause unacceptable moisture contents in the final gypsum product. The presence of growth retarding species may be countered by an increased rate of wastewater withdrawal, optimisation of the preceding particulate control device or a change of fuel/limestone. The nucleation rate, the crystal growth rate and the extent of breakage/attrition will determine the PSD obtained, thereby making the optimal operating conditions, in terms of gypsum crystallisation, plant specific and time dependent.

Foaming within industrial processes takes place because of an increased bubble persistence, caused by surfactants, macromolecules (such as polymers or proteins), or finely dispersed solids. Excessive foaming within wet FGD-plants has been associated with operational problems as well as an increased degree of absorption. Laboratory scale experiments concerning particles, electrolytes and buffers, present in a wet FGD-plant, showed that adipic acid, as well as a combination of small particles and an electrolyte, generated weak transient foams. Additional pilot plant experiments showed an increased absorption efficiency of SO_2

by a foaming tap water solution with small quartz particles and $CaCl_2$ compared to non-foaming tap water.

When foaming is encountered in a full-scale wet FGD-plant the initial approach will usually be the addition of foam breakers (defoamers), but an identification and elimination of the foaming agent will ensure a more lasting solution to the problem. Possible initiatives include: To avoid the addition of organic buffer, an increased rate of wastewater withdrawal, and an optimisation of the preceding particulate control devise. The potential increased absorption efficiencies by solutions creating weak transient foams may also be of interest to other industrial absorption processes.

6.2 Suggestions for further work

Growth & nucleation rate – Knowledge of the kinetic parameters (rate constants and exponents) of the nucleation rate and the surface integration controlled growth rate equations from the literature is necessary in order to model the gypsum crystallisation in a wet FGD-plant. To determine these parameters additional experimental data at different supersaturations, stirring rates and crystal concentrations must be performed. In order to transfer the results to full-scale wet FGD operation, the extent of breakage taking place in these plants needs to be quantified. The solution of transient population balances could furthermore increase the amount of information obtained from the individual experiments and help to validate the model against full-scale conditions.

Crystal morphology – Additional pilot plant experiments could be used to determine the concentrations of aluminium fluoride, and other impurities, that are capable of generating significant changes in gypsum crystal morphology. The influence of the limestone size and purity on the obtained gypsum quality could furthermore be investigated. Future full-scale episodes with poor dewatering properties, might be used to identify additional species/operating conditions that are capable of generating changes in morphology and PSD.

Foaming – One aspect that needs to be addressed is the evaluation of the efficiency of different potential defoamers, i.e. oils and hydrophobic particles. Bikerman experiments with either a prepared foaming solution or foaming slurry would be well suited for this purpose.

Nomenclature

a	Ionic activity [M]
a_1	Empirical parameter in Mydlarz & Jones growth model [μm^{-1}]
a_2	Empirical parameter in Mydlarz & Jones growth model [μm]
A	Area [μm^2]
B^0	Nucleation rate [$L^{-1}\ hr^{-1}$]
$B(l)$	Birth term [$\mu m^{-1}\ L^{-1}\ hr^{-1}$]
$B(v)$	Birth term [$\mu m^{-3}\ L^{-1}\ hr^{-1}$]
C	Ionic concentration [mol L^{-1} or equivalents L^{-1}]
C_m	Mass concentration [g L^{-1} or wt%]
D	Diameter [m]
D_{10}	Particle size under which 10 % of the particle volume is located [μm]
D_{50}	Particle size under which 50 % of the particle volume is located [μm]
D_{90}	Particle size under which 90 % of the particle volume is located [μm]
$D_{3.2}$	Sauter mean diameter [μm]
$D(l)$	Death term [$\mu m^{-1}\ L^{-1}\ hr^{-1}$]
$D(v)$	Death term [$\mu m^{-3}\ L^{-1}\ hr^{-1}$]
d_p	Particle diameter [μm]
e_1	Empirical nucleation rate parameter, eq. 2.05
e_2	Empirical nucleation rate parameter, eq. 2.05
e_3	Empirical nucleation rate parameter, eq. 2.05
e_4	Growth rate exponent, eq. 2.08
e_5	Empirical breakage rate parameter, eq. 3.06
F_v	Cumulative volume fraction of particles
G	Linear growth rate [$\mu m\ hr^{-1}$]

G_m	Maximal linear crystal growth rate [μm hr^{-1}]
Gi	Free energy of formation [J mol^{-1}]
h	Foam height [m]
H	Enthalpy of fusion [J mol^{-1}]
k_b	Boltzmann's constant; $k_b = 8.62\ 10^{-5}$ eV $K^{-1} = 1.38\ 10^{-23}$ J K^{-1}
k_d	Breakage rate constant, eq. 3.06 [$L^{0.5}$ $hr^{-1}dm^{-1.5}$]
k_g	Growth rate constant, eq. 2.08 [μm hr^{-1}]
k_{nu}	Nucleation rate constant, eq. 2.04 and 2.05
k_p	Precipitation rate constant, eq. 2.14 [L mol^{-1} hr^{-1}]
k_{we}	Shape parameter of weibull function
K_1	Constant in BCF growth rate expression, eq. 2.07
K_2	Constant in BCF growth rate expression, eq. 2.07
K_{so}	Solubility product
l	Characteristic particle size [μm]
m_1	First miller index
m_2	Second miller index
m_3	Third miller index
M	Molar mass [g mol^{-1}]
M_T	Crystal concentration [g L^{-1}]
n	Molar amount of a substance [mol]
n(l)	Population density in length coordinates [μm^{-1} L^{-1}]
$n(l_0)$	Population density of nuclei in length coordinates [μm^{-1} L^{-1}]
$n_v(v)$	Population density in volume coordinates [μm^{-3} L^{-1}]
N_a	Avogadro's number; $N_a = 6.02 \cdot 10^{23}$ mol^{-1}
N_b	Number of fragments formed per parent particle [μm^{-3}]
N_{gr}	Number of growth sites
N_{st}	Stirring rate [RPM]
pK_a	Acid dissociation constant
q	Elementary charge; $q = 1.6 \cdot 10^{-19}$ C
Q	Flow rate [Nm^3 hr^{-1} or L hr^{-1}]
R_u	Universal gas constant; $R_u = 8.314472$ J K^{-1} mol^{-1}
S	Degree of saturation

$S^{'}$	Approximation of the degree of saturation
t	Time [hr]
$\bar{t}$	Residence time e.g. V/Q [hr]
T	Temperature [K]
u	Velocity [m s^{-1}]
v	Particle volume [μm^3]
$\bar{v}$	Mean particle volume [μm^3]
V	Volume [L]
V_m	Molar volume [Nm^3 mol^{-1}]
w	Parent particle volume [μm^3]
x	Characteristic grid point
z	Ionic charge

Greek letters

α	Alpha/surface roughness factor
β	Breakage kernel
β_g	Growth affinity
Δl_j	Size/width of particle size interval "j" [μm]
ε_0	Permittivity of free space; $\varepsilon_0 = 8.85 \cdot 10^{-12}$ C^2 N^{-1} m^{-2}
ε_r	Dielectric constant
ξ	Anisotropy factor
μ	Chemical potential [J mol^{-1}]
γ	Activity coefficient
κ^{-1}	Debye length/thickness of electrostatic double layer [m]
Σ	Bikerman coefficient [s]
η_a	Absorption efficiency
ϕ	Volume fraction
ρ	Density [kg m^{-3}]
λ	Scale parameter of Weibull distribution

Subscript

ab	Absorbed
an	Anionic
cat	Cationic
eq	Equilibrium
fo	Foaming solution
g	Gas
gy	Gypsum
i	Inner
j	Interval j
in	Initial
l	Liquid
nu	Nuclei of critical size
s	Solid
sl	Slurry
su	Superficial
sur	Surface
v	Corresponding to volume “v”
w	Corresponding to volume “w”
wa	Water

Bibliography

(1) *World energy outlook*; International Energy Agency (IEA) & Organisation for Economic Co-operation and Development (OECD): Paris, 2004.

(2) Bartok, W., Ed.; Sarofim, A.F., Ed. *Fossil Fuel Combustion – A Source Book*; John Wiley & Sons, Inc: New York, NY, 1991.

(3) Wark, K.; Warner, C.F.; Davis, W.T. *Air Pollution – Its origin and control*, 3rd ed.; Addison Wesley Longman, Inc: Menlo Park, CA, 1998.

(4) Soud, H.N. *Developments in FGD*; IEA Coal Research: London, 2000.

(5) Takeshita, M.; Soud, H. *FGD Performance and Experience on Coal-fired Plants*; IEA Coal Research: London, 1993.

(6) Srivastava, R.K. *Controlling SO_2 emissions – A review of technologies*; Nova Science Publishers, Inc: Hauppauge, NY, 2003.

(7) *Vi springer ud i den rene luft – Røggasrensningsanlæg på asnæsværket blok 5*; Elkraft A.m.b.a.: Denmark, 1990.

(8) Buecker, B. FGD Gypsum Issues. *Power Engineering* **2007**, 111 (11), 112-116.

(9) Randolph, A.D.; Etherton, D. *Study of Gypsum Crystal Nucleation and Growth Rates in Simulated Flue Gas Desulfurization Liquors - technical report EPRI-CS-1885*; Arizona Univ. Dept. of Chemical Engineering: Tucson, AZ; Electric Power Research Inst: Palo Alto, CA, 1981.

(10) *300 New FGD Projects Planned in China*; The McIlvaine Company: Northfield, IL, 2006 Internet: http://www.environmental-expert.com.

(11) Siegfriedt, W.E.; Gaikwad, R.; DePriest, W. *Flue Gas Desulfurization Technology Evaluation – Dry Lime vs. Wet Limestone FGD*; Sargent & Lundy^{LCC}: Chicago, IL, 2007.

(12) *Flue Gas Desulphurisation (FGD) Technologies*, *technology status report*; Department of Trade and Industry: London, 2000.

(13) Soud, H.; Takeshita, M. *FGD handbook,* 2nd Edition; IEA Coal Research: London, 1994.

(14) Blankinship, S. Looking for good scrubbing: Today's FGD technology. *Power Engineering* **2005**, 109 (9), 19-24.

(15) Mullin, J.W. *Crystallization*, 4th Edition; Elsevier Butterworth-Heinemann: Oxford, 2004.

(16) Davey, R.; Garside, J. *From Molecules to Crystallizers – An Introduction to Crystallization*; Oxford University Press: Oxford, 2000.

(17) Randolph, A.D.; Kelly, B.J.; Keough, B. *Calcium sulfite and calcium sulfate crystallization: Volume 1, Effect of crystallizer type on gypsum size distribution – final report EPRI-CS-4861-Vol.1*; Arizona Univ. Dept. of Chemical Engineering: Tucson, AZ; Electric Power Research Inst: Palo Alto, CA, 1986.

(18) Zhang, J.; Nancollas, G.H. Influence of calcium/sulphate molar ratio on the growth rate of calcium sulphate dihydrate at constant supersaturation. *Journal of Crystal Growth* **1992**, 118 (3-4), 287-294.

(19) Bunn, C.W. *Chemical Crystallography – an introduction to optical and x-ray methods*; Oxford University press: Oxford, 1961.

(20) Rosenberger, F. Inorganic and protein crystal growth – similarities and differences. *Journal of crystal growth* **1986**, 76 (3), 618-636

(21) Myerson, A.S. *Handbook of Industrial Crystallization*, 2nd Edition; Elsevier Butterworth-Heinemann: Boston, MA, 2002.

(22) Randolph, A.D.; Larson, M.A. *Theory of Particulate Processes – Analysis and Techniques of Continuous Crystallization*, 2nd Edition; Academic Press: New York, NY, 1988.

(23) Bujac, P.D.B. Attrition and Secondary Nucleation in Agitated Crystal Slurries. In: Mullin, J.W. *Industrial crystallization*, *6th symposium on industrial crystallization*; Plenum Press: New York, NY, 1976:23-31

(24) Berglund, K.A.; deJong, E.J. The calculation of growth and nucleation kinetics from MSMPR crystallizer data including growth rate dispersion. *Separations Technology* **1990**, 1(1), 38-45.

(25) Kougoulos, E.; Jones,. A.G.; Wood-Kaczmar, M.W. Estimation of crystallization kinetics for an organic fine chemical using a modified continuous cooling mixed suspension mixed product removal (MSMPR) crystallizer. *Journal of crystal growth* **2005**, 273 (3-4), 520-528.

(26) Garside, J.; Jancic, S.J. Growth and dissolution of Potash Alum Crystals in the Subsieve Size Range. *AIChE Journal* **1976**, 22 (5), 887-894.

(27) Garside, J.; Jansen-Van Rosmalen, R.; Bennema, P. Verification of crystal growth rate equations. *Journal of Crystal Growth* **1975**, 29 (3), 353-366.

(28) Mydlarz, J.; Jones, A.G. On the estimation of size-dependent crystal growth rate functions in MSMPR crystallizers. *Chemical Engineering Journal* **1993**, 53 (2), 125-135.

(29) Hamm, H.; Kersten, H. J.; Hueller, R. 25 years experience gained in the European Gypsum Industry with the use of FGD gypsum. *Cement International* **2004**,4. 92-102.

(30) Hageman, E. *Gips*, 3rd Edition; Polyteknisk forlag: Lyngby, 1977.

(31) Hand, R.J. Calcium sulphate hydrates: a review. *British ceramic transactions* **1997**, 96(3), 116-120.

(32) Meijer, J.A.M.; Van Rosmalen, G.M. Solubilities and Supersaturations of Calcium Sulfate and its Hydrates in Seawater. *Desalination* **1984**, 51(3), 255-305.

(33) Ottmers, D.Jr.; Phillips, J.; Burklin, C.; Corbett, W.; Phillips, N.; Shelton, C. *A theoretical and Experimental Study of the Lime/Limestone Wet Scrubbing Process*. Technical report EPA-650/2-75-006; Radian Corporation: Austin, TX, 1974.

(34) Christoffersen, M.R.; Christoffersen, J.; Weijnen, M.P.C.; van Rosmalen, G.M. Crystal growth of calcium sulphate dehydrate at low supersaturation. *Journal of Crystal Growth* **1982**, 58 (3), 585-595.

(35) Liu, S-T.; Nancollas, G.H. The kinetics of crystal growth of calcium sulphate dihydrate. *Journal of crystal growth* **1970**, 6 (3), 281-289.

(36) Abdel-Aal, E.A.; Rashed, M.M.; El-Shall, H. Crystallization of calcium dehydrate at different supersaturation ratios and different free sulphate concentrations. *Crystal Research and Technology* **2004**, 39 (4), 313-321.

(37) Kruger, A.; Focke, W.W.; Kwela, Z.; Fowles, R. Effect of Ionic Impurities on the crystallization of Gypsum in Wet-Process Phosphoric Acid. *Industrial & Engineering Chemistry Research* **2001**, 40 (5), 1364-1369.

(38) Gilbert Jr., R.L. Crystallization of gypsum in wet process phosphoric acid. *I&EC – Process Design and Development* **1966**, 5(4), 388-391.

(39) Martynowicz, E.T.M.J.; Liao, L.; Witkamp, G.-J.; van Rosmalen, G.M. The influence of aluminim fluoride in hemi-dihydrate phosphoric acid processes. *Hydrometallurgy* **1996**, 41(2-3), 155-170.

(40) Martynowicz, E.T.M.J.; Witkamp, G.-J.; van Rosmalen, G.M. The effect of aluminium fluoride on the formation of calcium sulphate hydrates. *Hydrometallurgy* **1996**, 41(2-3), 171-186

(41) Martynowicz, E.T.M.J. *Impurity uptake in calcium sulphate during phosphoric acid processing*. PhD Thesis; Delft University of Technology: Delft, 1994.

(42) Koopman, C.; Witkamp, G.J. Ion exchange extraction during continuous recrystallization of $CaSO_4$ in the phosphoric acid production process: lanthanide extraction efficiency and $CaSO_4$ particle shape. *Hydrometallurgy* **2002**, 63(2), 137-147.

(43) Rashad, M.M.; Mahmoud, M.H.H.; Ibrahim, I.A.; Abdel-Aal, A. Crystallization of calcium sulphate dehydrate under simulated conditions of phosphoric acid production in the presence of aluminium and magnesium ions. *Journal of crystal growth* **2004**, 267 (1-2), 372-379.

(44) Pashley, R.M.; Karaman, M.E. *Applied Colloid and Surface Chemistry*; John Wiley & Sons, Ltd: Chichester, 2004.

(45) Shaw, D. J. *Introduction to Colloid and Surface Chemistry*, 4th Edition; Butterworth-Heinemann, Ltd.: Boston, MA, 1992.

(46) Thiele, R.; Brettschneider, O.; Repke, J.; Thielert, H.; Wozny, G. Experimental Investigation of Foaming in a Packed Tower for Sour Water Stripping. *Ind. Eng. Chem. Res.* **2003**, 42 (7), 1426-1432.

(47) Lu, S.; Pugh, R. P.; Forssberg, E. *Interfacial Separation of Particles*, 1st Edition; Elsevier: Amsterdam, 2005.

(48) Kostakis, T.; Ettelaie, R.; Murray, B. S. Effect of High Salt Concentrations on the Stabilization of Bubbles by Silica Particles. *Langmuir* **2006**, 22 (3), 1273-1280.

(49) Sebba, F. *Foams and biliquid Foams – aphrons*; John Wiley & sons, Ltd: Chichester, 1987.

(50) Denkov, N.D;, Cooper, P.; Martin, J.-Y. Mechanisms of Action of Mixed Solid-Liquid Antifoams: 1. Dynamics of Foam Film rupture. *Langumuir* **1999**, 15(24), 8514-8529.

(51) Bao, Y.; Zhang, J.; Yin, Q.; Wang. J. Determination of growth and breakage kinetics of L-threonine crystals. *Journal of Crystal Growth* **2006,** 289, 317-323.

(52) Kostoglou, M.; Dovas, S.; Karabelas, A.J. On the steady-state size distribution of dispersions in breakage processes. *Chemical Engineering Science* **1997**, 52 (8), 1285-1299.

(53) Brown, W.K.; Wohletz, K.H. Derivation of the Weibull distribution based on physical principles and its connection to the Rosin-Rammler and lognormal distributions. *Journal of Applied Physics* **1995**, 78 (4), 2758-2763.

(54) Villadsen, J.; Michelsen, M.L. *Solution of Differential Equation Models by Polynomial Approximation*; Prentice-Hall: New York, NY, 1978.

(55) Virone, C.; ter Horst, J.H.; Kramer, H.J.M.; Jansens, P.J. Growth rate dispersion of ammonium sulphate attrition fragments. *Journal of crystal growth* **2005**, 275 (1-2), 1397-1401.

(56) Kiil, S.; Michelsen, M. L.; Dam-Johansen, K. Experimental Investigation and Modelling of a Wet Flue Gas Desulfurization Pilot Plant. *Ind. Eng. Chem. Res.* **1998**, *37* (7), 2792-2806.

(57) Kiil, S.; Nygaard, H.; Johnsson, J. Simulation studies of the influence of HCl absorption on the performance of a wet flue gas desulphurisation pilot plant. *Chem. Eng. Sci.* **2002**, 57 (3), 347-354.

(58) Holdich, R. *Fundamentals of Particle Technology*; Midland Information Technology and Publishing: Leicestershire, 2002.

(59) Allen, T. *Particle Size Measurement – Volume 1*, 5th Edition; Chapman & Hall: London, 1997.

(60) Ulrich, J. Solution crystallization – Developments and new trends. *Chemical Engineering & Technology* **2003**, 26 (8), 832-835.

(61) Sherwood J.N.; Ristic R.I. The influence of mechanical stress on the growth and dissolution of crystals. *Chemical Engineering Science*. **2001**, 56 (7), 2267-2280.

(62) Frandsen, J. B. W.; Kiil, S.; Johnsson, J. E. Optimisation of a wet FGD pilot plant usng fine limestone and organic acids. *Chem. Eng. Sci.* **2001**, *56* (10), 3275-3287.

(63) Sparmann, A.; Liebmann, V.; Lemke, D. Operating Experience with the FGD Wet Scrubbing Process and Gypsum Processing at VEAG's Jänschwalde Power Station. *VGB Powertech – International edition* **1999**, 79 (1), 59-64.

(64) Gebhard, G.; Uerpmann, E.P. Gypsum grain shape and gypsum grain size-effects of method of operation of flue gas desulphurization. *VGB Kraftwerkstechnik* **1988**, 68 (8), 843-853.

(65) Lide, D. R., Ed. *CRC Handbook of Chemistry and Physics*, Internet version 2007 (87th Edition); Taylor and Francis: Boca Raton, FL, 2007 (available via the Internet at http:/www.hbcpnetbase.com).

(66) Lyregaard, M.; Rabia, O. *Våd røggasafsvovling*, B.Eng. thesis (In Danish); Department of Chemical Engineering, Technical University of Denmark: Lyngby, Denmark, 2000.

(67) Thomsen, K. *Aqueous electrolytes: model parameters and process simulation,* Ph.D. Thesis; Department of Chemical Engineering, Technocal University of Denmark: Lyngby, Denmark, 1997

(68) Roberts, W.L.; Rapp, G.R.; Weber, J. *Encyclopedia of Minerals*;.Van Nostrand Reinhold: New York, NY, 1974.

(69) Sloley, A. Is foam the culprit?. *Chem. Process.* **2006**, *69* (3), 62.

(70) Zheng, Y.; Kiil, S.; Johnsson, J. E. Experimental investigation of a pilot-scale jet bubbling reactor for wet flue gas desulphurization. *Chem. Eng. Sci.* **2003**, *58* (20), 4695-4703.

(71) Kister, H.Z. *Distillation Design*; McGraw-Hill: New York, NY, 1992.

(72) Kitchener, J. A. Foams and Free Liquid Films. *Recent Progress Surf. Sci*. **1964**, 1, 51-93.

(73) Buchardt, C. N.; Johnsson, J. E.; Kiil, S. Experimental investigation of the degradation rate of adipic acid in wet flue gas desulphurisation plants. *Fuel* **2006**, *85* (5-6), 725-735.

(74) Bikerman, J. J. *Foams*; Springer-Verlag: New York, 1973.

(75) Kiil, S. *Experiments and theoretical investigations of wet flue gas desulphurization*, Ph.D. Thesis; Department of Chemical Engineering, Technical University of Denmark: Lyngby, Denmark, 1998.

(76) Alvarez Nunez, F.A.; Yalkowsky, S. H. Foaming activity and pKa of some surface active compounds. *Int. J. Pharm.* **1997**, *151* (2), 193-199.

(77) Pugh, R. J. Foaming in Chemical Surfactant Free Aqueous Dispersions of Anatase (Titanium Dioxide) Particles. *Langmuir* **2007**, *23*(15), 7972-7980.

(78) Beenackers, A.A.C.M.; Van Swaaij, W.P.M. Mass Transfer in Gas-Liquid Slurry Reactors. *Chem. Eng. Sci.* **1993**, *48* (18), 3109-3139.

(79) Millero, F. J.; Hershey, J. P.; Johnsson, G.; Zhang, J.-Z. The solubility of SO2 and the dissociation of H2SO3 in NaCl solutions. *J. Atmos. Chem.* **1989**, *8* (4), 377-389.